DIPLOMARBEIT

Negative CO_2 Emissions with Oxygen Carrier in an Experimental Comparison

ausgeführt zum Zwecke der Erlangung des akademischen Grades eines Diplomingenieurs unter der Leitung von

Univ.Prof. Dipl.-Ing. Dr.techn. Hermann Hofbauer

am

Institut für Verfahrenstechnik, Umwelttechnik und Technische Biowissenschaften

betreut von

Projektass. Dipl.-Ing. Dr.techn. Josef Fuchs

Dipl.-Ing. Dr.techn. Benjamin Fleiß

eingereicht an der Technischen Universität Wien
Fakultät für Maschinenwesen und Betriebswissenschaften

von

Paul Söder

Matrikelnummer 12128307

[redacted]

[redacted]

Wien, am 01.06.2025

Ich nehme zur Kenntnis, dass ich zur Drucklegung meiner Arbeit unter der Bezeichnung

Diplomarbeit

nur mit Bewilligung der Prüfungskommission berechtigt bin.

Eidesstattliche Erklärung

Ich erkläre an Eides statt, dass die vorliegende Arbeit nach den anerkannten Grundsätzen für wissenschaftliche Abhandlungen von mir selbstständig erstellt wurde. Alle verwendeten Hilfsmittel, insbesondere die zugrunde gelegte Literatur, sind in dieser Arbeit genannt und aufgelistet. Die aus den Quellen wörtlich entnommenen Stellen sind als solche kenntlich gemacht.

Das Thema dieser Arbeit wurde von mir bisher weder im In- noch Ausland einer Beurteilerin/einem Beurteiler zur Begutachtung in irgendeiner Form als Prüfungsarbeit vorgelegt. Diese Arbeit stimmt mit der von den Begutachterinnen/Begutachtern beurteilten Arbeit überein.

Wien, am 01.06.2024

Paul Söder

Danksagung

Zunächst möchte ich mich bei Univ.-Prof. Dipl.-Ing. Dr.techn. Hermann Hofbauer bedanken für das Ermöglichen dieser Arbeit.

Mein außerordentlicher Dank gilt auch Dipl.-Ing. Dr.techn. Benjamin Fleiß für die Betreuung meiner Arbeit. Danke für die Ratschläge, danke für deine Zeit und deine Mühe, die du in diese Arbeit investiert hast, und danke für dein jederzeit offenes Ohr.

Ein weiteres großes Dankeschön gilt meiner Familie, meiner Mutter Petra, meinem Vater Rolf und meinem Bruder Lenz, die mich durch meine doch etwas längere Studienkarriere begleitet haben. Danke, dass ihr mir immer mit Tat und Rat zur Seite steht und ich mich jederzeit auf euch verlassen kann.

Abschließend gilt mein herzlichster Danke meiner Partnerin Clara. Danke für deine Zuversicht, deine Aufmunterungen, deinen Optimismus, deine Herzlichkeit und deine Fähigkeit mich in jeder Situation zum Lachen bringen zu können. Danke, dass du mich während meiner Zeit in Wien, ob nah oder fern, begleitet hast und dafür gesorgt hast, dass ich mein Ziel nicht aus den Augen verliere.

Danke

Abstract

To mitigate the emission of greenhouse gases and to reach a future without the use of fossil fuels, technologies are being developed that capture CO_2 from the atmosphere or from combustion processes. One of those technologies gaining more attention is chemical looping combustion (CLC). The CLC process is capable of producing a highly pure CO_2 stream with a lower energy penalty than conventional carbon capture methods. In combination with biomass as fuel CLC produces negative CO_2-emission, reducing the total concentration of greenhouse gases already present in the air. The characteristic of this process is that the fuel never comes into direct contact with the air; instead, the oxygen is fed into the reactor through a so-called oxygen carrier (OC). The OCs are the core element of the CLC process and the main focus of this study. The OC consists of metal oxides derived from natural ores or synthetically produced. Requirements for the OCs are high oxygen carrying capability, high reactivity, low attrition rate as well as low economic and environmental costs. In the scope of this work, six different synthetic OCs were tested in the laboratory at TU Wien and evaluated. The most promising of those OCs was then again tested in more detail during long-term experiments.

The OC that performed the best was a metal oxide comprised of manganese, iron and copper (MIC). It displayed high carbon conversion rates, CO_2 yield, as well as oxygen transport capabilities. The main drawback of MIC was, as shown during the characterisation test, because of its copper content the tendency to form agglomerations. During the long-term experiment, MIC was still showing high rates of CO_2 yield, as well as values of above 95% for the CO_2 selectivity. Finally, the lifetime of about 1920 h was determined. This study provides a framework for future experiments and investigations of synthetic OCs.

Kurzfassung

Um die Emission von Treibhausgasen zu verringern und eine Zukunft ohne fossile Brennstoffe zu erreichen, werden Technologien entwickelt, die CO_2 aus der Atmosphäre oder aus Verbrennungsprozessen abscheiden. Eine dieser Technologien, die zunehmend an Aufmerksamkeit gewinnt, ist „Chemical Looping Combustion“ (CLC). Der CLC-Prozess ist in der Lage, einen hochreinen CO_2-Strom mit einem geringeren Energieaufwand als herkömmliche Methoden der Kohlenstoffabscheidung zu erzeugen. In Kombination mit Biomasse als Brennstoff erzeugt CLC negative CO_2-Emissionen, wodurch die Gesamtkonzentration, der bereits in der Luft vorhandenen Treibhausgase verringert werden kann. Charakteristisch für diesen Prozess ist, dass der Brennstoff niemals direkt mit der Luft in Kontakt kommt; stattdessen wird der Sauerstoff über einen sogenannten Sauerstoffträger (OC) in den Reaktor eingebracht. Die Sauerstoffträger sind das Kernelement des CLC-Prozesses und der Hauptfokus dieser Arbeit. Die Sauerstoffträger bestehen aus Metalloxiden, die aus natürlichen Erzen gewonnen oder synthetisch hergestellt werden. Anforderungen an die Sauerstoffträger sind eine hohe Sauerstofftransportkapazität, hohe Reaktivität, hohe Abriebfestigkeit sowie niedrige wirtschaftliche und ökologische Kosten. Im Rahmen dieser Arbeit wurden sechs verschiedene synthetische Sauerstoffträger im Labor der Technischen Universität Wien getestet und bewertet. Der vielversprechendste dieser Materialen wurde anschließend in einem Langzeitexperiment erneut detailliert untersucht.

Der Sauerstoffträger, der die besten Ergebnisse erzielte, war ein Metalloxid bestehend aus Mangan, Eisen und Kupfer (MIC). Es zeigte hohe Kohlenstoffumwandlungsraten, CO_2 Ausbeute sowie Sauerstofftransportfähigkeiten. Der Hauptnachteil von MIC war, wie während des Charakterisierungstests gezeigt wurde, dass es aufgrund seines Kupfergehalts zur Agglomeration neigt. Auch während des Langzeitexperiments zeigte MIC weiterhin hohe CO_2 Ausbeuteraten, es wurden durchgängig Werte für die CO_2 Selektivität von 95% gemessen. Des Weiteren wurde eine Analyse der Lebenszweit erstellt, welche auf 1920h geschätzt wurde. Diese Studie dient als Grundlage für weitere Versuche an synthetischen Sauerstoffträgern.

Acknowledgements

This work was part of the Research Project BIO-LOOP of the cooperation partners BEST - Bioenergy and Sustainable Technologies GmbH (BEST), TU Graz: Institute of Chemical Engineering and Environmental Technology (CEET) and Institute for Thermal Engineering (ITE); National Institute of Chemistry: Department of Materials Chemistry; Spanish National Research Council: Department of Energy and Environment; Chalmers University of Technology; Rouge H2 Engineering GmbH; AVL List GmbH; Aichernig Engineering GmbH; Christof Project GmbH; SW-Energie Technik GmbH; TG Mess-, Steuer- und Geotechnic GmbH; Rohkraft - Ing. Karl Pfiehl GmbH. The COMET Module BIO-LOOP (Austrian Research Promotion Agency Project Number 872189) is funded within COMET - Competence Centers for Excellent Technologies - by the Federal Ministry for Climate Action, Environment, Energy, Mobility, Innovation and Technology (BMK), the Federal Ministry for Digital and Economic Affairs (BMDW) as well as the co-financing federal province Styria (SFG). The COMET programme is managed by FFG (Austrian Research Promotion Agency, the funding is gratefully acknowledged.

Table of contents

1 Introduction

Since the industrial revolution the economic model of the modern world has prioritized exponential growth, heavily reliant on fossil fuels and unsustainable resource extraction. The understanding that the Earth is not an inexhaustible source of resources but rather a fragile ecosystem with finite boundaries has only recently reached the awareness of the general public. For a long time, the economic activities of some societies were based on the assumption that growth and progress could be achieved through the unlimited exploitation of natural resources. This understanding ignores the ecological boundaries of our planet, which are becoming progressively more apparent in the form of climate change, species extinction and the destruction of whole ecosystems. A rapid shift in thinking is essential to prevent the continued exploitation of the earth for human growth.

1.1 Motivation

The fight against climate change and the prevention of increasing quantities of greenhouse gases is one of the most important political and social issues we face today. The effects of global warming have become increasingly apparent in recent years. The still rising emissions of greenhouse gas like carbon dioxide (CO_2) or methane (CH_4) are causing heat from solar radiation to be trapped inside the atmosphere and causing change in our climate. In actuality, the greenhouse effect is a phenomenon, that occurs naturally in our atmosphere and helps maintain a warm climate at Earth's surface. Only through the greenhouse effect of the atmosphere, a global mean temperature of about 14,5 °C becomes feasible [1]. The growing anthropogenic emission of greenhouse gases is intensifying this effect to such an extent that it is having an impact on the Earth's climate. The concentration of CO_2 has increased from 337 ppm in 1979 to 417 ppm in 2022, that's a growth of more than 20% in the last 44 years [2].

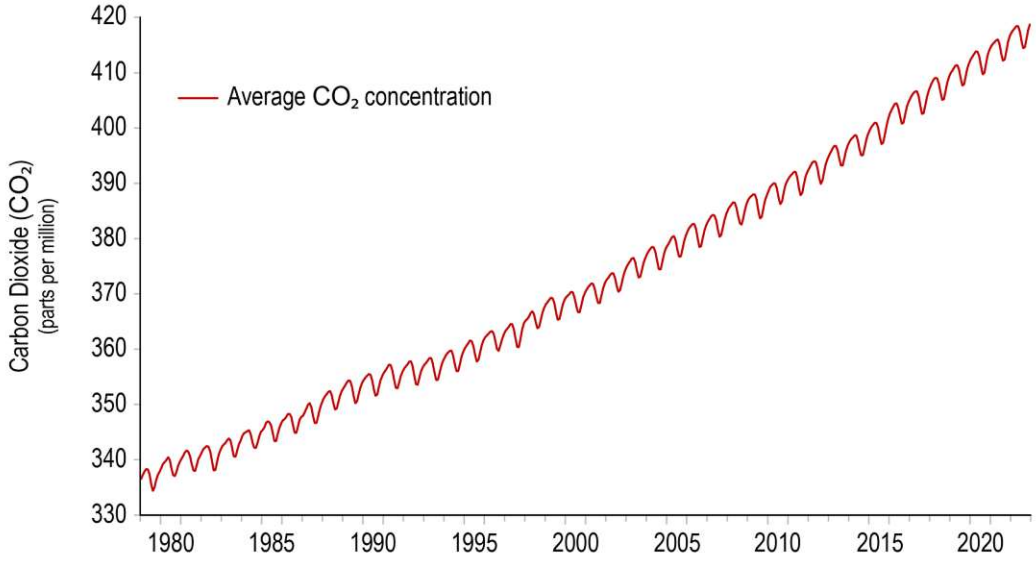

Figure 1: Global monthly average carbon dioxide concentration (adapted from [2])

As explained above, with rising levels of greenhouse gas in the atmosphere the surface temperature of the Earth is also increasing, which leads to a change in our climate. This change is characterized on the basis of long-haul temperature and precipitation trends as well as humidity and pressure levels in the surrounding environment. In addition, irregular weather conditions, the retreat of global ice sheets and the associated rise in sea levels are among the most critical effects of climate change. [3]

These changes have a profound impact on all life on Earth. According to the Intergovernmental Panel on Climate Change (IPCC), the negative influence contributed by climate change can be observed, among many others, in these areas [4]:

- Alternation of marine, terrestrial and freshwater ecosystems all around the world
- Stress on food and forestry systems, with negative consequences for food safety of hundreds of millions of people
- Water insecurity through climate induced water scarcity
- Harm to physical and mental health
- Involuntary migration and displacement mainly because of extreme weather events

The main source of greenhouse gas emission still remains the combustion of fossil fuels. The energy released in this process is used, among other things, to produce electricity, to drive means of transportation and to generate heat. For all those applications there are environmentally friendly alternatives, but transitioning away from fossil fuels is a slow and expensive process. As the current energy supply relies on fossil fuel in almost every sector and with the world-wide energy demand still rising, the task of replacing this energy source becomes an immensely complex procedure [5]. These changes require a reasonable policy framework. Achieving the necessary transformation of the energy system will require a combination of various measures and technologies. The focus must be on expanding renewable energy sources, as this is the only way to achieve a sustainable reduction in CO_2 emissions. Relevant technologies include the use of hydropower, solar, wind, geothermal, ocean, and bioenergy.[6]

The Paris climate summit in 2013 is considered a milestone in international climate policy. The countries that signed the document came to the agreement to restrict the temperature rise to a maximum of 2 °C compared to preindustrial times and to commit to reducing greenhouse gas emissions to net zero until the middle of the 21st century. This led to many countries integrating climate targets into their laws, like the Austrian federal government committing to achieving climate neutrality by 2040. Until then, the development and expansion of new technologies is crucial for helping in this transitioning phase. [7]

Carbon capture and storage/usage (CCS/CCU) technologies have been discussed controversially in politics in the last few years. They are counted as a necessary tool to mitigate CO_2 emission, primarily for hard or impossible emissions to avoid. While environmental agencies warn against the implementation of CCS with regards to the potential dangers of transporting and storing CO_2

underground. Carbon capture methods can be categorized into generation one and generation two technologies. While generation one is well established with some uses in the industrial sector, generation two is still being tested, and plants have only been constructed on a laboratory scale. This thesis focuses around one of the second generation technologies, the chemical looping combustion (CLC). [8]

CLC has been gaining more interest in the scientific community since the early 2000s, when a lot of research was conducted on the subject. Especially its ability to produce a highly pure CO_2 exhaust stream with lower energy penalty than generation one CCS technologies, sparked interest in more research. Furthermore, the CLC process allows to produce so called negative emissions, when biomass is used as a fuel. In contrast to CO_2 neutral technologies like using biomass as a fuel in a conventional combustion process, in which the CO_2 is release into the atmosphere with the flue gas, technologies with negative emissions reverse climate change by reducing the total concentration of greenhouse gases already present in the air, as opposed to merely reducing ongoing emissions. Now the technology has been seen a lot of development over the last 20 years, yet some questions are still not answered. A significant role in the CLC process belongs to the oxygen carrier (OC), which circulates between the two reactors of a CLC plant. This metal oxide transports the oxygen from the air reactor to the fuel reactor. The motivation of this thesis is to examine and evaluate different metal oxides and find the best suited one for a CLC process.

1.2 Aim & Scope

To evaluate different OCs a series of experiments and analyses have been conducted. The methodology behind this thesis was established through previous experiments done in a similar fashion [9]. All experiments were conducted in a laboratory at TU Wien. The reactor used throughout the research is a CLC batch reactor. This reactor simulates a larger scale CLC plant with only a single reactor, by switching between air and fuel reactor. It is perfectly suited for an investigation of OCs. The six characterisation tests are all executed in the same way. The OC are tested under various conditions like different temperatures, volume flows and fuel amounts. During the test samples of the bed materials were taken to require information about the oxygen transport capability of the OC. The data gathered during the test and from the samples are than used to evaluate the OC on several criteria. After the best performing OC was determined it was again tested during a long-term experiment. The objective here was to find more detailed information about the OC like, attrition rate, carbon conversion or magnetic permeability, which can be important when thinking about the recyclability of the OC. All together this experiment was to test the OC under longer reaction condition, to see how it would perform in the large CLC pilot plant.

2 State of the art

In order to understand the chemical looping combustion (CLC) process, the basics of this technology are explained in this chapter. As an introduction into the technology, this chapter gives a broad overview of the fundamentals of the CLC process. The fluidised bed technology, that is crucial for this process, is explained and the influence of the oxygen carrier (OC) on the process are illustrated. Furthermore, an overview of the existing CLC systems will be given and the possible direction in which the technology will continue to develop. Finally, the topic of utilization will be discussed.

2.1 Carbon capture methods

As mentioned before, CLC is categorized as a carbon capture and storage technology (CCS). The aim of those technologies is to capture CO_2 from industrial processes and produce a concentrated stream of it, to either store it safely or utilise it further. In the first generation of carbon capture methods, a distinction is made between pre-combustion, post-combustion and oxy-combustion technologies [10]. Figure 2 shows the process scheme as developed by Figueroa et al [8].

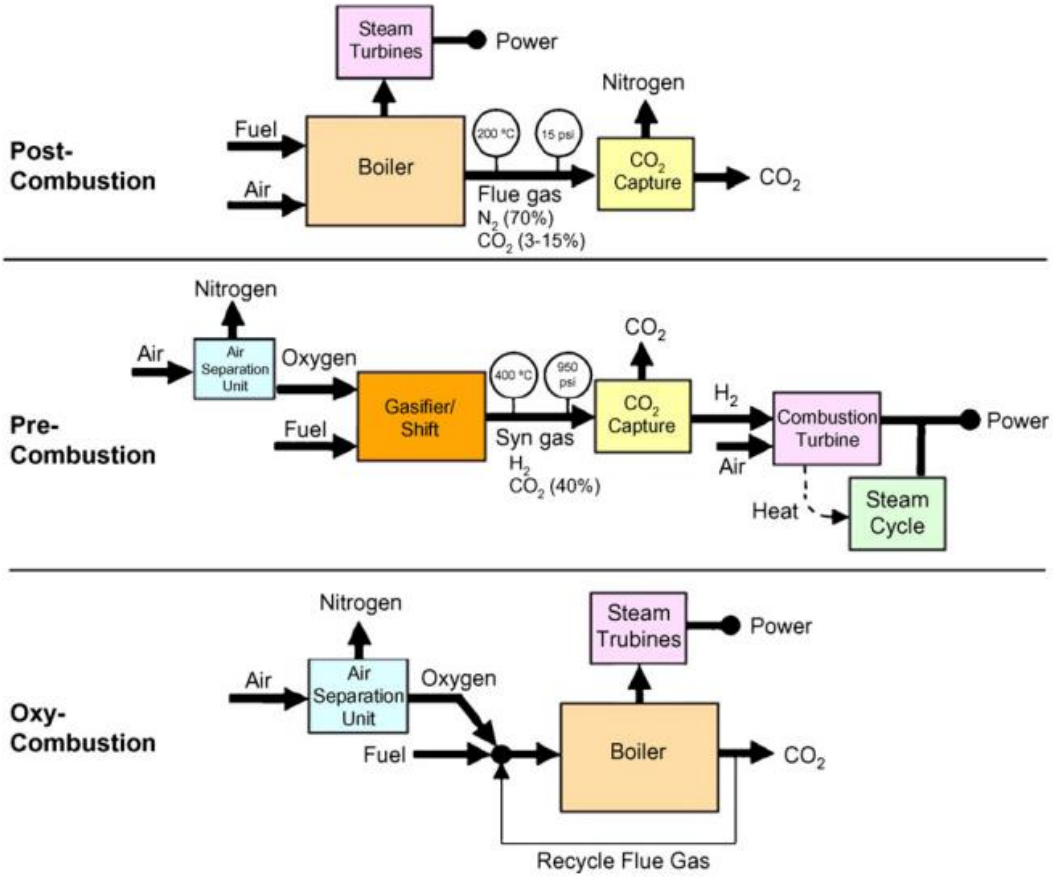

Figure 2: Schematic display of the Gen 1 CCS technologies: post-combustion, pre-combustion and oxy-combustion process (adapted from [8])

The post-combustion capture is the process of removing the CO_2 from the flue gas produced during the combustion. Conventional power plants use air, which contains around 79% nitrogen, to burn the fuels. This produces a flue gas with atmospheric pressure and a low CO_2 concentration of less than 15%. Thus, resulting in a flue gas with low thermodynamic driving force for CO_2 capture. Despite this considerable drawback, the post-combustion capture technology allows retrofitting of most existing power generation plants. Making it a viable solution for near-term reduction of greenhouse gas emissions [8, 10]. The CO_2 capture is achieved through absorption, adsorption, or membrane separation. The different post-combustion capture techniques can be found at Chao et al. [11]

With the pre-combustion carbon capture, the solid, liquid, or gaseous fuel gets converted into a synthesis gas, mainly containing hydrogen (H_2) and carbon monoxide (CO) [12]. The CO gets converted via the water gas shift reaction into CO_2 and combined with more CO_2 from the exhaust stream of the combustion to increase the CO_2 content. The higher CO_2 concentration allows the carbon capture with more conventional techniques, lowering its cost. The hydrogen is used as fuel for the power plant. [13, 14]

Since nitrogen in the air was the biggest problem for post-combustion technology, the approach of oxyfuel combustion technology is to use pure oxygen for its combustion. For this, the nitrogen gets separated out of the air. The fuel gets burned in a nitrogen-free atmosphere, which results in a flue gas containing mainly CO_2 and water vapor. By condensing the water vapor, this mixture can easily be separated. For the oxy-combustion technique, the cost of separating the CO_2 out of the flue gas is low, but the air separation unit, which produces the pure oxygen for combustion, increases the overall cost of the technology. [10, 15]

CO_2 capture is best suited for large-scale power plants or industries. It opens the way for low-carbon or carbon-free production of electricity and fuels for transportation. Capturing the CO_2 requires energy and thus reduces the efficiency of the power plant. This leads to more fuel requirements, solid wastes, and environmental impacts. However, the continuing research will make carbon capture more efficient, making older plants that are now in service obsolete. [14]

While these technologies have seen great development, their high energy penalty is still a drawback. Efforts were therefore made to develop a new low-cost CCS technology. In [16] different CCS technologies were evaluated with the goal of identifying the most promising CCS technology. Their results show that CLC offers considerable cost savings, as well as reduced NO_x production and emissions [16, 17]. In contrast to traditional combustion methods CLC uses an OC to introduce oxygen into combustion. The technology contains an air reactor, for the oxidation of the OC and a fuel reactor for the combustion of the fuel. The OC is a metal oxide which gets circulated between the two reactors. CLC shows higher energy efficiency as the other carbon capture methods because the capturing of the CO_2 is inherent to the process.

2.2 Chemical looping combustion

Chemical looping combustion (CLC) was first introduced as a method for producing pure CO_2 from carbon-rich fuel by Lewis et al. [18]. They presented their work, a basic process concept, as a patent in 1954. Proposing the ideas of OCs and two fluidised bed reactors in order to produce pure carbon dioxide. [19] Ishida and Jin later picked up that concept as a method for capturing CO_2 during a combustion process and they were the first to call it CLC [20]. Since then, a great number of studies have been conducted, mainly investigating reactor configurations, fuel types, the fluidised bed technology, and different materials for OCs. [21-23]

The concept of CLC is that the fuel is never burnt in direct contact with air. The oxygen needed for the combustion is transported into the reactor via the OC, which are metal oxides. For this system to work the CLC process relies on two reactors, with the OC constantly looping between the two reactors. This concept is illustrated in Figure 3.

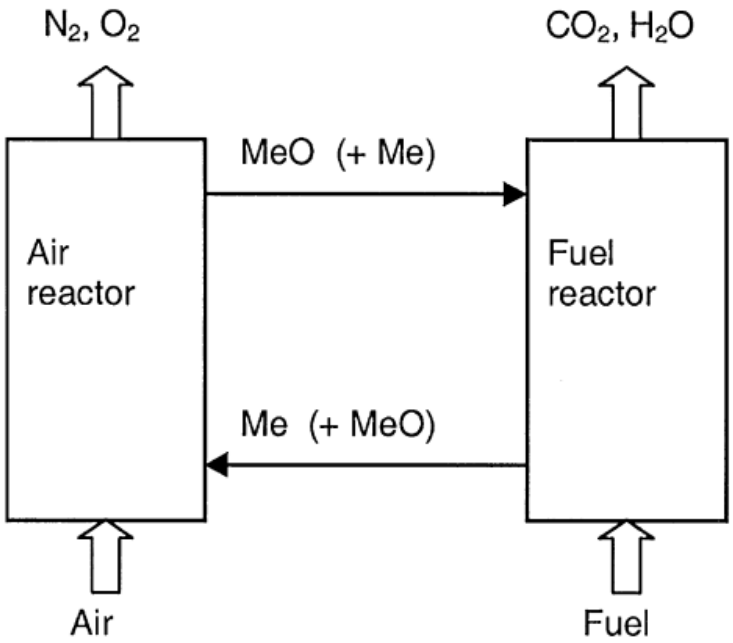

Figure 3: Chemical looping combustion concept (adapted from [24])

Inside the air reactor the metal oxide (Me) gets oxidised by the oxygen (O) in the air to produce an oxidized metal oxide (MeO).

$$Me + \frac{1}{2}\,O \rightarrow MeO \qquad (1)$$

This reaction creates a flue gas from the air reactor only containing nitrogen (N_2) and the unused oxygen (O_2). The MeO and some unoxidized Me (as a full conversion is only attainable in theory) circulate

inside the fuel reactor. Here the oxygen carried over by the metal oxide reacts with the fuel into water vapor (mH_2O) and carbon dioxide (nCO_2).

$$(2n+m)MeO + C_nH_{(2*m)} \rightarrow (2n+m)Me + mH_2O + nCO_2 \quad (2)$$

The reduced Me and some MeO get transferred back to the air reactor to be oxidised again. The exhaust gas coming from the fuel reactor containing mostly CO_2 and water vapor. It depends on the OC but the reaction inside the air reactor is often exothermic (producing heat) and the reaction inside the fuel reactor endothermic (consuming heat). The total amount of energy generated is the same as in a traditional combustion with direct contact between air and fuel. The inherent generating of a relatively pure CO_2 stream without any energy penalty is what makes the CLC process so interesting in regards to CCS. [24]

The first CLC experiments have been conducted using gaseous fuels, and a high effort of research has addressed this subject. More recently researcher have also considered solid fuels such as coal, or biomass. Solid fuels have considerable advantages over the gaseous fuels, so an adaption of the CLC process would be highly advantageous [25]. Coal is way more abundant than natural gas, lowering the overall cost of the operation. Considering the anthropogenic emission of carbon dioxide, capturing and storing CO_2, that is released burning biomass, would lead to negative emissions from generating power. Nonetheless the use of solid fuels comes with its own challenges. The high concentration of fixed carbon in coal shows only low solid-solid reaction with iron-based metal oxides [26]. Therefore, the solid fuel needs to be gasified for the OC particles to react with the produced gas. The gasification of the solid coal is much slower than the reaction of the gas with the OC particles, making it the time limiting step. If the char is not fully converted into gas, some residual char is going to circulate into the air reactor along with the OC. Unconverted char gets then burned in the air reactor leading to CO_2 not being captured, thus lowering the CO_2 capture efficiency of the system [27]. In contrast to this, most relevant biogenic solid fuels, compared to coal, contain a higher fraction of volatiles, which get released during gasification and combustion. These volatiles can, for instance, cause unwanted gas-phase reactions, resulting in increased production of CO, CH_4, or other hydrocarbons. Another challenge for the burning of solid fuels in a CLC process is the separation of fuel ash from the OC material [28].

Regardless of the fuel-type, adequate contact between the OC and fuel is required when considering CLC. To ensure a high conversion rate and minimizing unburnt material, CLC plants are often realized utilizing the fluidised bed technology [29]. The OC and the reactor design are two crucial features of the CLC process, both will be described in further detail in the next chapters.

2.3 Oxygen carrier

The oxygen carriers (OC) are one of the most important corner stone of the CLC technology. Their ability to transfer oxygen into the fuel reactor, their resistance to attrition and agglomeration, as well as their ability to convert the carbon into CO_2, are only a few of the necessary functions an OC has to fulfil for a CLC process to be viable. That's why a high research effort in the field of CLC is focused on testing and developing different OCs. OCs are metal oxides consisting of an electronegative oxygen and an electropositive metal, e.g., CuO or Fe_2O_3. The OC is used as a grain-sized powder (20-1000 µm) for optimal fluidisation capability. [30]

Table 1: Important properties for an OC [30]

Particle properties	**Explanation**
Attrition resistance	The higher the attrition rate the faster the OC carrier is used up during the CLC process
Agglomeration resistance	Agglomeration can influence the fluidisation of the bed and lower the recyclability of the OC
Density	Higher density and bulk density materials better dissipate heat
Bulk density	
Particle size distribution	A low variance in particle size results in a more stable fluidised bed and lower discharge rate
Reaction properties	**Explanation**
Carbon conversion	A complete carbon conversion is desired, to lower the formation of tars
CO_2 yield	A highest possible CO_2 yield is crucial for the viability of the CLC process
CH_4 conversion	The lower the CO- and CH_4 conversion the more carbon got converted into CO_2
CO conversion	
Oxygen transport	Higher oxygen transport results in more oxygen in the fuel reactor and better combustion
Exothermal heat release	Low exothermal heat release is desirable, as heat lost during the oxidation must be created during the reduction
Addition properties	**Explanation**
Toxicity	Non-toxic materials are easier to handle
Environmental compatibility	Impact on the environment of mining, producing and final storage of the OC
Costs	Lower costs increase the economic viability of the OC
Recyclability	Important for economic and environmental reasons

Table 1 shows the most important properties of an OC used in a CLC process. For this study the particle and process properties are especially important, their measuring and calculation are explained in further detail in the chapter 3.5.

There are two different groups of OCs that have been under investigation in recent years. The first group is natural ores (e.g., ilmenite, iron- or manganese-based ores) and the second is synthetic OCs, which are compounds of different metal oxides. Natural ores have the benefit of needing hardly any processing and are therefore relatively cheap. They can be harvested from mines, found in residual materials from the iron and steel industry, or as waste product from recycling plants [31]. Synthetic OCs on the other hand, are produced with different methods like freeze, granulation, spray drying, coprecipitation, Sol-Gel Synthesis, or impregnation [32]. As the OCs used in this work were produced using spray drying and impregnation techniques, those will be explained further in the next chapter.

As the name suggests a key quality of an OC is their ability to transfer oxygen from the air reactor to the fuel reactor, Figure 4 shows the oxygen transport capability of some redox systems of interest.

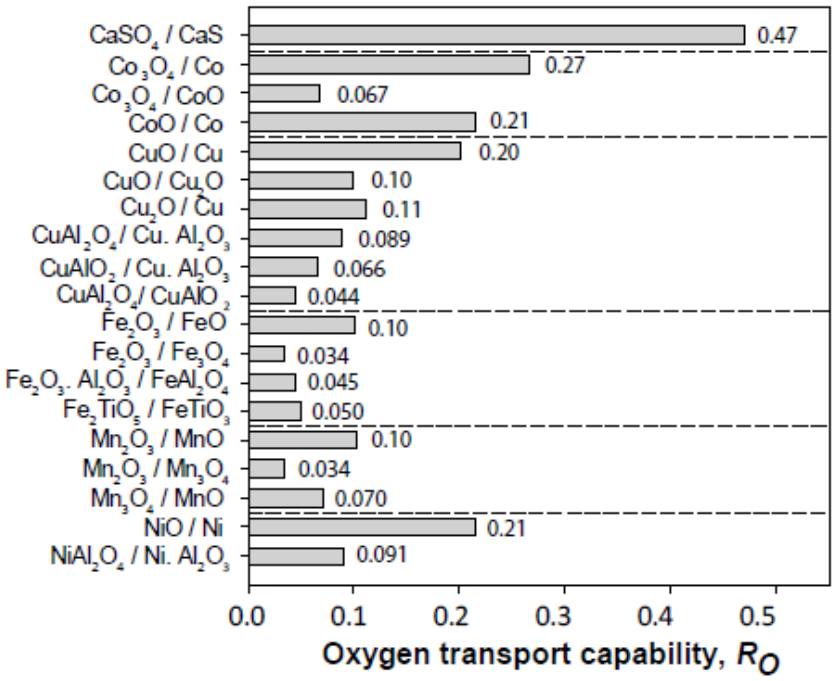

Figure 4: Oxygen transport capability R_O of different redox systems (adapted from [33])

The oxygen transport capability R_O is calculated using Formula 3, where m_o describes the mass of the OC in an oxidized state and m_r in a reduced state [12]:

$$R_O = \frac{m_o - m_r}{m_o} \tag{3}$$

Usual values for the oxygen transport capability are between 0.1 and 0.2, with the redox pair of $CaSO_4$/CaS being an exception.

2.3.1 Manufacturing of synthetic oxygen carriers

Chemical looping processes, in which gaseous, liquid, and solid fuels react with solid OC, are usually operated in fluidised bed systems, where the selection of particles with specific densities, shapes, and sizes is crucial for ensuring optimal transport and mixing, which directly affects productivity, heat transfer, and process control. Consequently, OC synthesis plays a far more important role than often recognized in chemical looping technology, as it can significantly influence the success or failure of the operation. The synthesis method used has a major impact on key properties of the OCs, including microstructure, morphology, porosity, strength, and overall cost. Therefore, choosing the appropriate synthesis method and parameters is essential to produce OCs suited for the intended application. Several methods have been used in the development of OCs, The OCs used in the scope of this work have either been developed using spray drying or impregnation. [32]

The spray drying procedure encompasses the atomization of a solution, slurry, or emulsion containing the desired product's components into droplets through spraying. This is succeeded by the swift evaporation of the sprayed droplets into solid powder using hot air at specific temperature and pressure conditions. The resulting solid powders, which consist of salts or hydroxides, undergo calcination to yield metal oxide powders [34]. The spray drying method is highly viable on an industrial scale and therefore used more frequently for generating engineered OCs. Other advantages of this method are its homogenous microstructure, the relatively low cost compared to more advanced techniques and a scalable process, to name only a few. [32]

The impregnation method can in general be divided into two different approaches, which can be differentiated by the amount of solvent used in the process. During the dry impregnation method, the porous substrates are first dried and then only the pores are filled with a metal salt solution. The wet impregnation, on the other hand, uses an excess amount of metal salt solution to submerge the porous substrates into. The next step is the evaporation of the solvent by drying, which is the same for both methods. During this step the salt solution gets supersaturated, which leads to a precipitation of metal salts in the pores and on the surface of the substrate. These precipitates are then converted into oxides in a suitably designed calcination step. The spray drying as well as the impregnation method undergo, after their fabrication, a post-treatment step. This step contains a heat-treatment, usually in the form of sintering, in which the particles receive a strengthening for the use in a fluidised bed. A more detail description of those two methods as well as an overview of all manufacturing processes of OCs for a CLC process can be found in a study by De Vos et al. [32]

2.3.2 Oxygen carrier and fuel combustion reactions

A key consideration of the CLC process is the reaction between the OC and the fuel. There are three different reaction methods for solid fuels: Syngas-CLC, heterogeneous CLC (Het-CLC) and Chemical looping with oxygen uncoupling (CLOU). They are dependent on the OC and the fuel type. Syngas-CLC has a lot in common with gaseous CLC because the solid fuel gets gasified in a separate process and enters the reactor as a gas. The schemes of the combustion reaction for Het-CLC and CLOU are depicted in Figure 5. [33, 35]

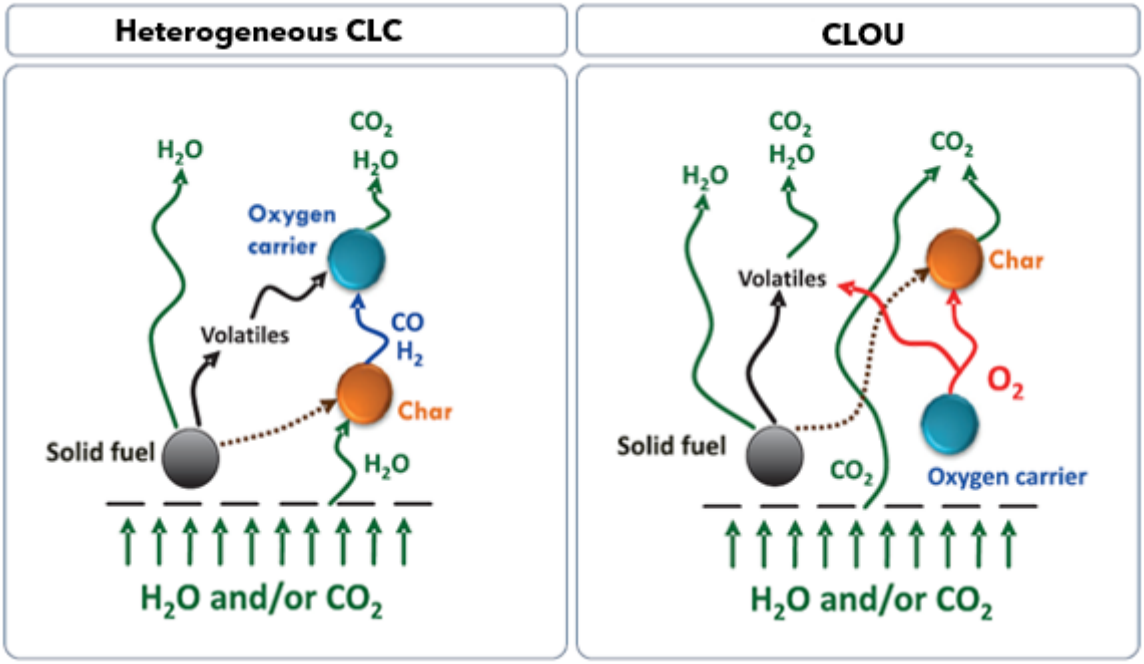

Figure 5: Reaction processes between OC and solid fuel (adapted from [27])

The Het-CLC avoids the need for a gasifier by directly gasifying the fuel inside the reactor. The solid fuel is mixed with the OC inside the reactor and fluidised by H_2O, CO_2 or a mixture of these gases. When CO_2 is used as a fluidisation agent, the energy for steam production can be avoided, as the CO_2 can be recirculated from the flue gas. The OC reacts with the volatiles and the gas products from the char-gasification, which are CO and H_2. The main reactions during heterogeneous CLC are as follows:

$$biomass \rightarrow volatile\ matter + char \quad (4)$$

$$char\ (mainly\ C) + H_2O \rightarrow H_2 + CO \quad (5)$$

$$char\ (mainly\ C) + CO_2 \rightarrow 2\ CO \quad (6)$$

$$H_2, CO, volaltile\ matter + n\ Me_xO_y \rightarrow CO_2 + H_2O + n\ Me_xO_{y-1} \quad (7)$$

$$H_2O + CO \leftrightarrow H_2 + CO_2 \quad (8)$$

$$Me_xO_{y-1} + \frac{1}{2}O_2 \rightarrow Me_xO_y \quad (9)$$

The solid fuel gets gasified during the heterogeneous CLC following the reactions (1-3), where the fuel (biomass) is first split into volatile matter and char. The char reacts with the gasification agent (H_2O, CO_2) and produces H_2 + CO and 2 CO respectively. These gases and the volatiles are oxidized through reduction of the OC (Me_xO_y) by means of reaction (4). The water-gas shift equilibrium, as seen in reaction (5) can also influence the gas composition in the reactor. The reduced OC is then oxidized again following reaction (6) inside the air reactor. The CO_2 capture should ideally be inherent to the CLC process, because the air is never in direct contact with the fuel. However, the CO_2 capture efficiency can be reduced when unburnt char gets transported into the AR with the OC. There the char is burnt, and CO_2 is mixed with the depleted air from the air reactor. This can happen when the residence time of the biomass inside the fuel reactor is too short. It has been identified that the gasification process is the speed-controlling factor of heterogeneous CLC. [33]

To compensate for the low reactivity of the char gasification stage in the heterogeneous CLC process, an alternative called the chemical looping with oxygen uncoupling (CLOU) has been proposed by Lyngfelt et al.[36]. The process relies on an OC that releases gaseous oxygen in the fuel reactor as schematically seen in Figure 9. This allows the fuel to burn with gas-phase oxygen, and avoiding the need for a slow gasification of the char. During the CLOU process the following reactions take place in the FR:

$$2\,Me_xO_y \leftrightarrow 2\,Me_xO_{y-1} + O_2 \quad (10)$$

$$biomass \rightarrow volatiles + char + H_2O \quad (11)$$

$$char\ (mainly\ C) + O_2 \rightarrow CO_2 \quad (12)$$

$$Volatiles + O_2 \rightarrow CO_2 + H_2O \quad (13)$$

First, during reaction (7) and (8), the OC releases the oxygen, and the fuel (biomass) begins devolatilization producing a porous solid (char) and gas product (volatiles). After that the volatiles and the char is burnt like a usual combustion, as seen in reaction (9) and (10). While designing a CLOU system, the relations between the different reactions are important to consider. If the oxygen release rate from the OC is much higher than the combustion rate of the fuel an almost equilibrium of the O_2 concentration in the reactor will be reached. This will result in a presence of oxygen in the flue gas of the fuel reactor, leading to a less pure CO_2 stream and possibly not fulfilling requirements for compression and sequestration of the flue gas. On the other hand, if the combustion of fuel is much faster than the OC combustion rate, the O_2 concentration inside the fuel reactor will be close to zero. The CLOU process likely implies that significantly less bed material is required in the system, leading to a reduction in reactor size and associated costs. Depending on OC system, always mixture of Het-CLC and CLOU occurs during operation of the process. An in-depth analysis of the processes described above can be found in a study by Adanez et al. [33]

2.4 Chemical looping combustion plants

Alongside the OC, an effectively designed reactor system, is crucial for the CLC process. CLC plants are almost exclusively built with a fluidised bed setup, there are some applications with a fixed bed, but they have some major disadvantages (e.g. lower heat distribution, worse reaction kinetics) compared to a fluidised bed. The reactor design depends mainly on the fuel type that is used. For a reactor that is operated with solid fuels (coal, woodchips, pellets), the formation and removal of ash, as well as the gasification of the fuel, has to be considered in the reactor design. Larger CLC plants are often realized with a dual fluidised bed (DFB) system [37]. Existing pilot plant vary in their size and thermal input. Ranging from a 100 kW_{th} reactor situated at Chalmers University of Technology, to a 3 MW_{th} facility build by Alstom in Connecticut, USA [38]. At TU Darmstadt a 1 MW_{th} reactor is in regular operations [39]. The currently largest CLC plant stands in the city of Chengdu in China. The plant, as of now, is still in the testing phase, but should be able to reach thermal input of up to 4 MW_{th} [40].

A dual fluidised bed (DFB) system is one of the most effective configurations for chemical looping combustion, particularly when dealing with solid fuels. Figure 6 illustrates a schematic representation of the DFB CLC reactor, designed specifically for methane as a fuel. The system consists of two interconnected reactors: a larger air reactor (AR) and a smaller fuel reactor (FR). The OC circulates between these two reactors, enabling continuous oxidation and reduction cycles. The loop seals (lower and upper loop seals) ensure that no gas crossflow occurs between the air reactor and the fuel reactor, which is crucial for maintaining process efficiency. Additionally, cyclones are integrated within both reactors to facilitate the separation and collection of the oxygen carrier particles. The green arrows in the diagram depict the continuous circulation of the oxygen carrier throughout the system, emphasizing the importance of its movement for sustained operation. [41]

A more specific example of a CLC pilot plant is depicted in Figure 7, which shows the 80 kWth DFB pilot plant at TU Wien. This facility is specifically designed for solid fuel combustion and fluidised-bed steam gasification. One of the distinguishing features of this plant is the innovative fuel reactor (FR) design, which is divided into two sections. The lower section operates as a bubbling fluidised bed, characterized by a high solids inventory that enhances the interaction between the fuel particles and the oxygen carrier. Meanwhile, the upper section functions as a counter-current column, facilitating extended gas-solid contact and improving the efficiency of gasification. The reactor internals are strategically positioned along the height of the column to minimize the free cross-sectional area, which ensures longer solid residence times and enhances char gasification. Additionally, steam is used as a fluidisation agent in the fuel reactor, further accelerating the gasification process by enhancing the reaction kinetics. The fuel is introduced into the lower part of the FR via a screw conveyor, which ensures a direct and controlled feed into the bed. This design innovation improves the overall performance of the CLC system, making it more suitable for biomass and coal-based applications. [37]

Overall, the fluidised bed remains the key technological component of modern CLC reactors, as it provides optimal conditions for solid fuel conversion, oxygen carrier circulation, and gas-solid interactions. The continuous advancements in reactor design, such as those demonstrated in the TU Wien pilot plant, play a significant role in increasing the efficiency and scalability of CLC technology for future large-scale applications. [42]

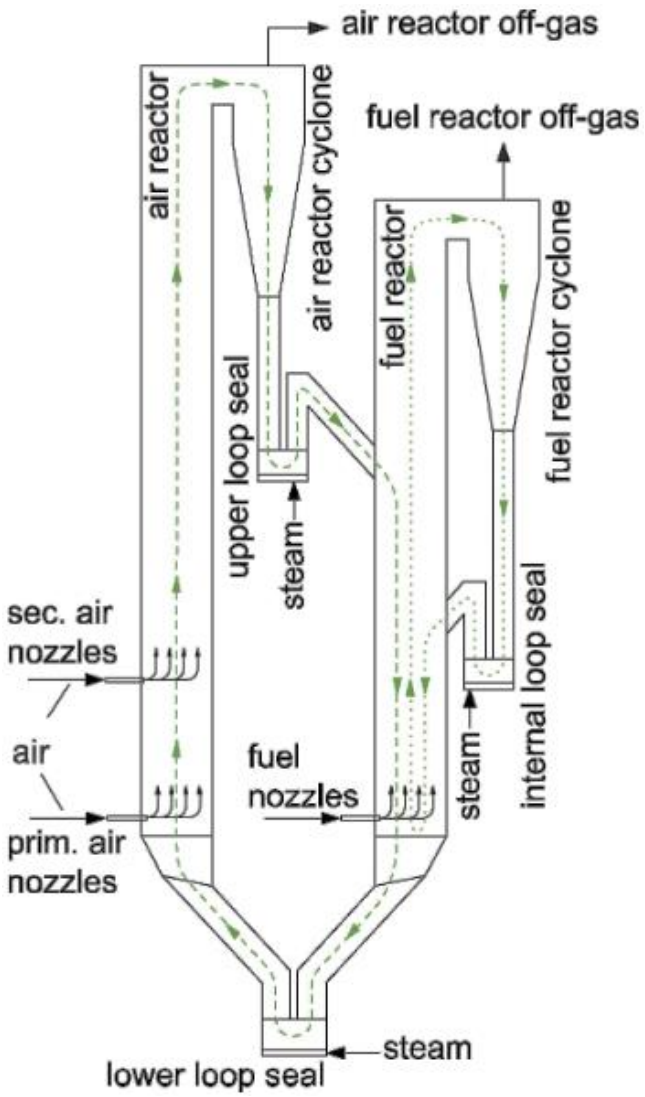

Figure 6: Scheme of a DFB pilot plant [41] [42]

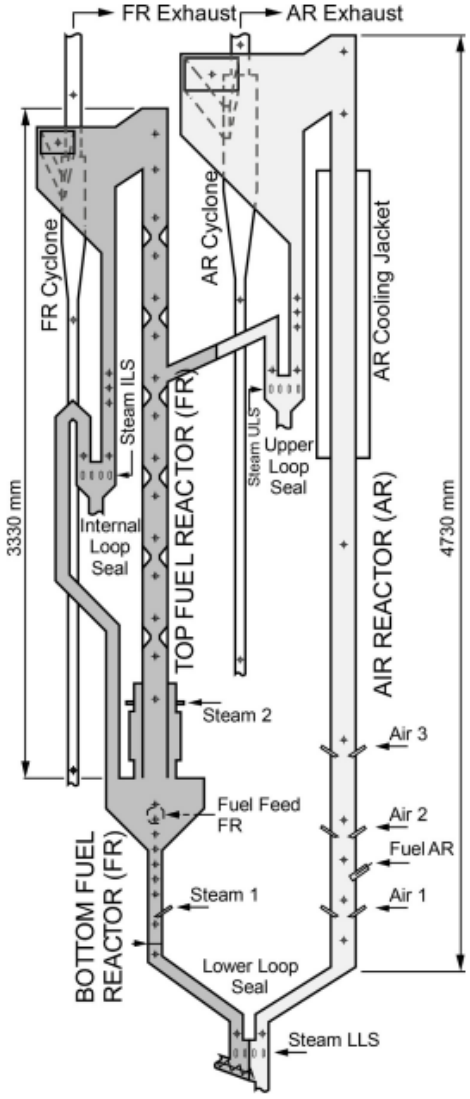

Figure 7: 80 kW_{th} CLC pilot plant at TU Wien

2.5 Fluidised bed technology

The fluidised bed technology is one of the most important technologies in solids process engineering [43]. When solid particles, in a defined and contained volume, are supported and allowed to move relative to each other as a result of vertical motion of a fluid (gas or liquid), fluidisation is achieved. The fluid, most commonly a gas, blows upwards through a perforated flat plate or a sequence of nozzles. Once enough particles have been actuated in this way, it is called a fluidised bed [44]. Flow patterns in the fluidised bed vary relatively to fluidisation velocity (U) as seen in Figure 8.

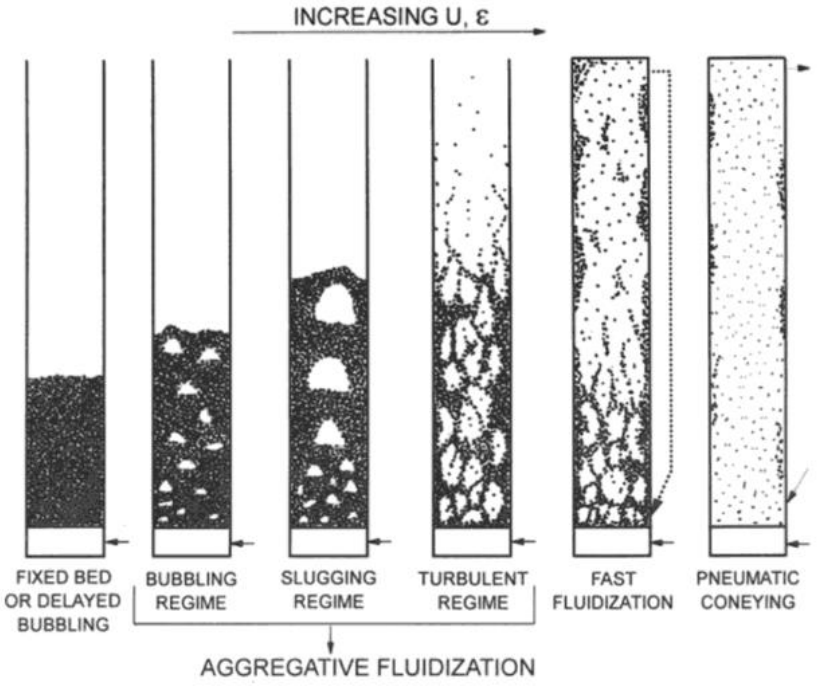

Figure 8: Flow patterns in fluidised beds (adapted from [45])

If the fluid velocity (gas or liquid) is kept low, a fixed bed is formed. The solid particles have a fixed position and do not move. If this speed is gradually increased, a point is reached at which the fixed bed begins to expand, and the particles start to move. The so-called minimum fluidisation velocity has been reached. With the continuous increase of the fluid velocity, the bed expands further, and the fluidised bed is reached. At this point, two different flow structures can occur. When using liquid fluidisation, a homogenous fluidised bed, where the particles are evenly distributed throughout, sets in. When using gaseous fluidisation, a bubbling fluidised bed arises. Fluidised beds can be maintained over a wide velocity range. If the velocity is increased further, a velocity is eventually reached at which particles can be discharged from the container. This point is called the terminal velocity and marks the upper ceiling for the fluidised bed. Velocities beyond this point are called pneumatic transport/conveying. [46]

The transition between a fixed bed and fluidised bed is best explained when looking at a pressure/velocity diagram, as it is shown in Figure 9. The so-called superficial velocity (U) is usually used as the velocity here, i.e., the empty pipe is used as the reference value for the velocity specification.

$$U = \frac{\dot{V}}{A} \tag{14}$$

The superficial velocity gets calculated using the gas volume flow ($\dot{V}$) and the cross-sectional area (A) of the pipe, according to Equation 3.

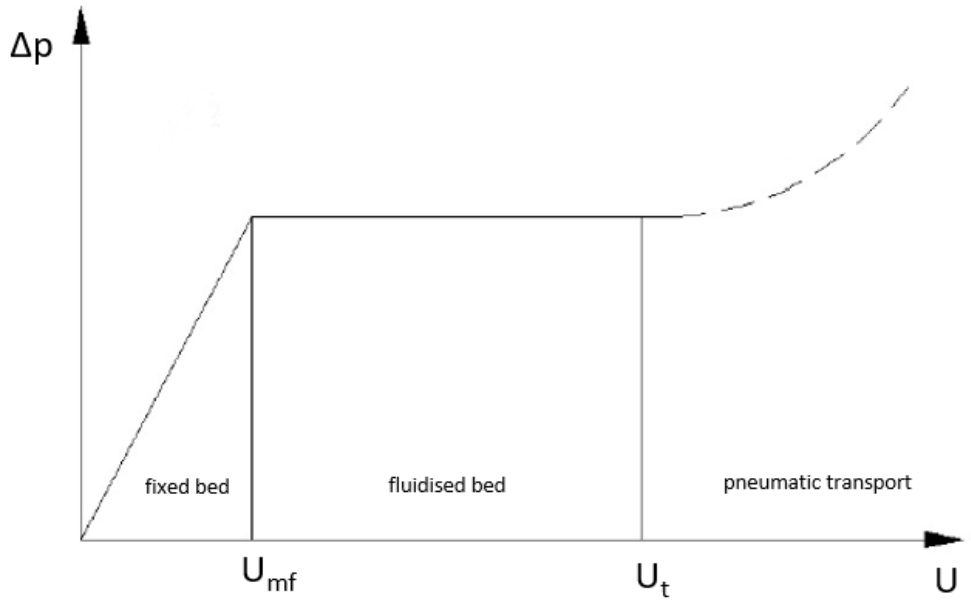

Figure 9: Pressure/velocity diagram for fluidised beds (adapted from [46])

Looking at a container, in which there are solid particles resting on a porous base, and introducing a fluid from below, first a fixed bed can be observed, as already explained above. In the area of the fixed bed, the pressure loss increases with increasing fluid velocity, as shown in Figure 4. Depending on the Reynolds number (will be explained in-depth in chapter 2.5.2), this can be a linear or a quadratic progression. After exceeding the minimum fluidisation velocity (U_{mf}), the difference of the pressure loss no longer changes but remains constant in the area of the fluidised bed. Once the floating velocity (U_t) is exceeded, the particles are discharged, and the fluidised bed is emptied. If the discharged particles are fed back into the fluidised bed, the pressure loss increases slightly. [46]

The two properties that have the most influence over the fluidised bed are the bed material and the fluidisation. Both are discussed in further detail in the next section.

2.5.1 Bulk material

The bulk material properties of the fluidised bed are influential factors for the operation. The behaviour of the particles under an inflowing gas changes depending on the structure, density, and surface. In order to define particle properties, the cluster of particles is considered, as the individual particles sometimes differ greatly in shape and size. The most important characteristic values for aggregates are the average diameter of individual particles, the particle density, the bulk density, as well as the porosity and the shape factor. [47]

As with most technically interesting solids, their particle shapes differ from that of a sphere. Therefore, in order to determine the size of the particles, an equivalent diameter must be formed. There are a variety of definitions of this diameter, of which the four most important are listed in Table 2. For the determination of the diameters, often a sieve analysis is utilised.

Table 2: Most important equivalent diameter: sieve diameter, volumetric diameter, surface area diameter, Sauter mean diameter [46]

Description	*Symbol*	*Explanation*	*Calculation*
Sieve diameter	d_p	Sieve width at which particles fall through	$d_p = \frac{d_i + d_{i+1}}{2}$
Volumetric diameter	d_v	Diameter for a sphere with the same volume as the particles	$d_v = \sqrt[3]{\frac{6\,V_P}{\pi}}$
Surface area diameter	d_s	Diameter for a sphere with the same surface area as the particle	$d_s = \sqrt{\frac{S_P}{\pi}}$
Surface/volumetric diameter	d_{sv}	Diameter of the sphere with the same surface area/volume ratio as the particle.	$d_{sv} = \frac{6V_P}{S_P}$

The so-called Sauter mean diameter (d_{sv}) is particularly interesting for the fluidised bed technology. The particle shape can be considered spherical or nearly spherical. Depending on that the Sauter mean diameter (SMD) can be assumed as follows:

$$\text{spherical: } d_{sv} \approx d_p \tag{15}$$

$$\text{nearly spherical: } d_{sv} \approx d_p * \psi \tag{16}$$

For spherical particles the SMD is approximately equal to the sieve diameter (d_p). For nearly spherical

particles a shape factor (ψ) has to be considered. The shape factor indicates the similarity of the particle to a sphere and assumes values between zero and one. A value of one indicates a perfect spherical shape.

$$\psi = \frac{{d_v}^2}{{d_s}^2} \tag{17}$$

A frequently used classification of the bulk material for fluidised bed technology are the Geldart classes. The particle diameter and the density difference between fluid and particle are used as criteria. According to Geldart the bulk materials can be divided into four different classes, as seen in Figure 10.

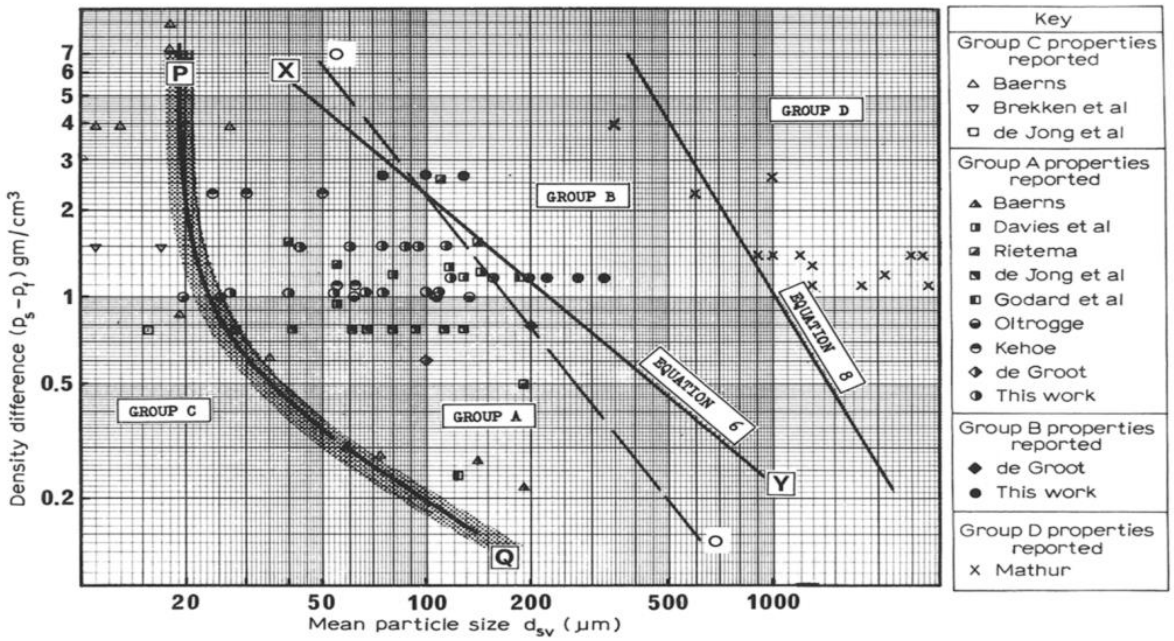

Figure 10: Geldart diagram (adapted from [48])

Group C: This group includes any powers that are cohesive in some form. Fluidisation of these materials is extremely difficult as they tend to form plugs or channels, because their high interparticle forces are greater than those that the fluid can exert on the individual particle. This Group is not very important for practical applications.

Group A: This category contains all bulk materials that have a small mean particle size and/or a low particle density. Categorical for this group is a homogeneous expansion when the minimal fluidisation point (U_{mf}) is exceeded. This is because they are still slightly cohesive. These materials are very suitable for highly expanded, circulating fluidised beds and are also easy to convey pneumatically.

Group B: In contrast to group A, in this category, interparticle forces are negligible. Bubbling formation starts as soon as the minimal fluidisation point (U_{mf}) is exceeded. The dominant phenomenon is the formation of bubbles, which cause good mixing of the solids. This group has the greatest practical significance in fluidised bed technology.

Group D: This group consists of bulk materials with high density and/or high mean particle size. Due to these properties, fluidisation of these particles is more difficult, but there are practical applications in the food industry. [46, 48]

2.5.2 Fluidisation diagrams

Dimensionless diagrams are usually used to visualise the existence of the fixed bed, fluidised bed and pneumatic conveying (solids discharge). Similarity variables (dimensionless key figures) that describe the flow behaviour are used for this purpose. Important diagrams used for fluidisation technology are the Reh-diagram and the Grace-diagram. The transitions between the different operating fields do not have sharp boundaries but are fluid. For this reason, an operating point should not be set or located too close to a boundary. As both the Grace-Diagram (Figure 11) and the Reh-diagram (Figure 12) were used during this work, they will be explained in further detail. [46]

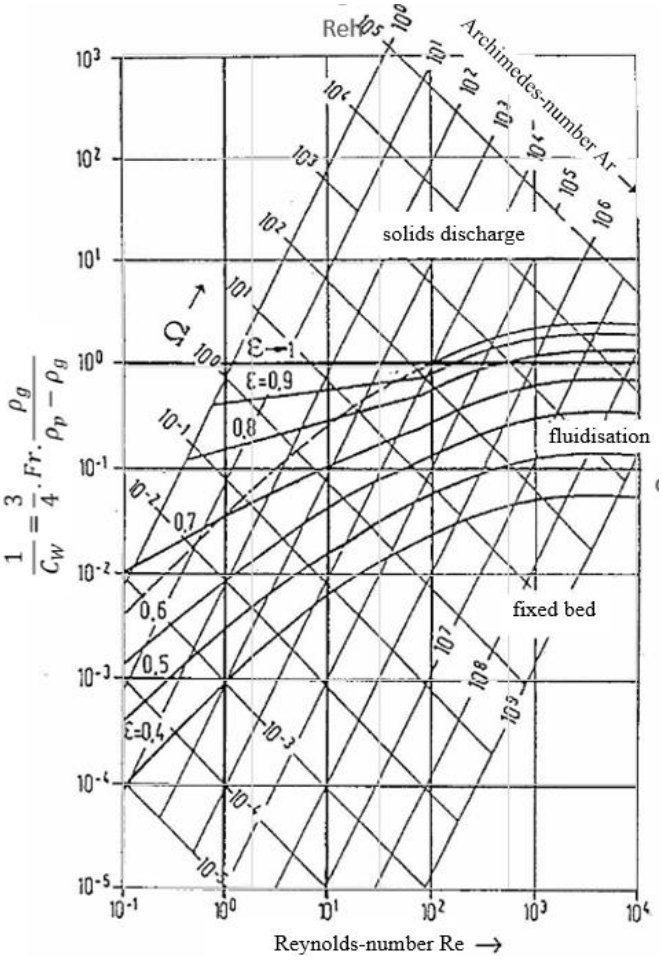

Figure 11: Reh-diagram, adapted from [47]

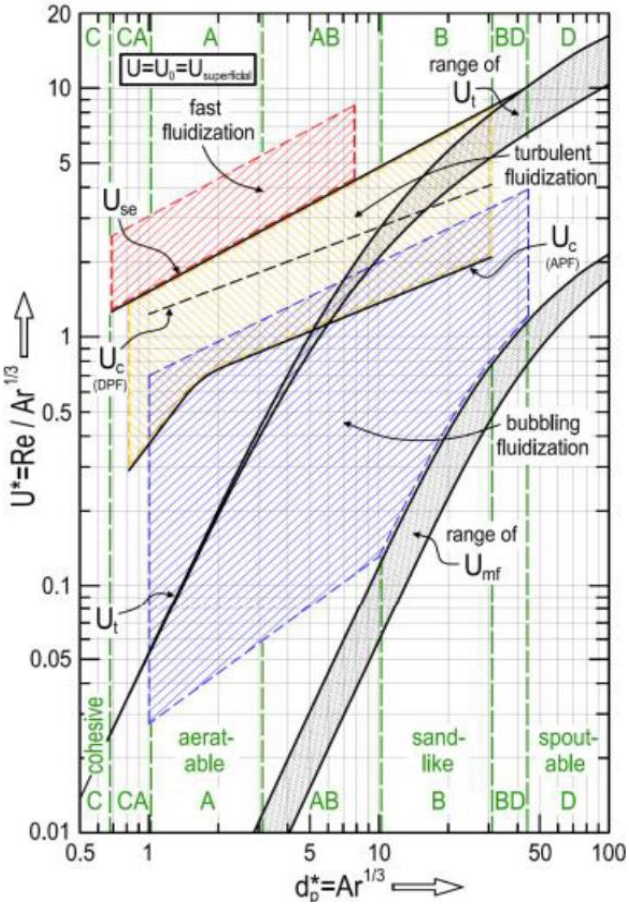

Figure 12: Grace Diagram, adapted from [49]

The formation of the fluidised bed depends on the flow velocity of the gas, the diameter and shape of the bed material as well as the density and viscosity of the gas. Those variables are defined in the dimensionless key figures, like the Froud-number (*Fr*), Archimedes-number (*Ar*), and the Reynolds-number (*Re*), which are all very significant figures for the fluidisation technology. For the Reh-diagram the Re as well as a modified version of the Fr are used:

$$Fr = \sqrt{\frac{inertial\ force}{particle\ weight}} = \frac{U^2}{d_p * g} \tag{18}$$

$$Re = \frac{inertial\ force}{viscous\ force} = \frac{U * d_p * \rho_g}{\mu} \tag{19}$$

The gas velocity required to set a specific regime, and the width of the operating range can now be estimated. The calculation requires the use of the relative velocity between the fluid and the particle. This velocity usually varies strongly between the reactor walls and the reactor core. This is a disadvantage in the usage of the Reh-diagram compared to the Grace-diagram. [46]

The Grace diagram uses the dimensionless particle size (d_p^*) and dimensionless velocity (U^*) resulting from the Archimedes number and the Reynolds number. Since the Grace diagram relies on superficial velocity, it is easier to use. The *Ar* can be calculated using the following formulas.

$$Ar = \left(\frac{sinking\ force}{viscous\ force}\right)^2 = \frac{(\rho_p - \rho_g) * \rho_g * d_p^3 * g}{\mu^2} \tag{20}$$

The definitions of the Reynolds and Archimedes are similar; they both describe a ratio between the encouraging and resisting force. However, the *Ar* is defined as the ratio between sinking force and viscous force, while the Re is defined as a ratio between inertial force and viscous force [50]. To use the Grace diagram, the dimensionless particle size (d_p^*) and velocity (U^*) have to be calculated, using the Archimedes - and Reynolds – number:

$$d_p^* = Ar^{\frac{1}{3}} \tag{21}$$

$$U^* = \frac{Re}{Ar^{\frac{1}{3}}} \tag{22}$$

The dimensionless variables are designed in such a way that working with the Grace diagram is quick and easy. As you can see the Geldart classes are also drawn into the Gace diagram, as well as different fluidisation regimes (bubbling, fast, turbulent fluidisation). A major advantage of the Grace diagram over the Reh diagram is that for the calculation, only the superficial velocity is needed. The superficial velocity, as mentioned before, is calculated simply using the fluid volume flow and the reactor inflow area. [46]

2.6 Carbon capture and storage vs. Carbon capture and utilisation

When evaluating carbon removal technologies, a crucial consideration is the utilisation of the captured CO_2. A large amount of research is being conducted on this subject. Although it is not the focus of this work, in this chapter a brief overview of the utilisation will be given.

There are mainly two options for the usage of captured CO_2. The first option are all methods that can be summarized as carbon capture and usage (CCU) technologies, for which the captured CO_2 is used in the production of chemicals or energy products. The second option is the carbon capture and storage (CCS) technology, which focuses around storing the CO_2. Both options only differ in the way the captured CO_2 is used, the capturing method of the CO_2 is irrelevant for the distinguishing.

2.6.1 Carbon Capture and Usage (CCU)

CO_2 already has a wide array of applications in several different industry sectors. Among many other employments it is used in the chemical industry to control reactor temperatures, liquid CO_2 is used for product transportation at low temperatures (-78 °C) in the pharmaceuticals industry, or as carbonation for beverages in the food industry [51]. Another important application of CCU, addressing both energy demands and carbon reduction, involves the conversion of captured CO_2 into fuels. There is a lot of recent research being conducted on this subject. Power-to-gas technologies, such as electrolysis, harness renewable energy to transform CO_2 into synthetic fuels like methane or methanol (e-fuels). These eco-friendly fuels offer a cleaner alternative to traditional fossil fuels and can be used across different sectors, including transportation and industry. The captured CO_2 can also be used as a primary product for manufacturing goods like carbon nanotubes, carbon fibre or graphene. These materials are required in various industries such as construction, aerospace or electronics. They offer a more sustainable alternative to the traditional manufacturing process. [52]

CCU offers several key advantages over CCS. Although storage capacity for CCS is currently abundant, it is a finite resource and could diminish rapidly as the technology scales up. Additionally, a pressing concern is that storage sites are often located far from CO_2 sources, necessitating extensive transportation infrastructure. This not only increases energy demands and costs but also raises the risk of CO_2 leakage. In contrast, CCU avoids these spatial constraints, as synthetic fuel production can occur directly at the carbon capture site [53]. CCU, when converting captured CO_2 into fuels while using electricity from renewable energy, is advocated as a climate change mitigation strategy that can avoid significant emissions of CO_2 from vehicles and other sources. However, a case study of methanol production shows the mitigation costs for CCU are much higher than for a CCS-based system delivering the same fuel product. The dominant contributor to the cost of CCU is the cost of the carbon-free electricity [54]. Moreover, CCU technologies cannot achieve negative emissions, meaning they are unable to actively decrease the concentration of CO_2 in the atmosphere.

2.6.2 Carbon Capture and Storage (CCS)

The carbon capture and storage technologies are widely discussed but also controversial methods. They are regarded as a key instrument in meeting climate change targets and facilitating a transition to a carbon-free industry. Besides storage, the transportation of the captured CO_2 are the two critical challenges for CCS technologies. After being captured, the CO2 gets dried and pressurised to a liquid state to maximise transportation rates and minimise corrosion [55]. The transportation is carried out via pipelines to onshore or offshore storage sites, where it gets injected into rock formations. Figure 13 shows different options for CO_2 storage sites. The Figure illustrates methods of CO_2 storage, including injection into depleted oil and gas fields (1), deep saline formations both offshore (3a) and onshore (3b), and mineralization (4). CO_2 can also be used for enhanced oil and gas recovery (2), where it is injected to increase production while some of it remains trapped underground.

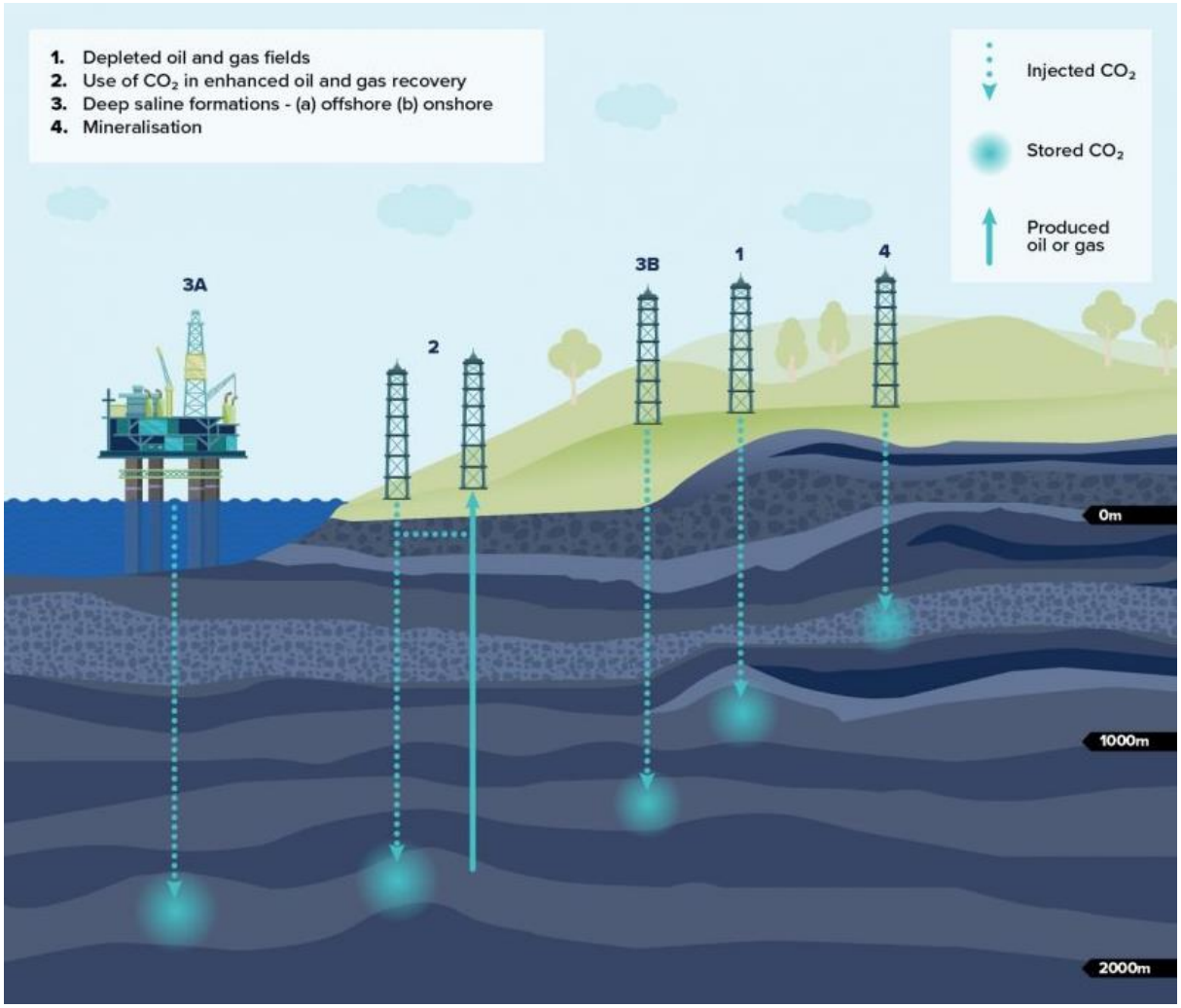

Figure 13: CCS, schematic image for different options of injecting and storing CO_2 (adapted from [56])

CO_2 can be stored using two main methods: deep geological storage and mineral storage. Deep ocean storage is another option, but it raises concerns about ocean acidification. Geological formations, such as those in the North Sea and the US Gulf Coast, are considered the most promising storage sites due to

their vast capacity. According to the IPCC, well-selected and well-managed geological storage sites can retain over 99% of injected CO_2 for thousands of years. [57]

Geo-sequestration involves injecting CO_2 in a supercritical state into sedimentary rock formations, including depleted oil and gas fields, saline aquifers, and unmineable coal seams. These formations are secured by impermeable caprocks and geochemical trapping mechanisms. CO_2-enhanced oil recovery (EOR) utilises CO_2 injection to increase oil production, but the subsequent burning of the extracted oil offsets much of the CO_2 reduction. Similarly, unmineable coal seams can absorb CO_2, releasing CH_4 that can be recovered and sold, though burning it also produces CO_2. [57]

Saline aquifers, which contain highly concentrated brine, offer significant storage potential due to their abundance. However, they are less studied than oil fields and do not provide economic byproducts. Mineral storage, or mineral carbonation, involves reacting CO_2 with iron, magnesium, or calcium-based minerals to form stable carbonates. While this method prevents CO_2 re-release, the natural reaction process is slow and requires substantial energy to accelerate, making it costly. The IPCC estimates that power plants using mineral storage could require 60–180% more energy than those without CCS. Despite these challenges, geological and mineral storage remain key options for long-term CO_2 sequestration. [57]

CO_2 injection into the subsurface has been used since the 1970s for (EOR) to increase the production of oil. Therefore the CO_2 storage and pipeline technology is well established [58]. The geological storage of anthropogenic CO_2 was first proposed in the same decade, but only gained traction after research in the early 1990s [14]. The technology is widely regarded as a necessary tool for climate mitigation; however, storing and transporting large amounts of CO2 has raised many issues for environmental organizations like Greenpeace, which argue that CCS could be used by big oil companies as a pretext to delay the phase-out of fossil fuel production [59]. With the concern of leakage of CO_2 during the transport, recent studies have shown that the likelihood of having a significant (potentially lethal) release of CO_2 from pipeline failure is likely in the range of 10^{-6} to 10^{-7}. These probability values as a proxy for individual risks are considered in the acceptable to negligible range. [60, 61]

When comparing CCU and CCS, both options have their advantages and disadvantages. Although CCU is a carbon-neutral alternative for the industrial usage of CO2, its high energy penalty and reliance on inexpensive carbon-free electricity are drawbacks that need to be considered. While there are still concerns about CCS, mainly with regards to the potential risk of storing CO_2, its potential to generate negative emissions presents a great asset for the fight against climate change.

3 Applied principles and methods

This chapter provides an overview of the reactor setup used for the experiments in this thesis. Furthermore, it describes the scientific principles and methods that the characterisation and long-term tests of the OC are based upon. Lastly, it explains important key figures and equations for the evaluation of the experimental results.

3.1 Experimental setup

The experimental setup consists of two major parts, the batch reactor, and the measuring setup. Both are described in more detail below.

3.1.1 Overview of the batch reactor

For the execution of the experiments a batch reactor, built in 2018 at TU Wien for OC screening and characterisation, was used. As shown in Figure 14, the batch reactor only consists of a single reactor, which functions both as AR and FR. During the experiment, the reactor simulates the oxidation process and reduction process by changing the fluidisation of the bed.

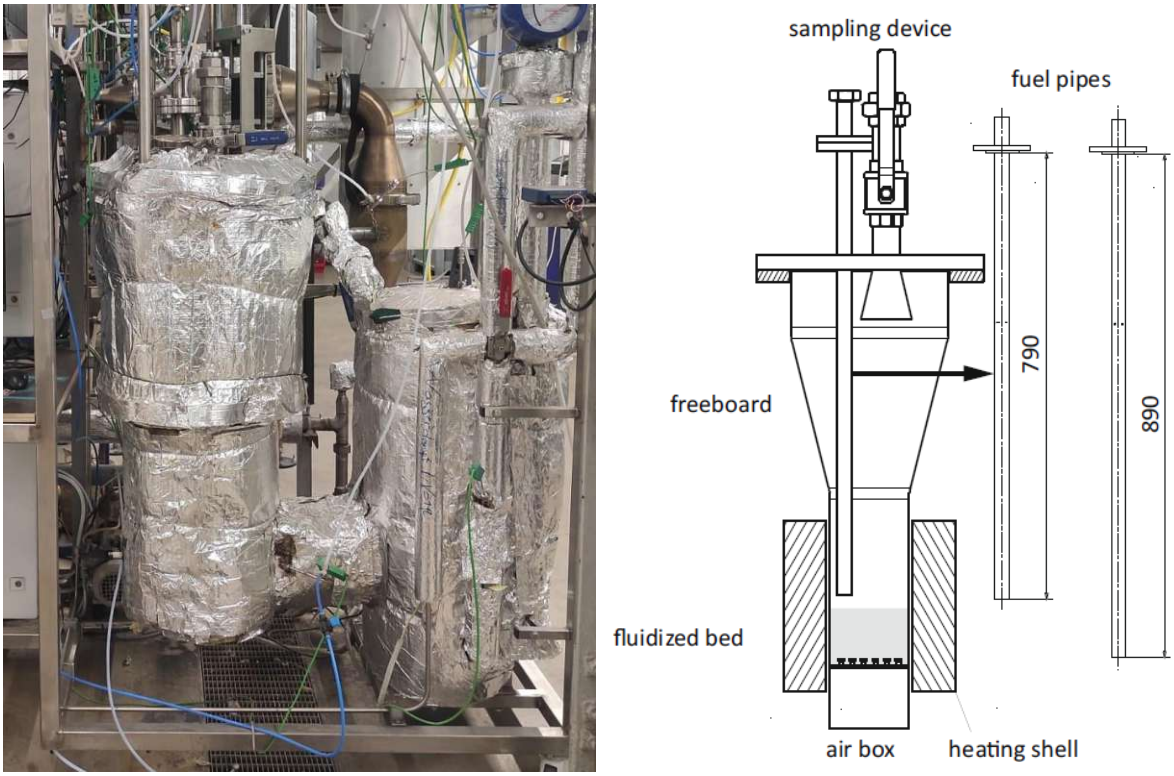

Figure 14: Left: picture of the batch reactor setup used for the experiment; right: schematic layout of the reactor with sampling device, different fuel pipes and heating shell (adapted from [62])

On the left side of Figure 14 you can see the batch reactor wrapped in aluminium foil for better insulation. Under the foil the reactor is encased with another layer of insulation material as well as a heating shell to keep the reactors bed temperature level during the experiments. On the right there is a gas preheater that heats up the air and respectively the steam gas before it flows into the batch reactor,

so the fluidisation does not cool down the reaction temperature.

Figure 15 displays a configuration plan of the batch reactor, for better understanding of the reactor setup. Air or steam flow through a 4-way ball valve (6) into the gas preheater (4). Wrapped around the preheater is a heating shell (3). After the gas passes through the preheater and gets heated up, it reaches the airbox. Inside the airbox the gas streams through small nozzles into the reactor (1) facilitating the fluidisation of the bed material. The reactor is also wrapped in a heating shell (2) to ensure a stable bed temperature. There a two different ways fuel can get introduced into the reactor. Gaseous fuel (e.g., CH_4) reaches the reactor, the same as the fluidisation gases, through the airbox. Because for the experiments in this thesis, only solid fuels were used, this won't be explained in detail. The solid fuels get into the reactor through the reactor lid. It is possible to use a screw conveyor to automatically feed in the solid fuels, though in the experiments in this thesis the solid fuels were manually put into the reactor. After the combustion, the exhaust gas flows out of the reactor and gets filtered and cleaned through a catalyst (5).

The reactor mode can be changed from AR to FR by turning the 4-way ball valve. During FR-operation steam flows into the reactor, pushing out the air and creating an oxygen-free atmosphere inside the reactor. Now the only oxygen left inside the reactor is tied up into the OC. By now, adding the fuel into the reactor, the oxygen inside the OC reacts with the wood pellets and creates the combustion. After the fuel is used up the 4-way ball valve gets turned and the reactor gets put into AR-operation again. At this time air is again flowing inside the reactor and the OC gets charged with oxygen again. This process describes one cycle of the batch reactor process, which will later be explained in further detail.

The reactor gets controlled with a PC and the software LabVIEW®, which also records all the data collected during the experiments. Further information about the design, construction and installation of the batch reactor can be found at Parzer (2018) [63].

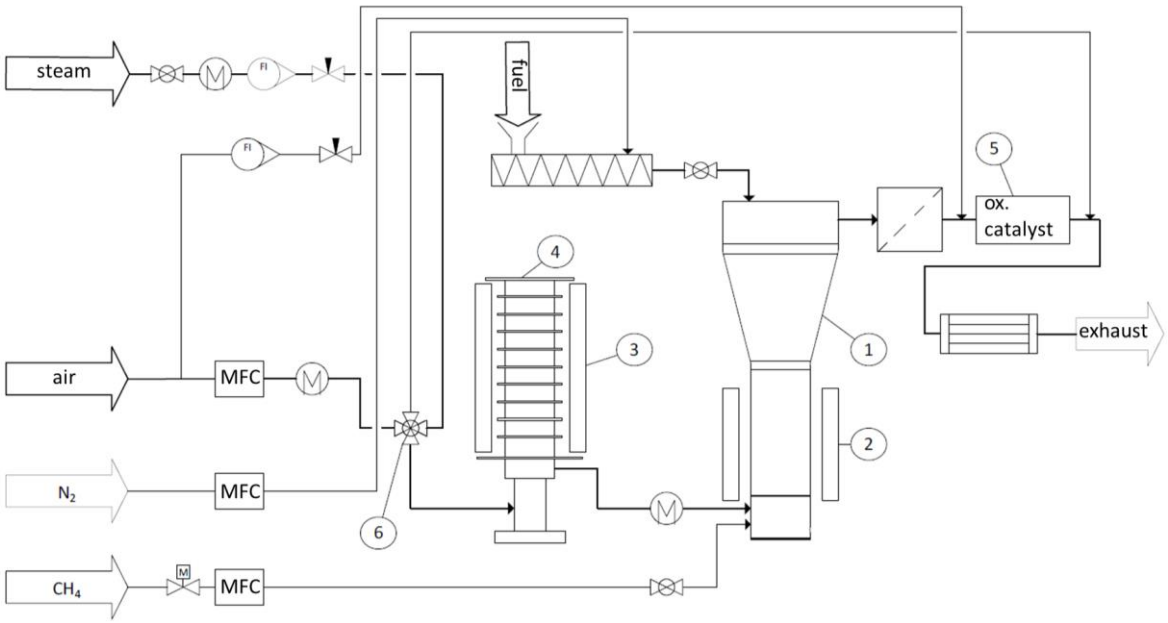

Figure 15: Batch reactor configuration plan; schematic representation of the gas flows and most important components of the batch reactor (adapted from [63])

3.1.2 Measuring equipment

To analyse the exhaust gas composition from the batch reactor a measurement setup, as shown in Figure 16, was devised. The bypass is connected to the exhaust outlet of the reactor via a ball valve. When opened, a pump draws the exhaust gas through the ball valve into the measuring setup. To cool the exhaust gas down and separate the water of the gas first enters a condenser. Following the condenser, the exhaust gas gets drawn into two scrubbers, one filled with rapeseed methyl ester to separate out any tars or higher hydrocarbons and the other, cooled and empty, is used to remove any residual water by condensation. A cryostat provides the cooling for the condenser and the scrubbers. The pump's performance is regulated by a downstream buoyancy flow meter. After the dust filter and water trap the gas is analyse in a gas-gauge. The 5-component gas analyser "NGA 2000" from Rosemount® is used in this measuring setup. It measures the concentration of H_2, CH_4, CO_2, CO, and O_2 in the exhaust stream. The collected data is transferred to a computer and is displayed and recorded using LabVIEW®.

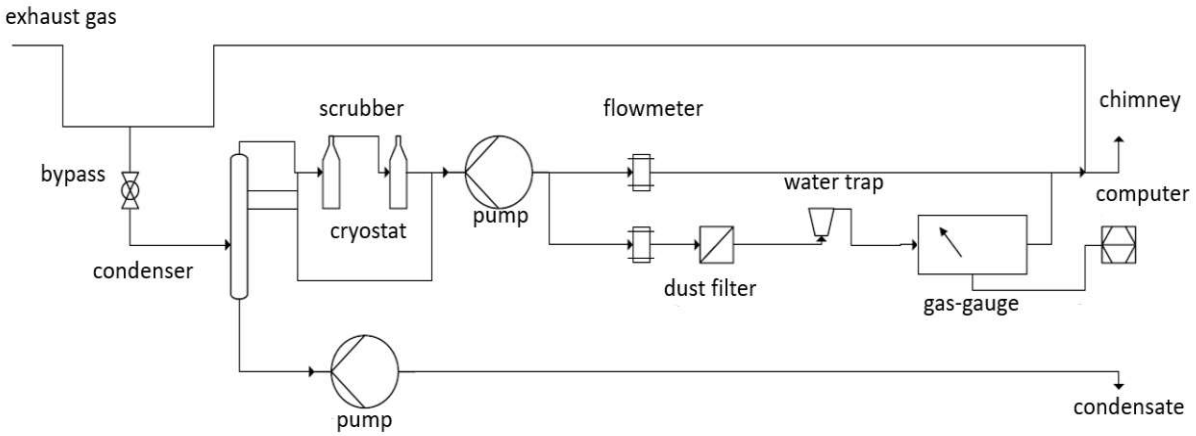

Figure 16: Configuration of the gas measuring and cleaning setup; schematic display of the most important components (adapted from [9])

3.2 Oxygen carriers and fuel composition

Six different oxygen carriers were tested during this master's thesis. In this chapter, the individual OCs are presented in more detail. The properties of the fuel used are also briefly listed.

Table 3 lists the composition of the OCs, how they were manufactured and whether they show CLOU behaviour. Some catalysts offer the advantage of CLOU ability, a well-documented phenomenon observed in certain compounds containing manganese or copper. This unique capability enables the material to release oxygen without directly reacting with the fuel. It relies on the instability of metal oxide at specific temperatures and oxygen partial pressures. [64]

Table 3: Oxygen carrier details: composition, production method, and CLOU abilities [41]; [65]

Oxygen carrier	*Composition*	*Production method*	*CLOU*
MIT	Mn_2O_3, Fe_2O_3, TiO_2	Spray drying	Yes
MIC	Mn_2O_3, Fe_2O_3, CuO	Spray drying	Yes
IB	ilmenite, braunite	Spray drying	No
C14/C28	perovskite	Spray drying	Yes
Vito A+B	NiO, Al_2O_4	Spray drying	Yes
Fe17	Fe_2O_3, AL_2O_3	Impregnation	No

As can be seen, all oxygen carriers except Fe17 are produced using spray drying, while Fe17 is produced by impregnation [34]. The Table shows that the names of the OCs are derived from the elemental compositions. MIT is made of manganese- iron- and titanium- oxide, whereas MIC is made of manganese- iron- and copper- oxide. The OC IB consists of the two natural ores ilmenite and braunite. Ilmenite consists of a mixture of iron oxide and titan oxide while braunite contains mostly manganese oxide. The exact elemental composition of IB can be found in Table 4. C14/C28 is a mixture of the two OCs C14 and C28, both are perovskites. A perovskite describes an oxide mineral, that commonly has the composition of $CaTiO_3$. In general, the perovskite structure can be simplified to ABO_3, where the cation on the A side is bigger than the cation on the B side. It is possible to replace parts of the A and B site cations to synthesize new multicomponent perovskites. The stochiometric composition for C14 is $CaMn_{0.9}Mg_{0.1}O_{3-\delta}$ and for C18 it is $CaMn_{0,775}Mg_{0.1}Ti_{0,125}O_{3-\delta}$ [64].

Vito A+B is a mixture of two nickel-based OCs. They both have a NiO content of 40 wt.%. The support material of OC-A is $NiAl_2O_4$, and a mixture of $NiAl_2O_4$ and $MgAl_2O_4$ for OC-B, respectively. For OC-B the ratio of the support material is 42% $NiAl_2O_4$ and 18% $MgAl_2O_4$. As the mixing ratio to create Vito A+B was 1:1 the final product contains 40% NiO, 51% $NiAl_2O_4$ and 9% $MgAl_2O_4$ [65] [66].

The Fe17 OC is produced by impregnating Fe_2O_3 on Al_2O_3. The active Fe_2O_3 content of the fresh material is 16.2 wt.%. The production and evaluation of this OC has been investigated in a study by Cabello et al. [67] Table 4 shows the detailed elemental composition of the OCs.

Table 4: Detailed elemental composition of the oxygen carriers in percentage

	MIT	*MIC*	*IB*	*C28*	*Vito A+B*	*Fe17*
Fe_2O_3	51	36	37,8	-	-	16,2
Mn_3O_4	34	33	28,3	41,8	-	-
TiO_2	15	-	26,1	12,5	-	-
Al_2O_3	-	-	-	-	-	83,8
NiO	-	-	-	-	40	-
$NiAl_2O_4$	-	-	-	-	51	-
$MgAl_2O_4$	-	-	-	-	9	-
CuO	-	31	1	-	-	-
CaO	-	-	1,9	35,7	-	-
MgO	-	-	1,5	10	-	-
SiO2	-	-	2,4	-	-	-
Rest	-	-	1	-	-	-

The fuel used during all experiments were wood pellets. For the characterisation test 10 g were used as established in earlier experiments. The fuel is a very high-quality fuel with a low water and ash content as well as a high calorific value. The data of the wood pellets are listed in Table 5 below.

Table 5: Composition of the wood pellets used as fuel

Value	*Wood pellets*	*Unit*
Water content	7,2	wt%
Ash content	0,2	wt%
Carbon content	50,7	wt%
Hydrogen content	5,9	wt%
Nitrogen content	0,2	wt%
Oxygen content	43	wt%
Content of volatiles	85,4	wt%
Heat value	20248	kJ/kg
Caloric value	18943	kJ/kg

3.3 Experimental plans

The goals of the experiments carried out in this thesis are to determine certain attributes of synthetic OC during a CLC process and to compare the performance of these synthetic OC. These test results are used to find out which process parameters are suitable for upscaling to the pilot plant.

First all six synthetic OC are characterized, and the most promising OC is further investigated during a long-term experiment. Both experimental plans are described below.

3.3.1 OC characterisation

The OC characterisation tests are conducted to identify the key attributes of the OC. Each OC undergoes the same test execution, in which 3 different process variables are tested. The process parameters are listed in the Table below.

Table 6: Process parameters during the characterisation test: OC to fuel ratio, fluidisation quantity of steam, bed temperature, fuel amount

Process parameter	*Unit*	*Explanation*
OC to fuel ratio	kg/kg	Theoretically available oxygen
Fluidisation quantity of steam	kg/h	Influences the mixing and formation of the fluidised bed
Bed temperature	°C	Has an influence on combustion and the release of oxygen from the OC
Fuel amount	kg	Influences the flue gas composition

Experiment execution

The experiment execution is divided into three different phases, the preparation, the execution, and the follow-up. During the preparation phase a preliminary examination of each OC takes place. Material values such as particle density, bulk density and particle diameter are determined. Those values are used to define the amount of OC and the fluidisation quantity of steam necessary for the process.

After the preparation is done the actual execution of the experiments can begin. For better understanding of the special mode of operation of the batch reactor, this step is now described in greater detail. The batch reactor, in contrast to a normal CLC plant, operates in two phases, the oxidation and the reduction phase. These phases substitute the AR and FR of a steady state CLC plant. During the oxidation phase the reactor gets filled with air and the OC is charged with oxygen atoms. This phase ends as shown in Figure 17 when the measured amount of oxygen is equal to the amount of oxygen in the air (~21%).

Now the 4-way ball valve is switched, and steam is flowing into the reactor. The reduction phase starts. The steam that flows into the reactor pushes out the air until an oxygen free atmosphere is reached. Now the only oxygen left in the reactor is bound to the OC. When at this moment the fuel is added, the OC reacts with the fuel and produces the exhaust gases as shown in Figure 17. After all the fuel is used up the exhaust gases reach 0 vol.% and the reduction phase ends. By now switching the 4-way ball valve, air is again flowing back into the reactor and the oxidation phase starts again. Those two phases together are called a cycle. During each phase samples of the OC can be extracted by lowering a basket into the reactor and removing a small amount of OC. Those samples are used to determine the oxidation state of the OC.

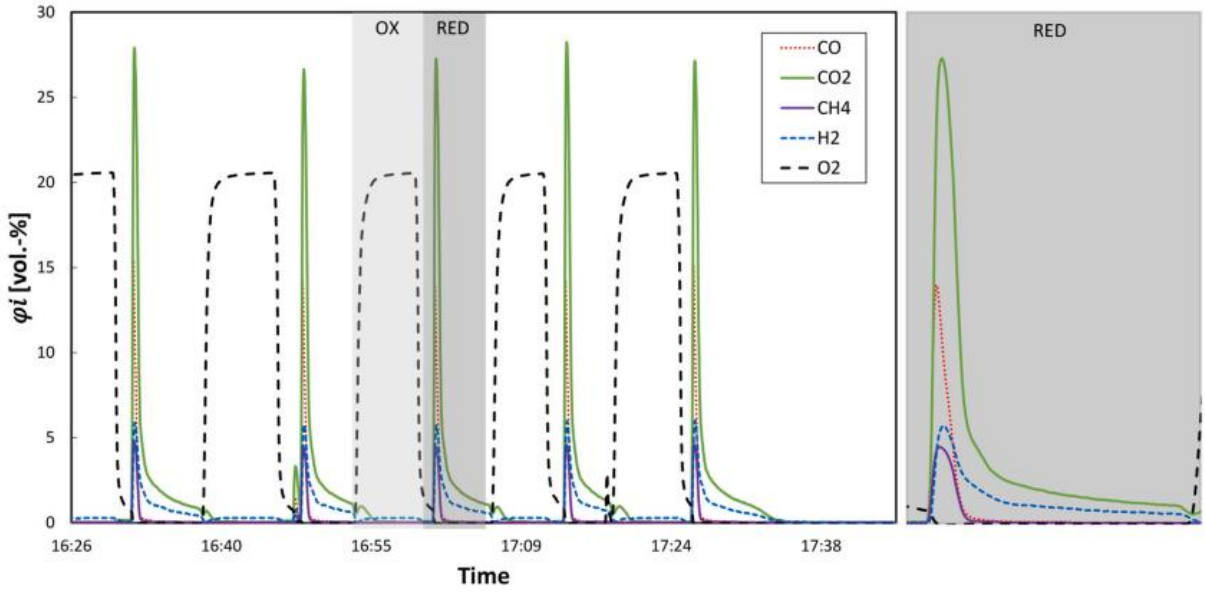

Figure 17: Oxidation and reduction phase shown as their exhaust gas streams (adapted from [30])

The execution process is divided into five different operating points, as listed in Table 7. You can see that for each operating point 3-5 cycles were performed, to reduce outliers and fluctuations. A solid sampling of the OC was extracted during the reduction and oxidation phase for the operating points Steam 1, Temp 2 and Temp 1. For the operating points Steam 2 and Fuel 1 the solid sample was only extracted during the reduction phase, since the oxidation state is independent of the amount of fuel and the amount of steam. After Steam 2 and Temp 1 the filter was drained to determine the attrition rate of the OC. The inventory and steam quantity are dependent on the OC and are set before the experiment. The fuel amount was set to 10 g for each cycle. During Fuel 1 double the amount of fuel was used. Exclusively wood pellets were used as fuel to reduce the impact of ash and fuel impurities on the experiment

For the first 3 operating points the bed temperature was set to 950 °C. During Temp 1 the temperature got lowered to 800 °C to identify the influence on the reaction. The different operating points are intended to illustrate the behaviour of the OC at different temperatures, steam quantities and fuel quantities. The last operating point Temp 2 had the same process parameters as the first operating point

Steam 2. Therefore, the initial and final process parameters were the same in order to investigate whether the behaviour of the bed material changes during all the cycles.

Table 7: Operating points of the characterisation test

Operating point	*Inventory in cm*	*Mass solid fuel in g*	*Temperature in °C.*	*Comments*
Steam 1	8,5	10	950	3-5 cycles, solid sample Red and Ox
Steam 2	8,5	10	950	3-5 cycles, solid sample Red, filter drain
Fuel 1	8,5	20	950	3-5 cycles, solid sample Red
Temp 1	8,5	10	800	3-5 cycles, solid sample Red, filter drain
Temp 2	8,5	10	950	3-5 cycles, solid sample Red and Ox

These five operating points together describe one characterisation experiment. The characterisations have been carried out for each OC and are further explained in chapter 3.4.

The follow-up takes place after the experiment. The remaining OC material gets cleaned out of the reactor, weighed, and again goes through a sieve analysis. The solid samplings taken during the experiment were divided into crucibles and weighed using a precision balance. They were then oxidized in the furnace for 24 h at 950 °C and then weighed again. At 950 °C, it was assumed that the OC was completely oxidized. The weight difference between before and after provides information on how much oxygen the OC can absorb. For evaluation purposes all collected data during the preparation, execution and follow-up were put into an excel sheet.

3.3.2 Long-term experimental plan

During the long-term experiment, the best-performing OC was tested in the batch reactor for 200 cycles. This test is primarily intended to examine the durability of the OC and the influence of ashes during the process. The cycles were run in the same way as the characterisation test, just the oxidization time was determined to 2 min per cycle. The ashes were added to the reactor after 100 cycles. A solid sampling was extracted after the first five cycles and after that ever 25 cycles. Also, the filter was drained at the same intervals. The aim was to ensure reaction conditions as similar as possible to those in the pilot plant. So, before the experiment the mass of the OC, the amount of fuel, the steam mass flow, the oxidation time, and the volume flow were calculated based on the results of an experiment in the pilot plant in which C28 was used as an OC. The detailed calculations of these values will be explained further below in Chapter 4.3.

The experiment took place over a period of 4 days, with 50 cycles being conducted each day. The aim of the long-term-experiment was to explore the behaviour of the OC, that performed the best out of all

the OCs tested in the characterisation test, undergoing a much higher number of cycles. Especially important was to see how the OC would perform regarding the attrition rate, the oxygen transport capability and the CO_2 yield. Another aspect that is important, when using an OC in a large scale CLC process, is its recyclability, not only to keep the costs of the operation low but also regarding environmental factors. As a measurement for recyclability the magnetic permeability of the OCs was used to determine the separability from of the OC from ash.

3.4 Key figures

The following chapter presents key figures and formulas for the CLC process. These are used to describe important properties and the quality of the reaction. They help understand the evaluation process used to determine and assess the quality of the OCs. In addition, they are standardized and can be compared with the results of other studies.

The degree of oxidation X_S indicates how much oxygen the OC has stored at a given time during the experiment. It is calculated from the mass m of the OC at the measured time and the oxygen transport capacity R_O as well as the reduced and oxidized masses m_r and m_o. For m_o the weight after the oxidization in the oven was used, m_r is calculated using R_O and m_o (Formula 3), and R_O is a value from the literature found in Figure 4. The two masses are characterized by the maximum possible release or absorption of oxygen from the OC. An OC with a degree of oxidation equal to 1 is fully oxidised and an OC with a degree of oxidation equal to 0 cannot release any more oxygen.

$$X_S = \frac{m - m_r}{R_O * m_o} \tag{23}$$

Another decisive parameter is the ratio of stoichiometric combustion Φ [33]. It is calculated from the total mass of OC inside the reactor m_{OC}, the oxygen transport capability R_O, as well as the mass of oxygen required for stoichiometric combustion m_{St}. The product of R_O and m_{OC} is the total mass of oxygen that can be released. This is compared with the amount of oxygen required for stoichiometric combustion. The usual values for ϕ in batch operation were 10. This corresponds to 10 times the amount of oxygen in relation to the fuel or that only 10% of the theoretical releasable oxygen is required by the OC [33].

$$\Phi = \frac{R_O * m_{OC}}{m_{St}} \tag{24}$$

To better understand the processes in the reactor the difference in oxidation degree ΔX_S [68] is an important value. It compares the degree of oxidation inside the AR $X_{S,ox}$ and the degree of oxidation inside the FR $X_{S,red}$. This difference in oxidation provides information on how much oxygen gets

released throughout the reaction process and whether the OC is fully oxidized again.

$$\Delta X_S = X_{S,ox} - X_{S,red} \tag{25}$$

The effective amount of oxygen released by the OC $\Delta\omega$ [33] is calculated using the Oxygen transport capability of oxide R_O, and the difference in oxidation degree ΔX_S. To be able to create a complete oxygen balance over the reactor system, the oxygen in the exhaust gas and in the fuel is also included.

$$\Delta\omega = R_O * \Delta X_S \tag{26}$$

The following section presents some characteristic values that can be used to quantify the quality of the CLC process and combustion in the reactor. These are specially adapted to the batch reactor used to ultimately ensure comparability with larger plants.

The first value of carbon loss percentage $Y_{C,loss}$ [9], determines the amount of carbon that actually reaches the exhaust stream, and, respectively, the amount that is lost during the combustion process. It is calculated by using the amount of carbon in the fuel and the amount of carbon measured in the exhaust stream. If the value goes towards 0, combustion strives for complete carbon conversion in the exhaust gas. Carbon loss occurs mainly in the form of higher hydrocarbons and tars, which are separated in the scrubber. This value is especially important for understanding the process inside the reactor and the carbon balances used for the evaluation of the OCs.

$$Y_{C,loss} = 1 - \frac{n_{C,exhaust}}{n_{C,fuel}} \tag{27}$$

In every combustion process, the carbon in the fuel should be converted as completely as possible to CO_2 and water vapor. The conversion rate is an indicator of the effectiveness of the combustion process. Two viable options for this value are discussed by Fleiß (2019) [9]. The selectivity S_{CO2} has proven to be a more suitable value for this application, as it is not dependent on carbon loss. The amount of CO_2 in the exhaust gas $n_{C,CO2}$ and the total amount of carbon in the exhaust gas $n_{C,exhaust}$ are necessary for the calculation of the selectivity. S_{CO2} is suitable for determining whether combustion is complete or whether carbon monoxide and methane remain in the exhaust gas.

$$S_{CO2} = \frac{n_{C,CO2}}{n_{C,exhaust}} \tag{28}$$

3.5 Evaluation method

For the evaluation of the OCs used in the characterisation experiments spider charts, as suggested by Fleiß et al. [30] and by J. Adànez [69], were created. They can be used to quickly assess the quality of the tested materials and allow for easy comparison. As shown in Figure 18 two OCs are compared using spider charts. The diagrams show directly in which categories the OC performed better and in which categories it performed worse. The aim of the diagram was also to create a standardized evaluation matrix for further comparison of OCs.

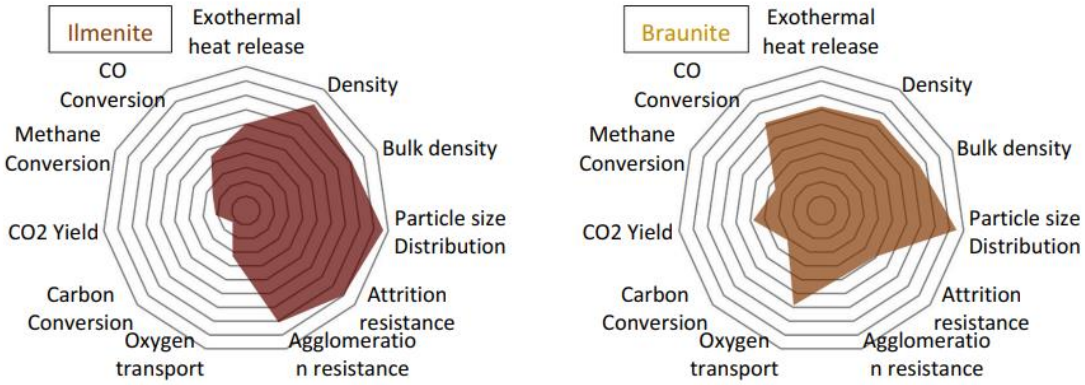

Figure 18: Spider charts used as the main validation tool for the OCs characterisation as proposed by B. Fleiß et al. [30]

Figure 18 presents exemplary spider charts as proposed by B.Fleiß et al. [30], serving as a visual template for how OC performance parameters can be effectively displayed. In total, eleven distinct parameters are considered to comprehensively characterize the performance of an oxygen carrier. These can be categorized into two primary groups: material properties and process performance indicators. The material properties include density, bulk density, particle size distribution, attrition resistance, and agglomeration resistance. These attributes are inherently linked to the physical and mechanical stability of the oxygen carrier particles under cyclic redox conditions and high-temperature fluidised bed environments. Conversely, the process-related parameters - oxygen transport capacity, carbon conversion, CO_2 yield, methane conversion, CO conversion, and exothermal heat release - are indicative of the reactivity and functional performance of the material during CLC operation. The boundaries and scales used in the spider charts are based on a normalization procedure against reference data from prior evaluations of oxygen carriers. This ensures consistency in comparative analyses and allows for direct benchmarking of new materials against established standards. The methodology for determining each of the eleven parameters, along with the respective normalization techniques, is described in detail in the subsequent sections. These explanations will also include the rationale behind the selection of each parameter and its relevance to the overall assessment of OC suitability for chemical looping combustion

applications.

3.5.1 Calculation and explanation of the properties

Density (particle density): The particle density is calculated by using a vessel of known volume. It gets filled to the brim with the OC material. Now because the OC is a made up of grains you can't just use the volume and mass to determine the density. First you must fill the spaces between those OC grains with water and calculate the volume of the water, by using the mass of water added (m_w) and the density of water (ρ_w). Afterwards you can calculate the particle density using formula 19. (M) represents the mass of OC (as determined for the bulk density) and (V_v) the volume of the vessel used. This process is repeated three times, to obtain an average value.

$$\rho_p = \frac{M}{V_v - \frac{m_w}{\rho_w}} \tag{29}$$

Bulk density: For calculating the bulk density, the commonly known formula 20 is used. (M) is the mass determined by using a bulk density apparatus and (V_v) the volume of the vessel.

$$\rho_b = \frac{M}{V_v} \tag{30}$$

The apparatus consists of a V-shaped funnel and a vessel of known volume. The funnel can be shut off to fill in the powder and opened to pour the powder into the vessel. It ensures an equal distribution of grains inside the vessel. This process is again repeated three times, to obtain an average value.

For performance of the OC in a CLC process a higher density and bulk density is advantageous, as high-density materials have a better heat capacity and can therefore dissipate heat better. So, OCs with high density perform better than those with low density.

Particle size distribution: The particle size distribution gets calculated with a sieve analysis. The grains of the OC material get divided into ≥ 400µm, 400-280µm, 280-224µm, 224-180µm, 180-140µm, 140-100µm, 100-63µm, and ≤ 63 µm fractions and the amount in each fraction is weighed. For the particle size distribution, the grains that get caught in the ≥ 400µm, 100-63µm, and ≤ 63µm mesh are of importance. For the CLC process you want the particle size distribution to be as narrow as possible. Particles that are too big won't get fluidised and too small particles are simply discharged during the process. So, the particle size distribution gets calculated by adding up those three fractions as seen in

formula x.

$$q_3 = w_{i,400\mu m} + w_{i,63\mu m} + w_{i,0\mu m} \tag{31}$$

The smaller q_3 is the smaller the amount of particle that are either too big or too small for the CLC process.

Attrition resistance**:** The attrition resistance is a very important property of an OC because it can influence the cycle stability and longevity of the OC. It can be calculated in two different ways. The first option is to take the sum of the discharged material inside the filter (m_f) and the test duration (t_t) and put it into relation with the total amount of bed material (m_{OC}).

$$A_{tot} = \frac{m_f}{t_t * m_{OC}} \tag{32}$$

The second option is to compare the initial sieve analysis to the sieve analysis after the experiment. However, due to the high losses in the cyclone, the second method did not provide representative values, and the first method was therefore used. Naturally you want the attrition of the OC to be as low as possible to guarantee longevity and cycle stability of the OC. Therefore, the higher the attrition resistance of the OC the better.

Agglomeration resistance: The agglomeration resistance was calculated using the quotient of two ratios. They are calculated using the mass percentage of the highest ($w_{i,400}$) and the second highest ($w_{i,280}$) sieve diameter from the initial sieve analysis and the highest ($w_{e,400}$) and second ($w_{e,280}$) highest sieve diameter of the sieve analysis done after the characterisation test, respectively.

$$A_R = \frac{\frac{w_{e,400}}{w_{e,280}}}{\frac{w_{i,400}}{w_{i,280}}} \tag{33}$$

Assuming the attrition of particles bigger than 400 µm is roughly equal to the attrition of particles bigger than 280 µm, an OC with low agglomeration has a A_R value equal to 1, as the ratio of the mass percentages before and after the test is roughly equal.

Oxygen transport: The oxygen transport (m_{OC,O_2}) is defined as the mass of the oxygen that was released from the OC. The highest value of the different operating points was chosen. To get the total amount of oxygen transported first the mass of the bed material in the oxidised state ($m_{OC,ox}$) and the reduced state ($m_{OC,red}$) must be calculated. This requires the oxygen change rate of the different states (ω_{ox}, ω_{red}) and the OC mass (m_{OC}).

$$m_{OC,ox} = \omega_{ox} * m_{OC} \tag{34}$$

$$m_{OC,red} = \omega_{red} * m_{OC} \tag{35}$$

Now the absolute mass of oxygen in the reduced state ($m_{OC,O_2,red}$) and in the oxidized state ($m_{OC,O_2,ox}$) can be calculated. This is done by using the weight of the samples before oxidisation ($m_{s,i,ox}$) in the oven and after oxidisation ($m_{s,ox,ox}$) and calculating a ratio. This ratio gets multiplied by the mass of the bed material ($m_{OC,ox}$) to get the absolute mass of the oxygen. The calculation is done for the oxidised and reduced state respectively.

$$m_{OC,O_2,ox} = m_{OC,ox} * \frac{(m_{s,ox,ox} - m_{s,i,ox})}{m_{s,i,ox}} \tag{36}$$

$$m_{OC,O_2,red} = m_{OC,red} * \frac{(m_{s,ox,red} - m_{s,i,red})}{m_{s,i,red}} \tag{37}$$

The final amount of oxygen transported between the oxidised state and reduced state can be calculated be simply subtracting the absolute mass of oxygen in the reduced state ($m_{OC,O_2,red}$) from the absolute mass of oxygen in the oxidized state ($m_{OC,O_2,ox}$), as seen in formula 28.

$$m_{OC,O_2} = m_{OC,O_2,red} - m_{OC,O_2,ox} \tag{38}$$

Carbon conversion: The carbon conversion (X_C) is calculated by dividing the total amount of carbon in the exhaust gas stream ($m_{C,exhaust}$) by the total amount of carbon in the fuel ($m_{C,fuel}$).

$$X_C = \frac{m_{C,exhaust}}{m_{C,fuel}} \tag{39}$$

The carbon conversion should aim for a value of 100%, if possible, as this means that the carbon in the fuel is completely released into the exhaust gas of the FR. A more detailed analysis of this can be found in the evaluation of the carbon balance (chapter 4.2.2).

CO_2 yield: Another important property of an OC in the CLC process is the CO_2 yield (Y_{CO_2}). It describes the amount of carbon in the fuel that got converted into CO_2. It gets calculated by dividing the amount of CO_2 (m_{CO_2}) measured in the exhaust stream divided by the amount of carbon in the fuel ($m_{C,fuel}$).

$$Y_{CO_2} = \frac{m_{CO_2}}{m_{C,fuel}} \tag{40}$$

This property is particularly significant with regard to the possible storage or further utilisation of the captured CO_2. Again, a value as close as possible to 100% is ideal.

The values for the carbon conversion and the CO_2 yield were selected from the maximum value of the operating point as described in diagram 7.

Methane conversion (CH_4 selectivity): The methane conversion (S_{CH_4}) expresses the proportion of methane in the exhaust fumes. For the calculation the amount of methane (n_{CH_4}) in the exhaust gets divided by the total amount of carbon ($n_{C,exhaust}$) in the exhaust.

$$S_{CH_4} = \frac{n_{CH_4}}{m_{C,exhaust}} \tag{41}$$

The value for the methane conversion should ideally be 0%, as all the methane was converted into CO_2.

CO conversion (CO selectivity): Like the methane conversion the CO conversion (S_{CO}) presents the share of CO in the exhaust stream. It also gets calculated by dividing the amount of CO (n_{CO}) in the exhaust by the total amount of carbon in the exhaust ($n_{C,exhaust}$).

$$S_{CO} = \frac{n_{CO}}{n_{C,exhaust}} \tag{42}$$

As the methane conversion, the CO conversion should be as low as possible to ensure more conversion of carbon into CO_2. For both properties, the values were selected from the minimum value of the operating point as described in Table 7.

Exothermal heat release: The exothermal heat release (ΔT_{heat}) gets calculated via the highest temperature difference ($\Delta T_{max,M}$) within a cycle. This value was normalized to the bed material mass (m_{OC}) and the oxygen released ($m_{OC,O2,M}$) within the selected cycle.

$$\Delta T_{heat} = \frac{\Delta T_{max,M}}{\frac{m_{OC}}{m_{OC,O2,M}}} \tag{43}$$

To achieve the same temperature level between the AR and the FR the heat losses between those two reactors should be as low as possible. Heat released in the oxidation process must be made available again during the reduction process. Therefore, a low exothermal heat release is to be preferred.

4 Results and Discussion

This chapter focuses on the presentation and interpretation of the results from the characterisation and long-term experiments. Lastly, it gives and estimation on the longevity of the OC used in the long-term experiment.

4.1 Results of the characterisation experiments

For greater clarity and better visualisation of the characterisation experiments a spider chart for each tested OC has been created. Furthermore, the influence of the fluidisation, the fuel amount and the bed temperature were evaluated.

4.1.1 Carbon balance

The carbon balance is used to clearly show how the OCs convert the carbon of the fuels. This allows conclusions to be drawn about unburnt materials, the coke content, and the higher hydrocarbons during the combustion process. The carbon balance was calculated considering the incoming and outgoing carbon flows, as shown in Equation 44. The entire reactor was defined as the reference limit for the balance. The only incoming carbon flow is carried into the reactor by the fuel $m_{C,f}$. The outgoing flows are calculated using the exhaust concentration of CO $m_{C,CO}$, CO_2 $m_{C,CO2}$, and CH_4 $m_{C,CH4}$.

$$m_{C,f} = m_{C,CO} + m_{C,CO2} + m_{C,CH4} \tag{44}$$

The differences in the balance can be explained by carbon losses. These are formed from higher hydrocarbons, unburnt material, coke content and tars.

Figure 19 shows the carbon conversion of each OC during the characterisation test. The values were calculated using the average of the four operating points (Steam 1, Steam 2, Temp 1, Temp 2), that use 10 g of fuel. The amount of carbon in 10 g of fuel is determined by the composition of the wood pellets. The Figure lays out what amount of the fuel got converted into CO, CO_2 and CH_4, as well as the amount of carbon that wasn't measured during the combustion. The stacked bars provide a good overview of the different carbon conversions of the individual OCs. There are differences in the height of the bars and differences in the respective amount of carbon of a certain exhaust gas. The higher the stacked bars on the right side, the less tar, coke, unburnt material or higher hydrocarbons have formed. For the CLC process ideally all carbon inside the fuel gets converted into CO_2, therefore the higher the CO_2 content the better.

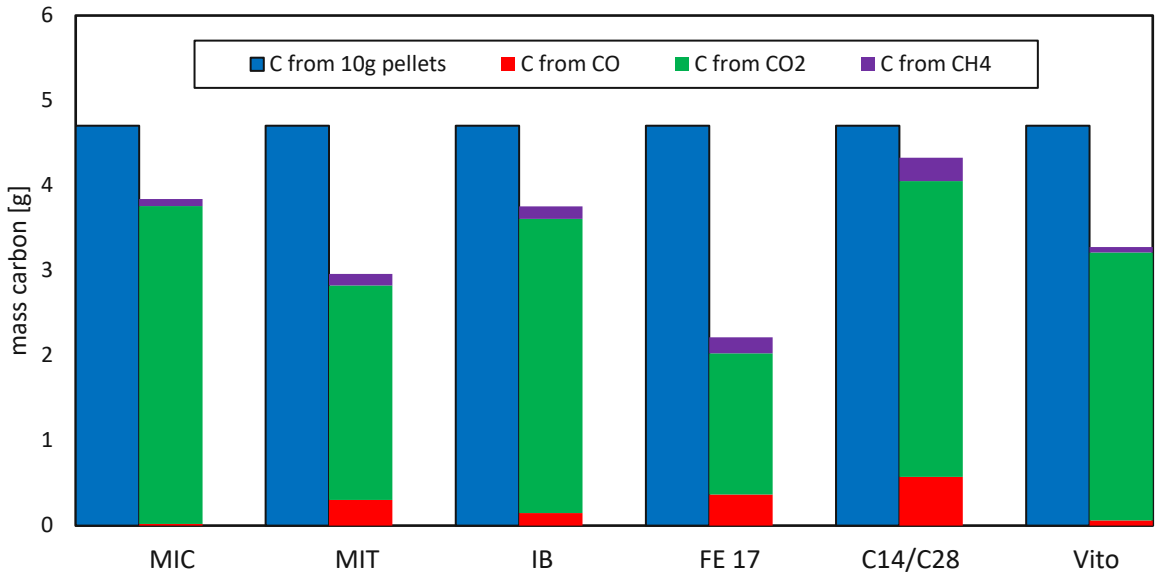

Figure 19: Carbon conversion of each OC

The OCs show very different results for the carbon conversion. The MIC OC has the highest C from CO_2 conversion of all the OCs, furthermore it has a very low C from CH_4 conversion and an almost negligible C from CO conversion. As previously stated, a complete conversion of carbon into CO_2 is strived for in this process and the amount of CH_4 and CO in the exhaust should ideally be as low as possible. Not counting the carbon loss, for MIC the average amount of CO_2 in the exhaust was 97%. Therefore, MIC shows the best carbon conversion out of all the OCs. Another interesting factor derived from the carbon balance is the carbon loss during the process. As mentioned before, the carbon loss is composed of unburnt material, coke, higher hydrocarbons, and tars. It can therefore be concluded that the combustion of Fe17 with a loss percentage of 52% is rather incomplete, whereas the combustion of MIC with a loss percentage of 18% demonstrates the lowest loss of all OCs. IB shows the second lowest carbon loss percentage with about 20%, followed by MIT with 37% and Vito with 42%. The carbon loss is therefore a function of reactivity with the different gas components and the oxygen release capacity of the OCs. In addition, the amount of available CLOU oxygen during combustion is of high impact, which could be specifically seen in the experiments with MIC and C14/C28. The oxygen release through CLOU is also quite visible by analysing the oxygen balance during the reaction.

4.1.2 Influence of fluidisation

As mentioned in Chapter 3.3.1 the OCs are being tested under different operating conditions. The influence of the fluidisation, the temperature and the fuel amount were examined. The following diagrams show the operating point Steam 1 and Steam 2. The difference between those two operating points only lies in the fluidisation amount. The volume flows during Steam 1 and Steam 2 are different for each OC, as their minimal fluidisation velocity is dependent on the bulk material. To understand the calculation for the fluidisation, an example for one OC (MIC) will be given:

As explained in a previous chapter the Grace-diagram uses the Archimedes-number and the Reynolds-

number. The AR is only dependent on the bulk material, so it does not change for Steam 1 and Steam 2. The goal for Steam 2 was to reach highest possible volume flow without crossing the U_t-line and possibly reaching turbulent fluidisation, although for bulk material with smaller particle diameters crossing the U_t-line does not necessary result in turbulent fluidisation. For Steam 1 the operating point in the Reh diagram (on the right) for a porosity of $\varepsilon = 0{,}6$ was chosen.

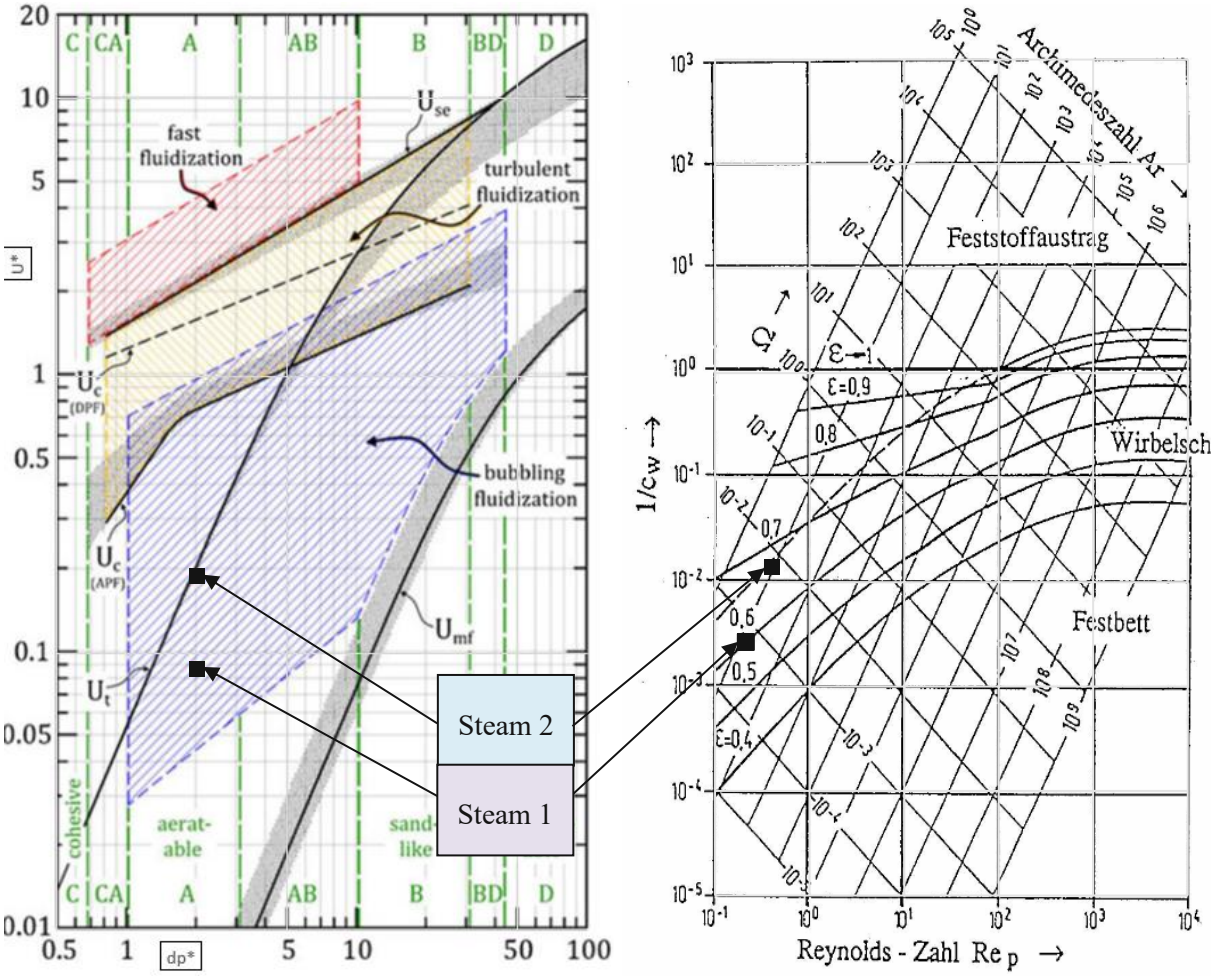

Figure 20: Exemplary fluidisation point calculation for MIC using the Grace (left) and the Reh (right) diagram (adapted from [49])

Table 8: Steam 1 and Steam 2 operating point for each OC in kg/h

Steam amount kg/h	*MIC*	*MIT*	*IB*	*Fe17*	*Vito A+B*	*C14/C28*
Steam 1	1,9	2,4	2,6	1,5	1,8	2,4
Steam 2	4,1	3,3	3,0	3,8	3,0	4,8

In Table 8 the operating points for each OC are shown. With increased fluidisation in a bubbling fluidised bed, the number of bubbles also rises. This can lead to improved solid mixing as well as better gas-solid contact. However, excessive fluidisation causes particle – OC, ash and char particles – entrainment from the fluidised bed and results in an insufficient gas residence time to form and oxidize

gasification intermediates. Additionally, the bubble size and amount increases, where gas components by-pass the bed material without sufficient gas-solid contact.

To compare the influence of the different volume flows on the six OCs, three key variables for the CLC process were used: The CO_2 yield, the carbon conversion as well as the CO_2 selectivity. The CO_2 yield describes the ratio of the CO_2 in the exhaust gas compared to the total carbon inside the fuel. Carbon conversion is the total amount of carbon inside the exhaust gas (only carbon from CO_2, CO, and CH_4 is measured) compared to carbon inside the fuel. And finally, CO_2 selectivity is the amount of CO_2 compared the amount of CO and CH_4 inside the exhaust gas. Those key variables are explained in more detail in 3.4.

Figure 22 shows the results of the CO_2 yield for each OC during Steam 1 and Steam 2. It is noticeable that C14/C28 performed the best out of all OCs, reaching a CO_2 yield of 87% during Steam 1 and 82% during Steam 2. MIC performed second best with values around 80%. MIT, IB and Vito A+B are all in the mid-range, while Fe17 with only around 40% performed the worst. For some OCs higher fluidisations seem to increase their CO_2 yield (MIC, Vito A+B, Fe17), while for the others it has a negative effect (MIT, C14/C28, IB).

Increased steam amounts primarily affect fluidisation, mixing of the oxygen carrier (OC), and gas-phase composition, thereby influencing the reaction pathways. A higher steam-to-carbon ratio promotes the water-gas shift reaction, leading to increased H_2 and CO_2 formation while simultaneously suppressing CO and CH_4. OCs such as MIC, Vito A+B, and Fe17 may benefit from these conditions, which could explain their improved performance at higher steam amounts. In contrast, OCs with strong CLOU abilities can perform efficiently even under low-steam conditions, as observed with MIC and C14/C28.

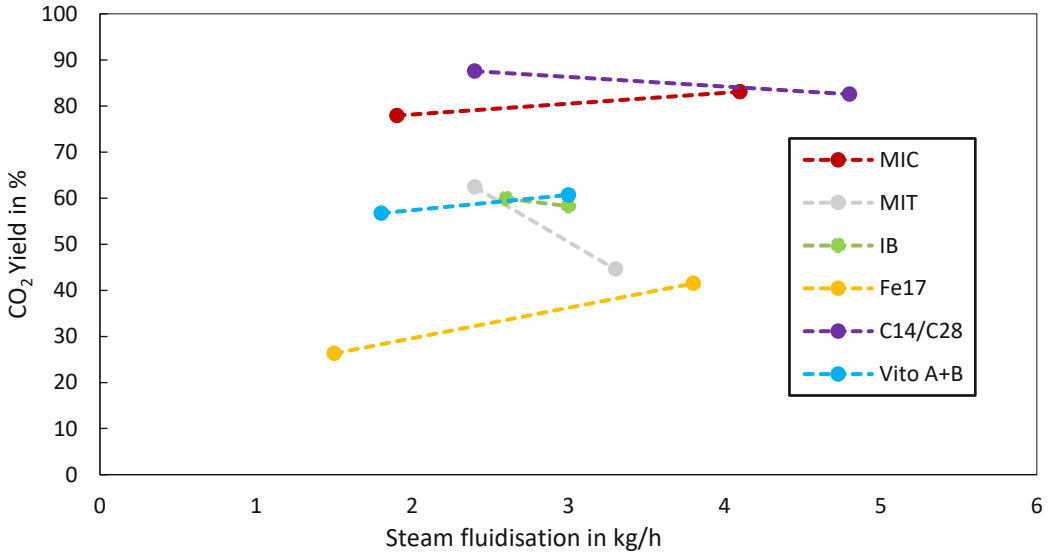

Figure 21: CO_2 yield during different fluidisation mass flows

For the CO_2 selectivity (Figure 23) there is not much notable change between Steam 1 and Steam 2 for all OCs. Both MIC and C14/C28 score very high with regard to their CO_2 selectivity, reaching values of up to 98%. A key observation is that CO_2 selectivity remains consistently high across all OCs, with only minor variations as steam flow increases. In contrast, Fe17 and IB exhibit slightly lower selectivity values but still maintain an increasing trend with higher steam amounts, suggesting that better fluidisation enhances complete oxidation.

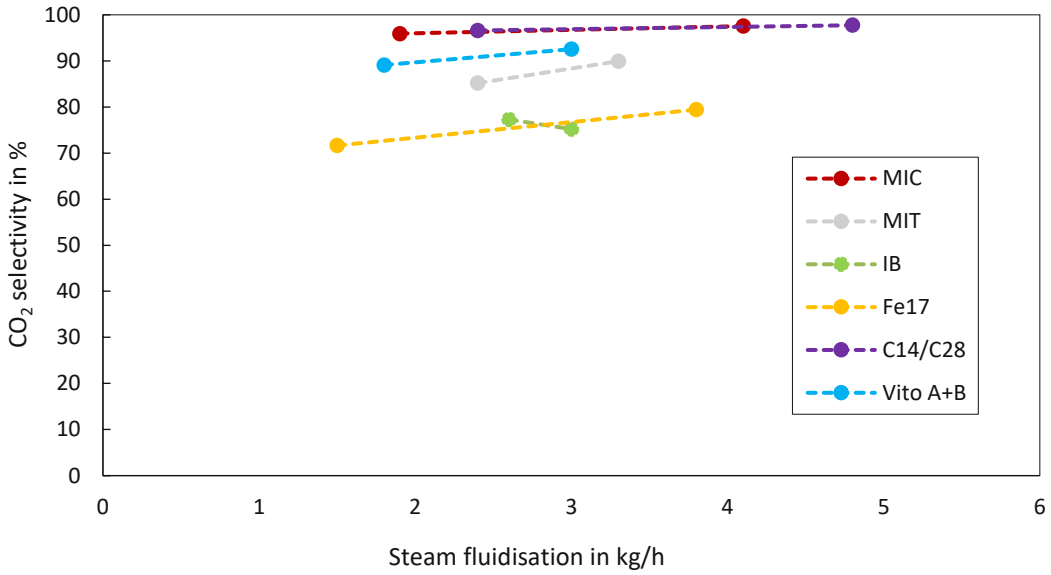

Figure 22: CO_2 selectivity during different fluidisation mass flows

Carbon conversion (Figure 24) shows again highest values for MIC and C14/C28 and IB is also performing better, reaching values of almost 80%. MIT has for the carbon conversion, as it has for the CO_2-slectivity, a lower value for Steam 2 than for Steam 1.

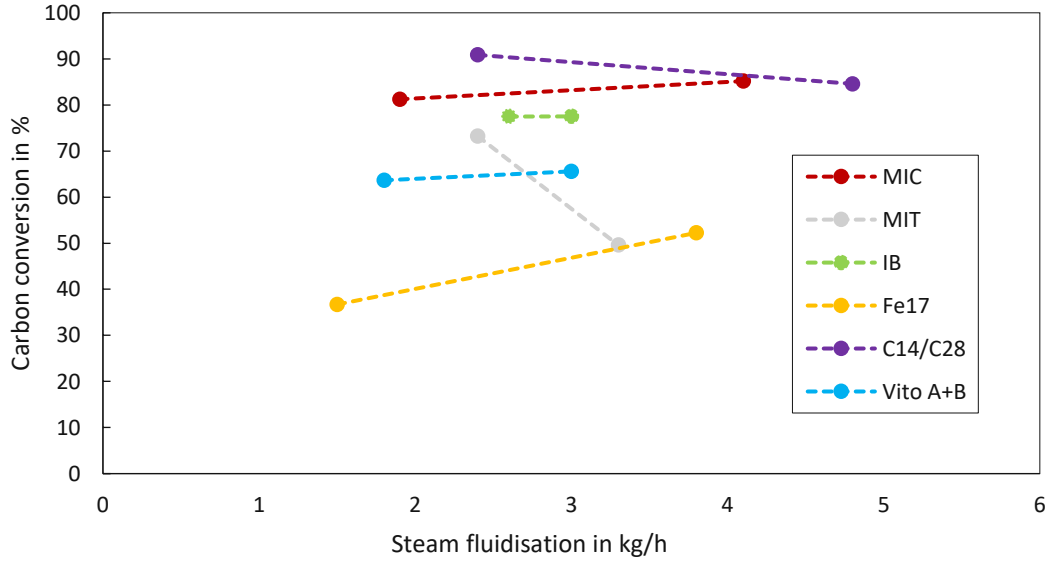

Figure 23: Carbon conversion during different fluidisation mass flows

In conclusion, the influence of the fluidisation is difficult to estimate. For some OCs, higher volume flows show better results, and for others, worse, and for IB, hardly any change was visible. Generally, a higher steam amount promotes better gas-solid contact and is therefore especially important for non-CLOU OCs like Fe17, which clearly shows better results with higher fluidisation.

An interesting phenomenon observed with MIT is that CO_2 selectivity increases with higher steam fluidisation rates, whereas CO_2 yield and carbon conversion decrease. This suggests that at higher steam flow rates, less fuel is being converted, but the fuel that does react is converted more efficiently into CO_2 rather than forming CO or other intermediate products. One possible explanation for this trend is the reduction in fuel-to-oxygen carrier contact time due to increased fluidisation. Higher steam flow enhances particle movement, leading to a shorter residence time of fuel within the reactor. This reduces the possibility for direct interaction between the solid fuel and the oxygen carrier, ultimately lowering the overall carbon conversion and CO_2 yield. However, the gas-phase oxidation reactions may still be highly efficient, ensuring that the fraction of converted fuel is predominantly oxidized to CO_2 rather than CO, resulting in an increase in CO_2 selectivity.

4.1.3 Influence of bed temperature

Finding the ideal temperature for an OC is crucial for the CLC process. The temperature of the fluidised bed influences the decomposition of higher hydrocarbons as well as the gasification of the fuel. Furthermore, the ability of OC to release oxygen via the CLOU effect has been shown to be influenced by the bed temperature. While elevated temperatures are generally advantageous, particularly for OCs containing low-melting-point metals such as copper, they also increase the risk of bed material agglomeration. The two bed temperatures tested were 950 °C and 800 °C. Again, CO_2 yield, carbon conversion and CO_2 selectivity were the key variables chosen to compare the six OCs.

At first Figure 25 shows the CO_2 yield of the OCs. It is clearly visible that all six OCs show an increase in CO_2 yield with higher temperatures. While Fe17 only increases slightly from 33 % to 36%, C14/C28 increases more than 20%. This is probably caused by the increased instability of the otherwise quite stable perovskite structure of C14/C28, which increased the release of CLOU oxygen during the combustion step. Overall, MIC and C14/C28 show the highest values for CO_2 yield, both reaching over 80% when being operated in a bed at 950 °C.

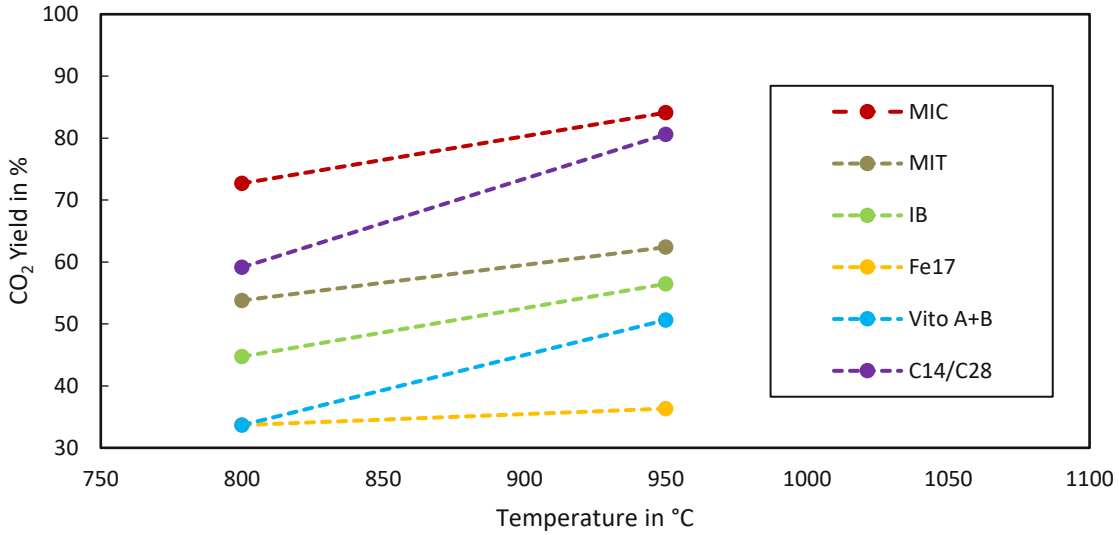

Figure 24: CO_2 yield during different temperatures

The carbon conversion in Figure 26 shows the same trends as the CO_2 yield before. All OCs exhibit better carbon conversion behaviour at higher temperatures. MIC and C14/C28 again performing best with values above 80% carbon conversion. Vito A+B and Fe17 only have a carbon conversion rate of around 50%, meaning that almost halve of the fuel did not get converted into CO, CO_2, or CH_4. Again, the increase of Fe17 is small compared to the other OCs.

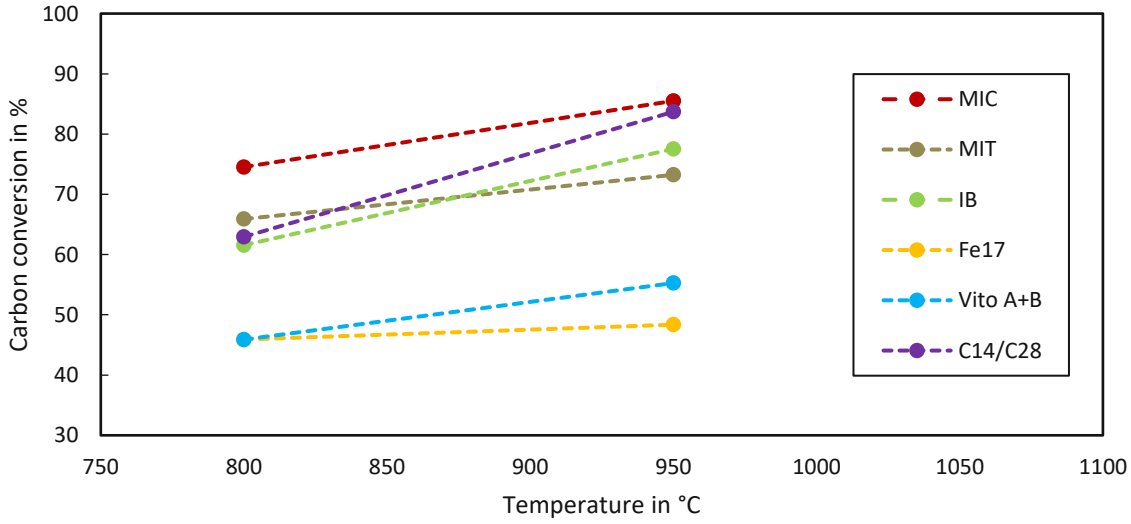

Figure 25: Carbon conversion during different temperatures

For the CO_2 selectivity the temperature does not seem to have a big influence. All OCs show a relatively stable CO_2 selectivity only varying in the 1-2 % range.

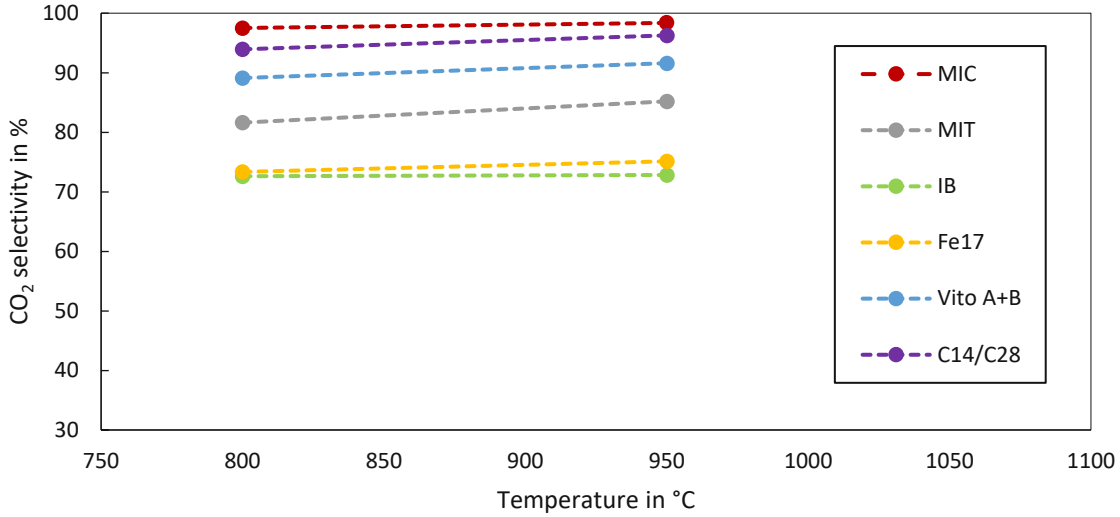

Figure 26: CO_2 selectivity during different temperatures

In conclusion, it is apparent, that an increase in temperature of the bed influences the CLC-process regarding the carbon conversion, CO_2 selectivity, and CO_2 yield. The performance of OCs and the overall combustion efficiency are highly dependent on operating temperatures. At higher temperatures, reaction kinetics are significantly enhanced, allowing faster redox reactions between the fuel and the oxygen carrier. This results in more complete oxidation of the fuel to CO_2, leading to higher carbon conversion efficiency. Elevated temperatures may also favour the thermodynamic conditions for oxidation reactions, minimizing the formation of incomplete combustion products such as CO, CH_4 and hydrocarbons. Additionally, the oxygen carrier's ability to release improves at elevated temperatures due to enhanced surface reaction rates and increased availability of active phases.

However, due to the exothermic reaction and the thermodynamic boundaries, it is possible that the total stored oxygen decreases with elevated temperatures. This is also shown, by comparing the maximal oxidation states of the materials at 800 and 950 °C. When evaluating Xs at different temperatures, as presented in Table 9, it is observed that for MIC, Vito A+B, and C18/C28, the oxidation degree exhibits an increase from 800°C to 950°C. Although this increase is minor, it indicates that these OCs can absorb oxygen at lower temperatures as effectively as, or even more efficiently than, at higher temperatures. In contrast, for MIT, IB, and Fe 17, the oxidation degree is significantly lower at 800°C compared to 950°C, which may be attributed to reduced reaction rates at lower temperatures. This suggests that the oxidation behaviour of these materials is more temperature dependent.

Table 9: Comparison of Xs for different temperatures

	MIC	*MIT*	*IB*	*Fe 17*	*Vito A+B*	*C18/C28*
$X_{s,ox}\ 950°C$	98,89	93,20	75,67	96,82	99,32	99,09
$X_{s,ox}\ 800°C$	99,33	83,98	74,81	81,25	99,91	99,75

Furthermore, excessively high temperatures can in addition negatively impact the structure of OCs. Sintering, or particle fusion, may occur, reducing the surface area and active sites available for reaction, ultimately degrading the carrier's long-term reactivity. The stability of the oxygen carrier must therefore be carefully considered when selecting operating temperatures.

CO_2 yield is also directly influenced by temperature. At optimal temperatures, CO_2 yield is maximized as complete combustion of carbon occurs with minimal formation of byproducts. Conversely, at lower temperatures, incomplete oxidation is more likely, resulting in reduced CO_2 yield and a higher likelihood of carbon deposition (coking) on the oxygen carrier surface. This not only lowers the overall efficiency but also risks deactivating the carrier over time.

While higher temperatures generally improve carbon conversion and CO_2 yield, operational challenges such as increased energy requirements, carrier degradation, and material sintering must be considered. Therefore, selecting an optimal temperature ensures a balance between high process efficiency and the long-term stability of the OC. By operating within this optimal range, the CLC process can achieve maximum efficiency and maintain carrier integrity over extended cycles.

4.1.4 Influence of fuel amount

This chapter explores the behaviour of the bed material when the fuel quantity is doubled, with a detailed comparison of the operating points Steam 1 and Fuel 1. In the first mode, 10 g of wood pellets are introduced into the fuel reactor, while in the second mode, the fuel quantity is increased to 20 g. This comparison provides insight into the effect of fuel load on system performance and stability. To evaluate the outcomes, again the three key performance indicators are used as benchmarks: CO_2-yield; CO_2 selectivity; and carbon conversion. The results of these performance metrics are illustrated in Figures 29, 30, and 31, providing a clear depiction of how the bed material and process parameters respond to changes in fuel input. This comparative analysis highlights the dynamic interactions within the fuel reactor and helps to identify trends or deviations when the fuel load is doubled.

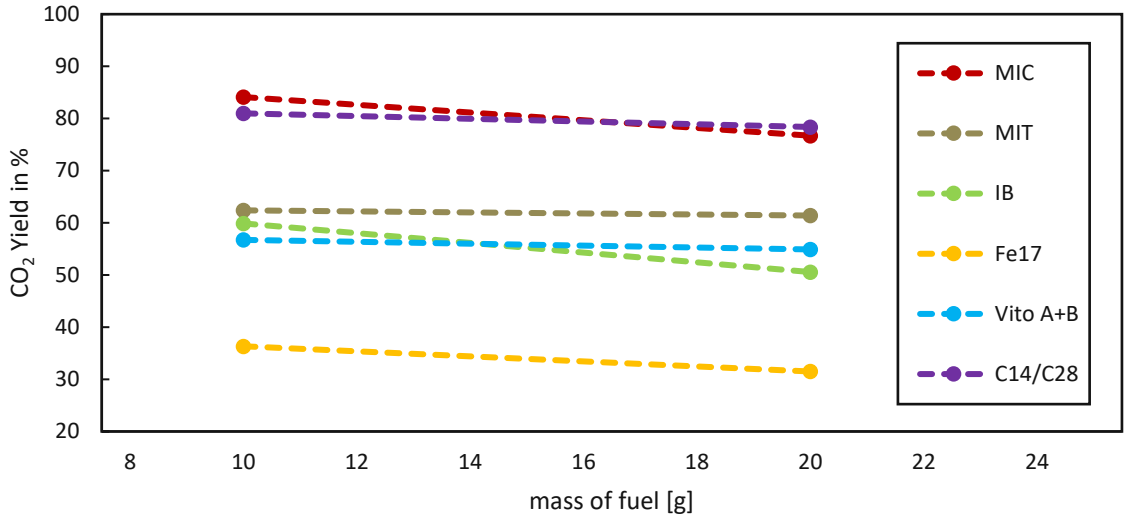

Figure 27: CO_2 yield for different amounts of fuel

In general, the CO_2 yield decreases as the fuel mass increases for all oxygen carriers. This trend indicates a reduction in the efficiency of carbon oxidation at higher fuel inputs. The oxygen carriers MIC and C14/C28 show the highest CO_2 yields, maintaining values above 80% even as the fuel mass increases. This demonstrates that these carriers are the most effective at converting carbon in the fuel to CO_2. Their consistent performance suggests high oxygen transport capacity, faster reaction kinetics, or other favourable properties, making them ideal candidates for CLC systems.

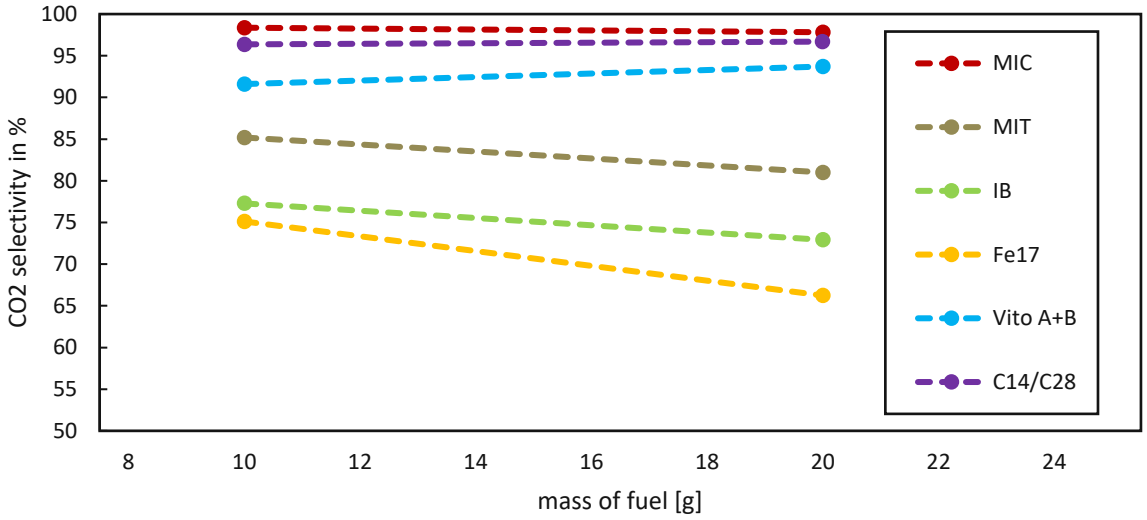

Figure 28: CO_2 selectivity for different amounts of fuel

For all three variables, doubling the amount of fuel has a negative effect on the OCs. The CO_2 yield of MIC and C14/C28 drops by around 10%. For the other OCs the loss percentage is not that high. MIT

and VITO A+B seem to be affected the least by the increasing amount of fuel, with regards to their CO_2 yield. C14/C28 seems to be less affected by the doubled amount of fuel as MIC, while its values are dropping in the higher fuel category it slightly outperformed MIC.

For the CO_2 selectivity, MIC and C14/18 show no significant changes by increased fuel. IB, MIT and, Fe17 show decreased performances. Only Vito A+B exhibits a slight increase in the CO_2 selectivity.

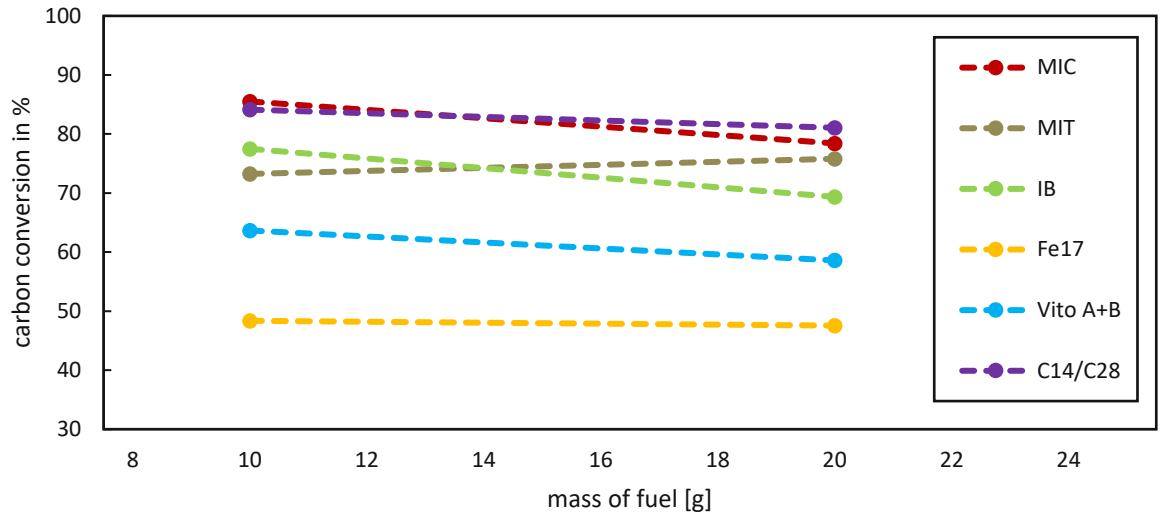

Figure 29: Carbon conversion for different amounts of fuel

For the carbon conversion again, most OCs only show a slight negative change, except MIT, which posts a slight increase. In conclusion, it can be stated that the increased fuel amount has a negative effect on most variables and most OCs.

In can be concluded that, with the CO_2 selectivity not being affected but the carbon conversion rate being negatively affected, the ratio of CO_2 to CO and CH_4 stays the same regardless of the double fuel amount. But the drop in carbon conversion indicates that unburnt material, tars or higher hydrocarbons have formed at a higher rate.

OC to fuel ratio

When considering the fuel amount during the experiment another important quality that has an influence on the OC performance is the OC to fuel ratio. The OC to fuel ratio can be calculated as explained before in Chapter 3.4 with Formula 24. It describes the ratio of the maximum amount of oxygen, that is transported into the reactor via the OC, to the amount needed for a full stoichiometric combustion of the fuel. This becomes more important when considering that for a higher fuel amount more oxygen is needed for a full combustion. There are two OC properties that have an influence on the OC to fuel ratio. Firstly, a higher density of an OC leads to more bed material that can be filled into the reactor without reaching its height limitations. Secondly, the oxygen transport capacity of the OC is essential; the greater

the amount of oxygen delivered to the FR, the higher the achievable OC-to-fuel ratio.

In Table 10 the calculated values of the OC to fuel ratio for all OCs are listed. The stoichiometric oxygen demand of 10 g and 20 g fuel are 12,42 kgO_2/kg and 24,83 kgO_2/kg, respectively. Among the evaluated oxygen carriers, MIC exhibits the highest density, whereas Vito A+B demonstrates the greatest oxygen transport capacity. The oxygen transport capacity is estimated by applying the corresponding redox pairs (as illustrated in Figure 4) to the compositional data of each oxygen carrier and calculating a weighted average. It is important to note that this approach provides only an approximate estimation of the oxygen transport capability. For a more accurate and material-specific determination, advanced characterisation techniques such as X-ray diffractometry are required, as they enable direct identification of the active phases and the extent of redox transformation [30]. Vito A+B being made up of NiO causes its high oxygen transports capability.

A higher OC to fuel ratio is important for several aspects of a CLC process. The higher oxygen supply ensures that the fuel undergoes a complete combustion, maximizing the conversion of carbon in the fuel to CO_2 and minimizing the formation of incomplete combustion products like CO, CH_4 or other hydrocarbons. Furthermore, this improves the overall carbon conversion efficiency of the process and enhances the purity of the CO_2 stream, which is a critical advantage in CLC for carbon capture applications

Furthermore, Table 10 presents the oxidation degree Xs of the oxygen carriers during both reduction (Xs,red) and oxidation (Xs,ox) phases for Steam 1, along with Xs,red values for Fuel 1. As previously discussed, Xs quantifies the fraction of lattice oxygen retained after reduction or restored after oxidation. Notably, the Xs,red values for C14/C28 are unrealistically high, indicating almost no oxygen release. This contradicts the expected behaviour of a CLOU-active material and likely results from an experimental error—possibly during sample weighing or oxidation. In general, lower Xs,red values are favourable, as they indicate a greater degree of oxygen release. For Fuel 1, which involves double the fuel quantity, more reduction is expected due to the higher oxygen demand for complete combustion. Regarding Xs,ox , values near 100% are ideal, signifying full reoxidation. All oxygen carriers except IB achieve this. IB shows a significantly lower Xs,ox (~75%), highlighting its limited reoxidation capacity and explaining its low reduction performance as well. MIC and MIT demonstrate high Xs,ox values but show a significant drop during reduction, consistent with their CLOU properties, which enable substantial oxygen release. Fe17, in contrast, exhibits only a minor change between oxidation and reduction, suggesting limited oxygen transport capability. Vito A+B shows unexpectedly high Xs,red in Steam 1, which may also stem from a measurement issue, as its value decreases markedly under Fuel 1, indicating greater oxygen release with increased fuel load.

Table 10: Comparative Analysis of the OCs focusing on OC to fuel ratio and oxygen transport capability (X_s)

	MIC	MIT	IB	Fe17	Vito A+B	C14/C28
Bed material in kg	2,42	1,66	1,57	1,24	2,28	1,98
Oxygen transport capacity in %	0,066	0,041	0,033	0,043	0,130	0,029
Stochiometric oxygen demand Steam 1 in kg/kg				12,42		
Stochiometric oxygen demand Fuel 1 in kg/kg				24,83		
OC to fuel ratio Steam 1	12,96	5,48	4,12	4,32	23,96	4,66
OC to fuel ratio Fuel 1	6,48	2,74	2,06	2,16	11,98	2,33
$X_{S,red}$ *of Steam 1 in %*	65,59	66,20	54,11	84,57	96,88	98,48
$X_{S,red}$ *of Fuel 1 in %*	35,17	30,70	32,04	79,23	42,40	98,86
$X_{S,Ox}$ *of Steam 1 in %*	99,27	93,20	75,67	96,82	99,79	99,32

4.1.5 Spider charts

Table 11 displays the exact calculated values for each OC and its properties. The calculation of the value is explained in Chapter 4.1. For the evaluation of those values, it is important to know that not all properties are equally important for the CLC process. Density, bulk density, and carbon conversion are most essential. The former two have a great influence on the fluidisation of the bed material, whereas the latter is a prerequisite for CLC. Agglomeration resistance, exothermal heat release and CO-conversion is considered with a lower priority for the CLC process. Agglomeration resistance can be compensated by additives and exothermal heat release by circulation rate and process cooling. A lower CO-conversion can for example be compensated by downstream cleaning steps, which is probably needed in case due to the low requirements of CO impurities. As the CLC process is regarded as a method for CCS, a very important property is the CO_2 yield, since it describes the amount of carbon that got converted into CO_2.

It should be noted that for some OCs the calculated values exceed the boundaries set before the experiment; for example, the oxygen transport of MIC, IB, and MIT or the exothermal heat release of Fe17. For those outliers, the values were set to the boundaries.

Table 11: Detailed calculated values of the particle and reaction properties of all OCs for the evaluation used in the spider charts

Particle properties	***Boundaries***		***MIC***	***MIT***	***IB***	***C14/C28***	***Vito A+B***	***Fe17***	***Unit***
Density	2400	6000	4301,19	4208,31	3703,9	3626,57	4040,07	2969,67	kg/m^3
Bulk density	1000	2500	2141,73	1462,33	1385,07	1747,13	2015,98	1097,83	kg/m^3
Particle size distribution	0,5	0	0,07	0	0,03	0,1	0,11	0,03	kg/m^3
Attrition resistance	0	0,8	0,04	0,2	0,182	0,3	0,07	0,38	%/h
Agglomeration resistance	15	-2	14,06	1,4	6,03	0,91	0,47	0,56	kg/kg
Reaction properties	**Boundaries**		**MIC**	**MIT**	**IB**	**C14/C28**	**Vito A+B**	**Fe17**	**unit**
Carbon conversion	60	95	85,6	75,88	77,6	83,79	65,65	54,5	%
CO_2 Yield	24	85	84,2	62,46	59,95	80,67	60,76	43,14	%
CH_4 conversion	12,5	-5	1,47	3,65	3,32	1,42	2,51	7,69	%
CO conversion	60	0	0,13	6,43	13,26	0,84	3,78	13,16	%
Oxygen transport	0	25	95,15	47,15	28,37	20	10,11	8,44	g
Exothermal heat release	5	-1	0,13	1,59	1,66	1,43	-0,22	6,37	K/g*kg

It is noticeable, that MIC exhibits the highest values for density, bulk density as well as carbon conversion. It therefore performs best in the three most important categories.

The spider charts in Figure 18 were created by normalisation of the calculated values of Table 8. This puts the values on a scale between 0 and 1 to enable a comparison. Based on the standardised values a surface value can be calculated for each particle property and for each reaction property. The sum of the surface values of the OCs is listed in Table 9.

Table 12: Surface area of the oxygen carriers based on their performance during the characterisation tests

OC	*MIC*	*MIT*	*IB*	*Fe17*	*Vito A+B*	*C14/C28*	*Unit*
Surface area	53,93	44,56	37,66	14,46	47,66	53,67	%

This allows the results of the characterisation tests to be compared directly. It should be noted that this does not put the before mentioned difference in importance of the individual properties into

consideration. It can be seen that MIC and C14/C28 perform best, and both have an almost identical surface value.

MIC, as already mentioned, shows the highest values for carbon conversion, density, and bulk density. It furthermore outperforms the other OCs regarding CO conversion, CO_2 yield, oxygen transport, and attrition resistance. Only in terms of agglomeration resistance MIC performed the worst. When retrieving the MIC-OC out of the reactor after the characterisation test, the agglomeration was visible. Loose clumps of metal oxide had formed, which could easily be broken apart by hand. This can be explained by the copper content of the OC. Copper has a melting point of 1085 °C and the reactor was operated at 950 °C, which increased during the exothermic oxidation reaction with air close to 1000 °C. A complete melting of the copper probably didn't occur, but agglomeration of particles and surface was possible. Copper based OCs have shown mixed results in the past regarding their agglomeration resistance. A study done on 2003 by Cho et al. [70] used a OC with 60% CuO as the active metal oxide and 40% $CuAl_2O_4$ as the support material in a CLC process operated at 850 °C, resulted in a complete sintering of the OC inside the reactor. Another study in 2011 by Gayan et al. [71] compared different copper-based OC at 950 °C showing no sign of agglomeration. The OC in the study done by Gayan et al. had a CuO-content of 15% or less. MIC has a CuO-content of 31%, leading to the possible conclusion that the higher the CuO-content in the OC the more prone it is to form agglomerations.

IB demonstrates a moderate to low performance across most properties, particularly excelling in oxygen transport and particle size distribution. However, its carbon conversion and CO conversion are moderate, indicating possible limitations in its reaction kinetics. A key limitation appears to be its bulk density and density, which are lower than other OCs.

Fe17 demonstrates high agglomeration resistance and strong particle size distribution, suggesting that it maintains structural integrity well over multiple redox cycles and is resistant to sintering. However, its bulk density and density are relatively lower as other oxygen carriers like VITO A+B or MIC. Its oxygen transport capability and CO_2 yield are moderate, indicating that while it can support oxidation reactions, it is not as reactive as Mn-containing oxygen carriers like C14/C28 or MIC. The low carbon conversion and moderate CO conversion suggest that it does not fully utilise its oxygen transfer potential, which is expected for iron-based oxygen carriers that do not exhibit CLOU behaviour.

MIT performs great in oxygen transport and well in CO conversion, indicating that its Mn-Fe composition contributes to effective oxidation and reduction cycles. However, it has one of the lower values for CO_2 yield and methane conversion, which suggests that not all the carbon is completely oxidized, potentially due to the influence of TiO_2. Titanium dioxide is known to enhance structural stability but can also hinder oxygen diffusion and reaction rates, leading to lower CO_2 selectivity. This explains why MIT does not perform as well in fuel conversion metrics despite having reasonable oxygen transport properties.

C14/C28 shows strong performance in CO_2 yield, carbon conversion, and oxygen transport, making it one of the most reactive OCs in the dataset. Its MnO-based composition is well known for its CLOU properties, which enhance fuel oxidation by directly releasing molecular oxygen into the gas phase. This leads to high combustion efficiency and excellent CO_2 selectivity. However, it has relatively low agglomeration resistance and attrition resistance, suggesting that it may suffer from structural degradation or sintering over multiple redox cycles. The bulk density is also lower compared to MIC or IB. Despite these drawbacks, C14/C28 is an extremely promising OC for applications that require high reactivity and efficient fuel combustion.

Vito A+B is characterized by a notably high CO conversion, despite exhibiting comparatively lower performance across other process properties. In terms of material properties, the carrier displays moderate to high performance, particularly with respect to bulk density and attrition resistance. These characteristics suggest structural robustness and mechanical stability over extended redox cycling. As a nickel-based material, Vito A+B benefits from inherently fast redox kinetics, which are advantageous for applications involving gaseous fuels. However, its oxygen transport capacity is relatively limited compared to materials such as C14/C28 or MIC, indicating a reduced contribution from CLOU mechanisms. Instead, the material likely favours direct gas-solid oxidation pathways.

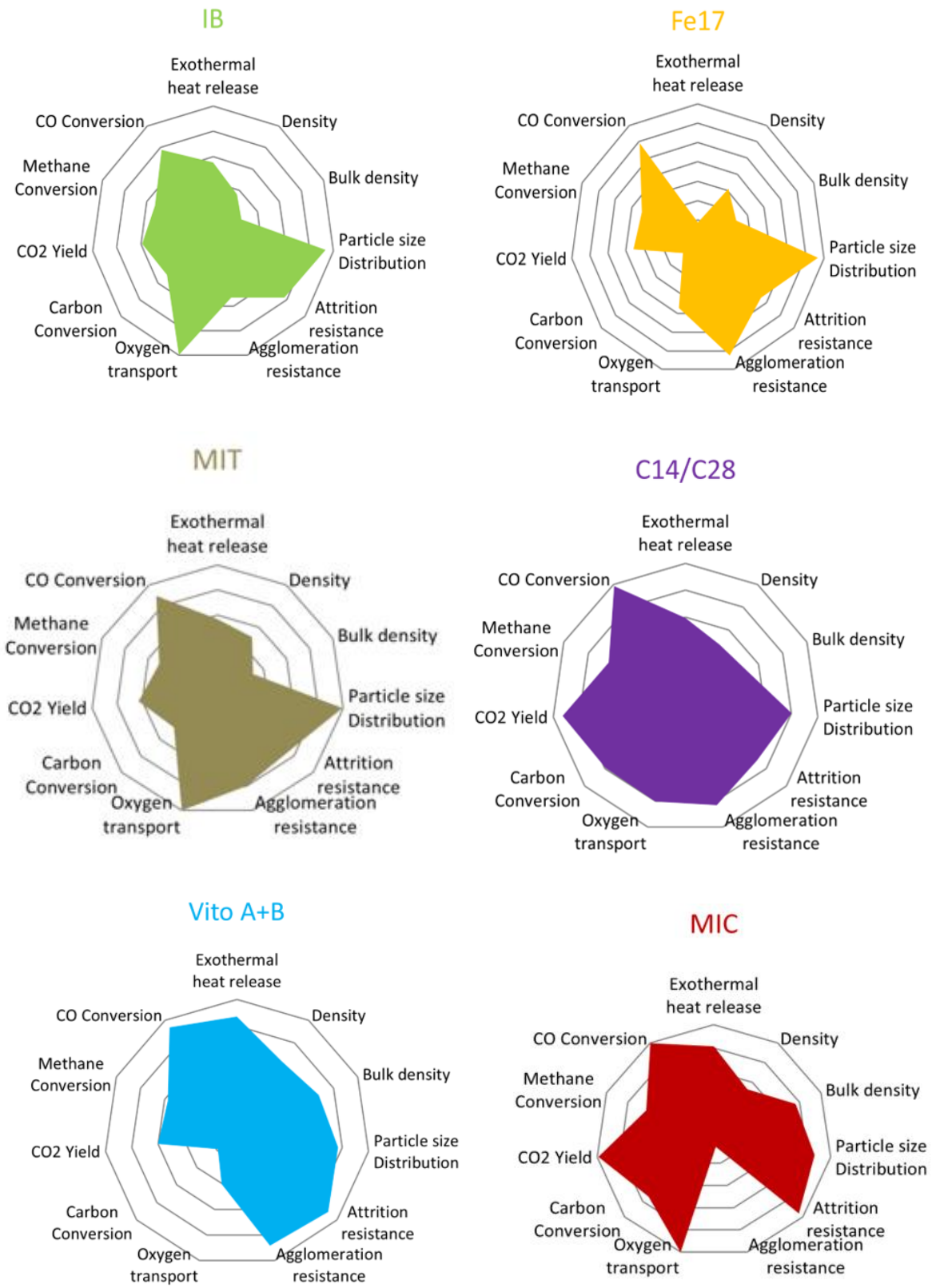

Figure 30: Spider charts of the six synthetic OCs tested during this study

4.2 Results of the long-term experiment

The long-term experiment focuses mainly on determining the longevity of MIC. As metrics for longevity the carbon conversion, the CO_2 selectivity, the magnetic permeability and the attrition rate of MIC were calculated. Before discussing the results, a detailed description of the calculation for the long-term experiment is necessary.

4.2.1 Detailed description of the calculation for the long-term experiment

The goal for the long-term experiment was to create similar reaction condition as in the pilot plant. The OC to fuel ratio (φ), the steam to carbon ratio (S/C ratio) as well as the air to fuel ratio (λ) were assumed to be equal for the batch reactor and pilot plant. As a reference for the calculations a test at the pilot plan using C28 (an OC, with similar properties as MIC) and wood pellets as the fuel were used. The operating temperature was again set to 950 °C, which might risk agglomeration, but the higher temperature was chosen to guarantee optimal reaction condition for the OC. As MIC showed only minor agglomeration during the characterisation test so there was no risk of sintering. Furthermore, as later in the test ash was added to the reactor, statements about the agglomeration would be hard to make.

The values in Table 11 were calculated as follows: The amount of OC (m_{MIC}) was determined by the volume of the reactor. Using the bulk density calculated in the characterisation test, the maximum amount of OC was determined. The mass of the ash should correspond to 25% of the mass of the OC. Using the mass of MIC and its oxygen transport capabilities, the amount of fuel (m_{fuel}) necessary can be calculated. First the mean transport capability of MIC was determined via Figure 8. By dividing the mean transport capability with the OC to fuel ratio, the amount of O_2 necessary for the fuel can be calculated. Now by dividing the amount of O_2 through the O_2 demand of wood, the fuel amount (m_{fuel}) was calculated. In order to calculate the steam mass flow ($\dot{m}_s$), the carbon content of the fuel amount, the steam quantity and the combustion time are required. For the carbon content of the fuel amount the fuel amount is multiplied by the carbon content of wood pellets. The steam quantity gets calculated by multiplying the carbon content of the fuel amount with the steam to carbon ratio (S/C ratio). Now the steam mass flow ($\dot{m}_s$) gets calculated with steam quantity and the combustion time, which is set to 10 seconds. In order to calculate the oxidation time (t_{ox}), the amount of oxygen in the air had to be determined. It was calculated from the product of the air to fuel ratio and the oxygen required for the fuel. Assuming that the ratio of volume flow and total bed material for the pilot plant and batch reactor are equal, the volume flow can be calculated using those values from the C28 pilot run and the determined total amount of MIC for the long-term experiment. The calculated values and reference values can be found in Table 13.

Table 13: Calculated and reference values of the long-term experiment

	Description	Abbreviation	Value	Unit
MIC calculated values	Mass MIC	m_{MIC}	2,829	[kg]
	Fuel amount	m_{fuel}	16,95	[g]
	Steam mass flow	$\dot{m}_s$	1,875	[kg/h]
	Oxidation time	t_{ox}	106	[s]
	Volume flow	$\dot{V}_{air}$	2,9	[nm^3/h]
C28 test at the pilot plant	OC to fuel ratio	φ	7,23	/
	Steam to fuel ratio	*S/C ratio*	0,65	/
	Flow rate air	$\dot{V}_{air,C28}$	55,68	[Nm3/h]
	Mean mass flow	$\dot{m}$	1102	[kg/h]
	Bed material total	$m_{OC,C28}$	55	[kg]
	Air to fuel ratio	λ	1,20	/
	Length of stay	t	180	[s]
Fuel	Carbon content	ω_{Holz}	0,47	wt%
	O_2 demand wood	$c_{fuel,C}$	1,2	[g/g]

An obstacle for the long-term experiment was to ensure a consistent stoichiometric ratio between OC and fuel, as more bed material was removed from the reactor with each solid sampling, changing the ratio of oxygen carrier to fuel amount. Therefore, the amount of fuel, the steam mass flow as well as the volume flow were recalculated after each solid sampling and filter drainage using an excel sheet. Only the oxidation time remained constant throughout the experiment. It should be mentioned that human error can influence the accuracy of the results. The volume flow for example has to be set by hand with a flowmeter. The fuel has to be weight for each cycle and reduced to smaller pieces so it can fit inside the fuel inlet. If some pieces get stuck inside the fuel inlet, the amount of fuel is less for a cycle resulting in falsified values. If this happened the values from those cycles were not put into the calculations.

4.2.2 Carbon conversion

In order to make statements about the quality of the OC during the long-term tests, the ability of MIC to convert carbon is analysed first. Three important key figures were determined for this purpose: CO_2 selectivity, carbon conversion and CO_2 yield. As stated before, those figures describe different ratios of the carbon in the flue gas. The carbon conversion is the ratio of the total amount of carbon in the exhaust gas to the amount of carbon from the fuel. The CO_2 yield describes the ratio of CO_2 in the exhaust gas to the amount of carbon from the fuel. Finally, the CO_2 selectivity is the ratio of carbon dioxide in the exhaust gas to the total amount of carbon in the exhaust gas. Detailed descriptions of those values can be found in Chapter 3.4.

The same evaluation sheets as in the characterisation test were used to calculate the afore mentioned values. The sheets provide the amount of CO, CO_2 and CH_4 inside the exhaust gas, and the total amount of carbon for five cycles and as well as an average. The average was used to calculate the three key figures, which were then plotted into the Figure 31.

Figure 31 shows the CO_2 selectivity, carbon conversion and CO_2 yield for the whole long-term experiment. The experiment took around 32 hours to complete, over a time period of four days. Each day 50 cycles were run in about 8 hours, not counting the preparation and cool down phase. The Figure shows that the CO_2 selectivity is high and steady throughout the whole experiment, averaging at about 95%. The carbon conversion and CO_2 yield fluctuate while showing a similar path. The similarity can be explained by the calculation of the two values. The CO_2 amount in the exhaust gas is equal to the total amount of carbon in the exhaust gas minus the CO and CH_4 concentration. Therefore, a corresponding path of CO_2 yield and the carbon conversion was expected. It is noticeable that the carbon conversion starts of at around 80% and increases after the first five cycles. This initial increase is caused by the attrition. The smaller particles get discharged from the reactor immediately causing the ratio of OC and fuel to be of balance resulting in a lower carbon conversion. This gets corrected after the first five cycles by weighting the amount of OC that got caught in the filter and subsequently adjusting the ratio of fuel and OC. After that the carbon conversion stays consistently above 80% for the first 100 cycles, while peaking at about 93%.

Despite the variance during the first 100 cycles MIC stills averages a carbon conversion rate of around 88%, which is higher than any other OC tested in the characterisation tests.

After the first 100 cycles (16h) the ash was added into the reactor causing a drop of more than 10%-points of the carbon conversion and CO_2 yield. The high amount of ash content during the combustion process lowers the contact between OC and fuel causing both values to decline significantly. Ash accumulation in the reactor can form a layer on the oxygen carrier particles or disrupt mixing within the reactor, both of which result in a decline in reactivity. The formation of an ash layer can inhibit gas-solid interactions, reducing the efficiency of oxygen transfer and fuel conversion. Additionally, poor

mixing caused by excessive ash can lead to temperature gradients and localized deactivation of the oxygen carrier, further impairing reactor performance. After the drop both values get progressively lower during the next 100 cycles. Carbon conversion reaches its lowest point at around 67%, while CO_2 yield bottoms out at around 65%. The results of the long-term experiment vividly demonstrate the negative influence a high ash content has on the carbon conversion and therefore on the viability of the whole CLC process. Therefore, the removal of ash from the fuel reactor should be of high importance when designing a CLC reactor.

During the whole test the CO_2 selectivity stays consistent. Showing that a higher number of cycles does not decrease the reactivity of MIC even after adding the ash. The capability of persistently reaching CO_2 concentrations of 95% in the flue gas is what makes MIC a great candidate for an OC used in a CLC process.

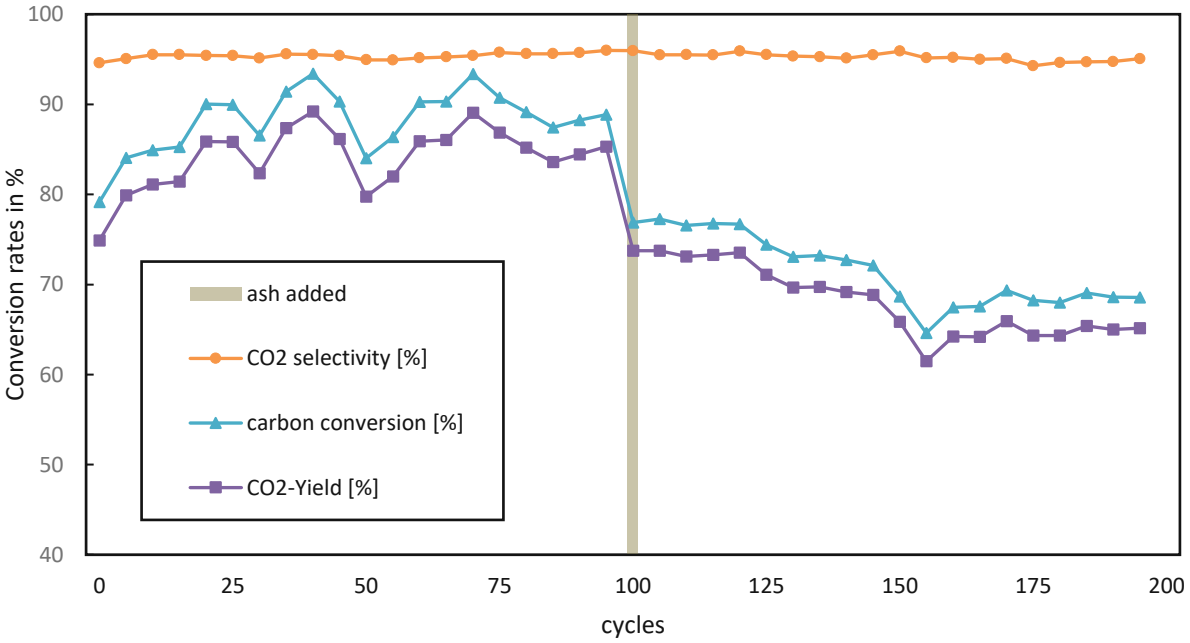

Figure 31: Conversion rates during long-term experiment: CO_2 selectivity, carbon conversion, and CO2 yield

4.2.3 Attrition rate

As already explained, there are two established ways to determine the attrition rate of the OC. It can either be calculated using the discharged mass inside the cyclone and the time of the experiment, or it can be estimated by comparing the initial and the end sieve analysis. Both methods have their drawbacks when considering that ash was added into the reactor after 100 cycles. A sieve analysis of the ash shows that it contains a large fraction of particles smaller than 63µm as well as particles larger than 400µm. The smaller particles will be discharged and trapped in the cyclone immediately. They will falsify the attrition rate when using the first method of calculating. The second method will not work either, as

there will be a lot of ash mixed with the OC when extracting the material out of the reactor. The only reliable way to estimate the attrition is to use the first method but only considering the first 100 cycles before the ash was added to the reactor. The results won't show the attrition for the whole experiment but only for the first 100 cycles of time. Figure 32 illustrates the results of the attrition rate calculation.

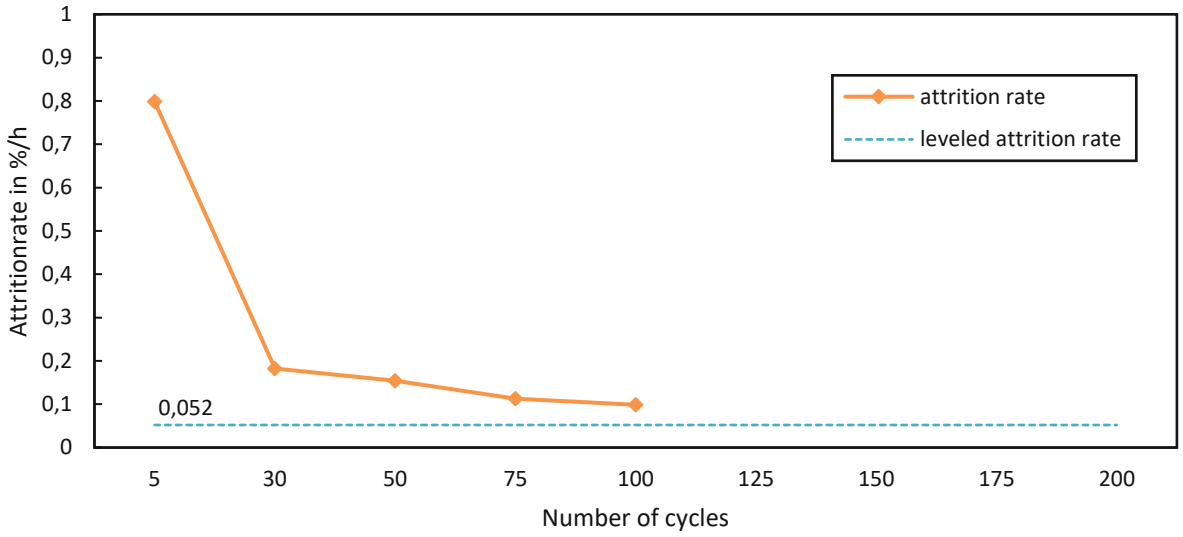

Figure 32: Attrition rate MIC; long-term experiment

As explained the attrition was only calculated for the first 100 cycles because of the ash, that got added into the reactor, so the Figure shows only values for the attrition of the first halve of the long-term experiment. It is noticeable, that the attrition starts very high at about 0,8 %/h and drops to 0,2%/h after the first filter drainage. After 30 cycles and the second filter drainage the attrition rate is levelling off at around 0,1 %/h. The drop off can be explained by the discharge of finer fractions during the first cycles. The bed material contains particles of different sizes. The fluidisation is so high that all small particles get discharged during the first few cycles and the attrition rate seems very high, but once all finer fractions have been expelled from the reactor, only the particles that get created through actual attrition get discharged from the reactor.

The levelized attrition rate gets calculated using all discharge samples and the total time for the first halve of the experiment. To factor in the finer fractions of the OC material, all particles smaller than 63µm are not put into consideration during the calculation of the levelized attrition rate. The final levelized attrition rate was calculated to 0,052%/h. Comparing this attrition rate to other synthetic OCs, 0,052 %/h appears to be a very low attrition rate. In a 2016 study from Cabello et.al [72] evaluating the attrition resistance of different synthetically produced OCs, the attrition rate measured ranged between 0,03%/h and 0,4%/h.

4.2.4 Magnetic permeability

When considering an OC for a CLC process another important aspect should be the reusability and recyclability of the material used for the OC. MIC, as it contains 36% iron oxide, is a magnetic metal oxide. The magnetic properties can be used for separating the OC from ash after the use in a CLC process. This would make the recycling of the material considerably easier. It is important to know that magnet metals lose their magnetic properties when exposed to high temperatures. This temperature is called the Curie point and for raw iron it starts at 770 °C. At this point the crystal structure of iron starts transforming from a body-centred-cubic (BCC) to a face-centred-cubic (FCC). When reaching a temperature of 910 °C the iron becomes completely FCC. With this structural change the iron loses its ferromagnetic properties [73]. As the reactor reaches temperatures of up 950 °C the ferromagnetic properties of MIC will decrease over time. As the recycling of the material is important, it would be interesting to see how fast the ferromagnetic properties of MIC will decrease and if it will lose its magnetic quality completely.

To test this, a study was conducted to determine the magnetic inductance of the material. The samples taken during the long-term experiment were each put inside a magnetic field and the deviation of the magnetic field was measured. From this deviation the magnetic inductance of the material after a set number of cycles can be determined. It is important to mention that the values for the magnetic inductance are only qualitative as the OC is a powdered material and the air pockets inside the bulk material effect the actual magnetic inductance. Though in the context of this work these values were satisfactory as the goal was only to measure the decrease of magnetic property of the OC.

Figure 35 shows the result of this test. The red points each correspond to a measured value for the magnetic inductance. The first red point indicates unused material and consecutively every 25 cycles. As expected, you can see a considerable drop after the first 25 cycles. After that the values decrease a little over time but stay relatively close together in a range of 150-160 µH. The yellow curve describes a trend line of the plotted points. As a comparison quartz sand, a material with no ferromagnetic qualities, was also tested. It reached a value of 147 µH. Following the trend line, it would take about 960 cycles for the material to reach the same magnetic inductance as the quartz sand, which means an operating time of over 150 h. By testing with a magnet, all samples of the long-term experiment showed magnetic properties and a separation from ash was still possible.

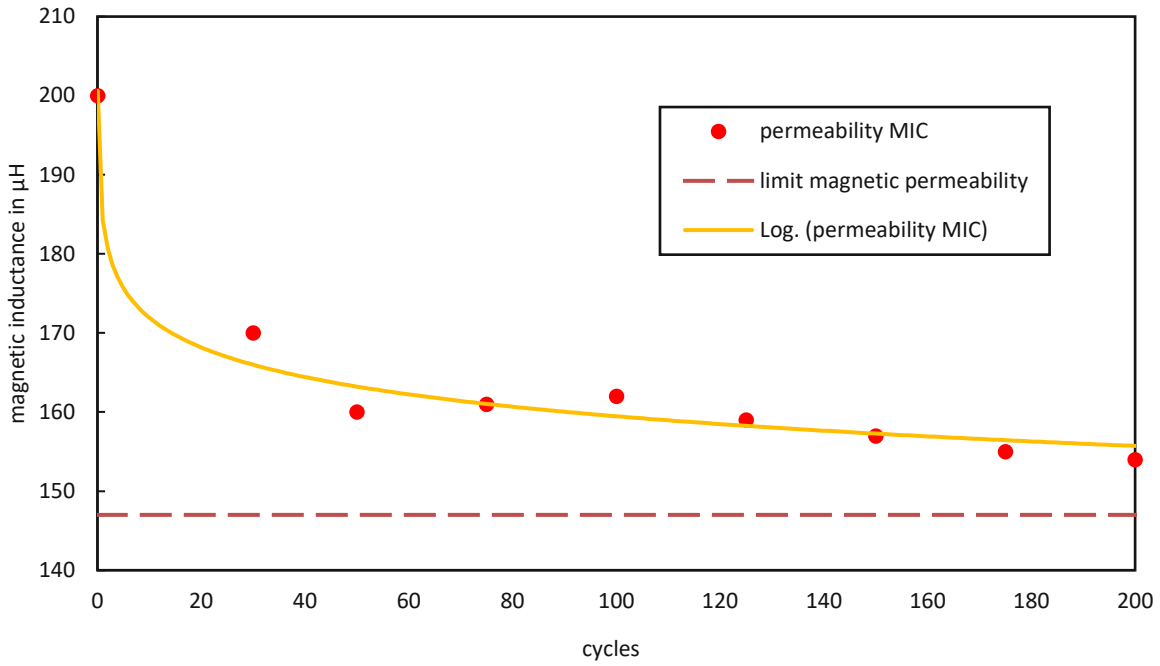

Figure 33: Magnetic inductance long-term experiment

4.2.5 Lifetime of MIC

As a final step, the long-term experiment was also conducted to determine a lifetime of the bed material. The lifetime of the OC is a very important variable, especially when considering a techno-economic assessment of a technology. A longer lifetime of the OC may reduce the price of a larger CLC plant considerably. Particularly when working with a synthetic OC the lifetime is important as the production is more expensive than when using natural ores. To get an estimation of the lifetime of MIC, the three different variables (attrition rate, magnetic permeability, CO_2 selectivity) introduced in the previous chapters were compared. Attrition rate is the standard when considering the lifetime of an OC, it is used in many studies because the lifetime can be directly deduced from the attrition rate (see Formula 45). The CO_2 selectivity is also suited to give an estimation about the lifetime through the cycle stability of the conversion rates, since it is such an important metric for the carbon capturing process. Once the percentage of CO_2 inside the flue gas is too low, the CLC process is no longer viable. Finally, the magnetic permeability as a unit for recyclability, can be used to give an estimation on how long it would take for the OC to lose its ferro magnetic ability, making the recycling process more difficult and therefore raising the price of operating a larger scale CLC-plant. For the comparison of all three values, Figure 36 shows the attrition rate, magnetic permeability and CO_2 selectivity in a single diagram. Furthermore, it shows the trend lines for all three values. The horizontal line at 200 cycles indicates the endpoint of the experiments.

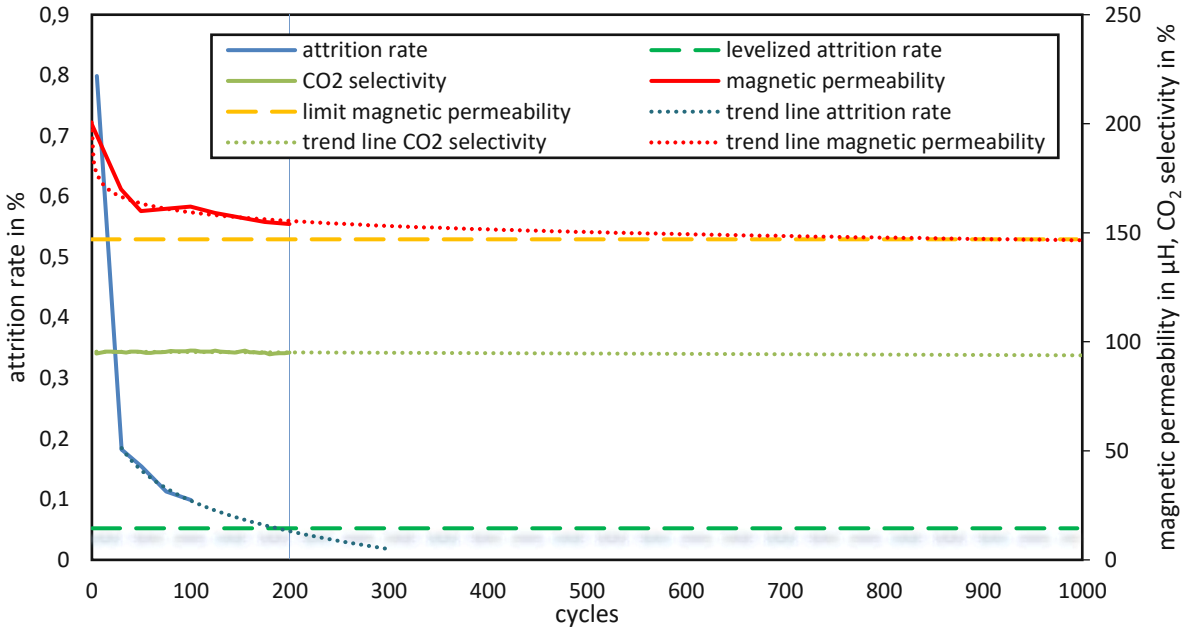

Figure 34: Attrition rate, magnetic permeability and selectivity of MIC during the long term experiment; measured and predicted values

Firstly, as described in Chapter 4.3.1, the CO_2 selectivity is level during the whole 200 cycles, showing no significant change. Averaging about 95% throughout the entire long-term experiment, which is higher than any other OC, achieved during the characterisation test. It can be concluded that the CO_2 selectivity will not be the determining factor of the lifetime, when considering 200 cycles. It is difficult to make a prediction on whether the CO_2 selectivity will change over time, this can only be established with certainty by running even more cycles. But for the scope of this thesis the following can be stated: No significant change of the CO_2 selectivity was noted during 200 redox cycles in a CLC process.

The magnetic permeability dropped considerably after the first 30 cycles, which can be explained by the Curie Point, as mentioned in chapter 4.3.3. After 200 cycles the material was still showing signs of its ferromagnetic ability when being tested by a magnet. The lower limit for the magnetic permeability of 147 µH would be reached after 960 cycles when following the trendline, rendering the material non-ferromagnetic. Again, it is difficult to estimate whether the bed material would lose its ferromagnetic ability altogether or whether it would be levelling off higher than the lower limit.

Finally, the lifetime can simply be inferred from the attrition rate according to Equation 45.

$$particle\ lifetime = \frac{100}{attrition\ rate} \tag{45}$$

Using the levelized attrition rate of 0,052 %/h a total lifetime of MIC can be calculated to 1920 hours. Compared to other synthetic oxygen carries this value ranges in the upper class [72]. When compared to ilmenite, a natural ore commonly used in CLC-processes with an estimated lifetime of 1315 h, MIC will last more than 600 h longer than ilmenite.

4.3 Error Analysis

Measurement Errors from the Measuring Device

The Rosemount® gas analyser used in this study has a specified accuracy of ±1% of the full-scale measurement range. Measurement uncertainties of this magnitude can influence the accuracy of the calculated results, particularly in the determination of gas conversion metrics. To mitigate such effects, the gas concentration data are converted into molar flow rates by referencing the known flow rate of the nitrogen carrier gas. Subsequent integration of the molar flow rate over time enables the determination of the total molar quantities, thereby reducing the impact of transient fluctuations and individual measurement inaccuracies on the overall mass balance calculations.

Another potential source of measurement uncertainty arises from the cross-sensitivity of the gas analyser in the presence of both oxygen and hydrogen. Under such conditions, the co-existence of oxygen may result in an overestimation of the detected hydrogen concentration due to instrumental interference. Nevertheless, within the scope of the present experimental procedure, this effect is largely inconsequential, as oxygen is not present during the fuel introduction phase—when hydrogen measurements are typically conducted. Since the primary evaluation focuses on carbon-based gas species and their corresponding performance metrics, the influence of this cross-sensitivity on the overall experimental outcomes is considered negligible.

Carrier Gas Flow (Nitrogen)

The total exhaust gas quantity can only be determined based on the carrier gas flow of nitrogen, as water vapor in the exhaust gas is not measured. After condensing out the water vapor, the five-component measuring device detects O_2, H_2, CO_2, CO, and CH_4. It is assumed that the remaining gas corresponds to the nitrogen carrier gas flow, which, however, is not directly measured. Any fluctuations in nitrogen supply or other exhaust gas components may affect the results. The carrier gas flow consists of two nitrogen streams: one supplied through a screw feeder via a mass flow controller, and another used for flushing a pressure measuring chamber in the airbox via a rotameter. However, since the concentration of each gas changes proportionally, these fluctuations do not affect selectivity but do influence yield and conversion rates.

Sample Collection

Samples are collected during reactor operation, with mixed bed material being extracted. The particle size deviation of the sampled bed material fluctuates, indicating that the extraction process is non-selective. The collected sample is split into two crucibles and weighed, followed by oxidation in a sample furnace. During transport to the furnace or while placing the samples into the crucibles, individual oxygen carrier particles may fall out of the containers, potentially distorting the measurement results. Additionally, all measurements were performed manually, introducing the possibility of

systematic and random errors. Further potential sources of error include uncertainties in mass measurement due to the sensitive nature of oxygen uptake, slight weight losses due to adhesion effects on the weighing containers, and possible inhomogeneities within the sample mixture, which could lead to slight deviations in oxygen determination. Furthermore, the heterogeneity of the particle size distribution within the sample can influence the measurement results, particularly if smaller particles are preferentially oxidized or unevenly distributed.

Temperature Dependence

The most critical temperature parameter in the CLC batch reactor is the bed temperature, which is measured using a thermocouple mounted vertically within the bed. Apart from instrumental inaccuracies, the bed temperature fluctuates due to heat losses, exothermic, and endothermic reactions.

Fluidisation

The amount of steam used for fluidisation plays a crucial role in mixing efficiency within the reactor. The steam dosage is controlled via a rotameter, which is calibrated for steam at 180°C and 2 bar. Steam dosage fluctuations occur due to pressure pulses in the steam drum system, causing instantaneous variations of 30–40%.

5 Summary

In the scope of this master thesis, different experiments, revolving around the OC of a CLC process, were conducted. In the first chapter a detailed overview of the core principles necessary for understanding the technology were presented. Explanation of different carbon capture methods, the CLC-process, the fluidised bed technology, the OC, existing CLC-plants, as well as the difference between CCS and CCU were given. The second chapter focuses on the applied methodology; giving a description of the batch-reactor and the measuring setup, that was used during the experiments, as well as explaining key variables for the evaluation of the OCs. Finally in the third chapter all results gathered from the test are being presented. In the following a brief overview of the results from both the characterisation test and the long term-experiment is summarized.

5.1 Characterisation tests

During these test six OCs were evaluated. For assessing the OCs spider charts were created, ranking the ability of the OCs, according to established parameters for a CLC-process. Furthermore, the influence of temperature, fuel amount, and volume flow on the performance of the OCs were assessed. The results can be summarized as follows:

MIC: This OC composed of manganese, iron and copper oxides ranked the highest out of all the other OCs, with regards to the parameters of the spider charts, reaching 53,93 surface area. It ranked highest for carbon conversion, CO_2 yield and oxygen transport capability, in the category of reaction properties. For the particle properties MIC had the highest scores for density, bulk density and attrition rate. These results show MIC clearly as the best OC for a CLC-process. Only the low agglomeration resistance, because of its copper content, is a drawback of this OC.

C14/C28: C14/C28 is a mixture of two perovskite OCs. It scored very close behind MIC with a score of 53,67 %. Reaching almost the same surface area as MIC. C14/18 was outperformed by MIC in all the before mentioned properties, but only by a small margin. It however, performed better with regards to its agglomeration resistance. Therefore, it should not be ruled out at all as a viable candidate, especially if the agglomeration problem of MIC causes

Vito A+B**:** This OC is mixture of two nickel-based metal oxides. It performed decently during the characterisation tests, scoring the third highest surface area of 47,66%. Vito A+B examines high values for all particle properties, especially for agglomeration resistance where it performed best out of all the OCs. The values for carbon conversion and oxygen transport of Vita A+B are rather low. Its biggest disadvantage, however, is that nickel is a carcinogenic metal, making the handling of this OC more complicated and dangerous.

MIT: MIT contains, manganese, iron and titanium. It scored close behind Vito A+B with a score of 44,45%. It has the highest possible score for particle size distribution as well as oxygen transport. However, it did not perform too well in and other category for its use as an OC in a CLC process to be justified.

IB: IB is a mixture of ilmenite and braunite, two natural ores that are often used as OCs. It did perform second worst with a surface area of 37,66%. It also has the highest possible oxygen transport capability but performed badly in all other categories. The only redeeming quality is that as it is produced from natural ores, therefore its production prices are lower than those of the other metal oxides.

Fe17: This metal oxide performed by far the worst with a surface value of only 14,46%. There is no reason for this OC to be used in CLC-process.

In conclusion, both MIC and C14/C28 are highly viable OCs and should be studied in more detail. For the long-term experiment MIC was chosen as it did perform slightly better than C14/C28. All other four are with respect to the characteristics applied by this study no viable candidates for a CLC-process, except for IB, because of the theoretically lower production cost due to the use of natural ores as feedstock material. Finally, the influence of temperature, volume flow, and fuel amount, can be summarized as follows: Higher temperature has a positive effect on the CLC-process because of better combustion condition leading to a more complete combustion and less unburnt material in the flue gas. The higher fuel amount had the opposite effect on the combustion as higher temperatures, causing a less complete combustion and more unburnt material in the flue gas. The difference in volume flow had only a small influence on OC, causing some to perform better (MIC, Vito A+B) and others worse (Fe17, C14/18, MIT). All together the influence was not that noticeable, and more testing is necessary to make a reliable statement.

5.2 Long-term experiment

For the long-term experiment MIC was tested for 200 redox cycles in the CLC batch reactor. This study was done over 4 days with 50 cycles being run each day. The experiment should simulate the conditions of the pilot plant at TU Wien as closely as possible. The goal was to gather important data on the performance of the OC during a longer runtime. Particularly interesting was to determine the lifetime of the OC, which is important for a techno-economic assessment. During the experiment ash was added into the reactor to examine the influence of a higher ash content. The results are as follows:

CO_2 yield, carbon conversion and CO_2 selectivity were used as quantifying variables. The CO_2 selectivity stayed constant throughout the whole experiment, averaging levels of 95%, even after the ash was added into the reactor. CO_2 yield and carbon conversion fluctuated during the first 100 cycles. CO_2 yield reached values between 80 % and 90%, while carbon conversion fluctuated between 85 % and 95%. Both values dropped considerably after the ash was added, during the last 50 cycles CO_2 yield levelled off at 65% and carbon conversion at around 68%. The magnetic permeability was determined as an indicator of recyclability of the material. It showed a significant decrease from after the experiment in comparison to before the experiment. However, when tested with a magnet the material still exhibited its ferromagnetic properties. Finally, the attrition rate and the resulting lifetime were calculated. Because of the ash a reliable estimation for the attrition rate could only be determined for the first 100 cycles. The attrition rate was calculated to 0,052%/h, resulting in a lifetime of 1920 h for MIC. The results of the long-term experiment showed a reliably high CO_2 selectivity throughout the entire test as well as high lifetime for a synthetic OC and the magnetic permeability of the material was still measurable after the test. Regarding the agglomeration problem MIC exhibited during the characterisation test, the long-term test did not show any negative influences of the possible agglomeration. Unfortunately, the agglomeration resistance could not be measured accurately after the long-term experiment as the bed material was mixed with the added ash, making a sieve analysis pointless. Although, while retrieving the bed material out of the reactor there was no visible sign of agglomeration as it had been during the characterisation tests.

6 Outlook

During this thesis several experiments were conducted, providing an evaluation of six OCs for a chemical looping combustion process. Two OCs have proven to be particularly suitable; the manganese, iron, copper, metal oxide MIC as well as C14/C28, a mixture of two perovskites. Both showed remarkable qualities with regards to their ability to transport oxygen and convert carbon. All other four OCs performed considerably worse making them no suitable options for a larger-scale CLC-process when including the high production costs of the synthesis. MIC was then again tested in a long-term experiment to determine its lifetime. During this experiment MIC was still performing great, reaching high values for the CO_2 selectivity. The experiments discovered the strengths of MIC while also revelling a potential downside. Because of its copper share MIC tends to form agglomeration at higher temperatures.

The next step for MIC would be a test on a larger-scale pilot plant, to examine its performances and scalability. A technoeconomic assessment could provide important information for the industrial scale viability of MIC, but this was no longer possible within the scope of this work. The agglomeration problem of MIC must be observed with more detail, more experiments should be conducted to examine this further. The decrease of the copper content during production could decrease the affinity for agglomeration. However, the comparison of MIC with a lower cost OC like ilmenite in regards their particle lifetime could provide insides on the economic viability of MIC. This would show if the superior reaction and particle properties of MIC could compensate for its higher production cost in comparison to a lower cost OC.

Conducting more experiments for C14/C28 could show some more information on this OC and could be interesting for future research. This would include another long-term experiment similar to the one performed for the MIC OC. Following that, a test on a larger-cale pilot plant and a technoeconomic assessment, as suggested for MIC, would be a meaningful step towards learning more insides about this OC.

Finally, the CLC development has seen a lot of research during the last few years, still there has not been an industrial scale plant successfully implemented yet. There is not much time left in the fight against climate change, making it even more urgent, that larger scale plants are being constructed in the next few years, for this technology to have a significant positive impact on CO_2 emissions. The greatest strength of the CLC process is its ability to create negative CO_2 emissions when biomass is used as a fuel, giving this technology the potential for being more than just a transitional solution. As mentioned above, more in-depth research with regards to the OCs, but also the scaling to larger plants, are useful research areas to advance this technology further.

7 Abbreviations and symbols

7.1 Abbreviations

Ar	Archimedes-number
AR	Air reactor
CCS	Carbon capture and storage
CCU	Carbon capture and usage
CLC	Chemical looping combustion
CLOU	Chemical looping with oxygen uncoupling
DFB	Dual fluidised bed
EOR	CO_2-enhanced oil recovery
Fr	Froud-number
FR	Fuel reactor
het-CLC	Heterogeneous-CLC
Me	Metal oxide(reduced)
MeO	Metal oxide(oxidized)
MW_{th}	MW thermic
ppm	Parts per million
Re	Reynolds number
TU	Technical University
USA	United States of America
BCC	Body-centred-cubic
FCC	Face-centred-cubic
°C	Degree Celsius

7.2 Symbols

A_R	Agglomeration resistance	[-]
A_{tot}	Total attrition rate	[%/h]
d_p	Sieve diameter	[m]
d_p^*	Dimensionless particle size	[-]
d_s	Surface area diameter	[m]
d_{sv}	Sauter mean diameter	[m]
d_v	Volumetric diameter	[m]
g	Acceleration of gravity	[m/s^2]
h	Hour	[h]
M	Mass of OC	[g]
$m_{C,exhaust}$	Total amount of carbon in the exhaust gas stream	[g]
$m_{C,fuel}$	Total amount of carbon in the fuel	[g]
$m_{C,fuel}$	Amount of carbon in the fuel	[g]
m_{CO2}	Amount of CO_2 in the exhaust stream	[g]
m_f	Discharged material	[g]
m_{fuel}	Mass of fuel	[g]
m_{MIC}	Mass of MIC	[g]
m_O	Oxidized mass	[g]
m_{OC}	Total mass of OC inside the reactor	[g]
$m_{OC,O2}$	Oxygen transport	[g]
$m_{OC,O2,M}$	Oxygen released within a selected cycle	[g]
$m_{OC,O2,ox}$	Absolute mass of oxygen in the oxidized state	[g]
$m_{OC,O2,red}$	Absolute mass of oxygen in the reduced state	[g]
$m_{OC,ox}$	Mass of the bed material in the oxidised state	[g]
$m_{OC,red}$	Mass of the bed material in the reduced state	[g]
m_r	Reduced mass	[g]
$\dot{m}_s$	Steam mass flow	[kg/h]
$m_{s,i,ox}$	Weight of the samples of the oxidized state before oxidisation	[g]
$m_{s,i,red}$	Weight of the samples of the reduced state before oxidisation	[g]
$m_{s,ox,ox}$	Weight of the samples of the oxidized state after oxidisation	[g]
$m_{s,ox,red}$	Weight of the samples of the reduced state after oxidisation	[g]
m_{ST}	Mass of oxygen required for stoichiometric combustion	[g]
m_w	Mass of water	[g]
$n_{C,exhaust}$	Total amount of carbon in the exhaust gas	[g]
$n_{C,fuel}$	Total amount of carbon in the fuel	[g]
n_{CH4}	Amount of methane in the exhaust	[g]
n_{CO}	Amount of CO in the exhaust stream	[g]
$O_{exhaust}$	Oxygen in the exhaust stream	[g]
O_{fuel}	Oxygen from the fuel	[g]

O_{OC}	Oxygen from the OC	[g]
$O_{water\ vapor}$	Oxygen in the water vapor	[g]
q3	Particle size distribution	[-]
R_O	Oxygen transport capability	[-]
S/C ratio	Steam to carbon ratio	[-]
S_{CH4}	Methane conversion	[%]
S_{CO}	CO Conversion	[%]
T	Oxidation time	[s]
t_t	Test duration	[s]
U	Superficial velocity	[m/s]
U^*	Dimensionless velocity	[-]
U_{mf}	Minimum fluidisation velocity	[m/s]
U_t	Floating velocity	[m/s]
$\dot{V}_{air}$	Volume flow air	[m^3/h]
V_v	Volume of the vessel	[m^3]
$w_{i,0\mu m}$	Weight percentage sieve diameter 0	[-]
$w_{i,280\mu m}$	Weight percentage sieve diameter 280	[-]
$w_{i,400\mu m}$	Weight percentage sieve diameter 400	[-]
$w_{i,63\mu m}$	Weight percentage sieve diameter 63	[-]
X_C	Carbon conversion	[-]
X_s	Degree of oxidation	[%]
$X_{S,ox}$	Degree of oxidation inside the FR	[%]
$X_{S,red}$	Degree of oxidation inside the AR	[%]
$Y_{C,loss}$	Carbon loss percentage	[%]
Y_{CO2}	CO_2 yield	[%]
Δp	Pressure difference	[Pa]
ΔX_S	Difference in oxidation degree	[%]
$\Delta\omega$	Effective amount of oxygen released by the OC	[%]
ρ_g	Gas density	[kg/m^3]
ρ_p	Particle density	[kg/m^3]
ρ_w	Density of water	[kg/m^3]
ϕ	Stochiometric combustion	[kg/m3]
ψ	Shape factor	[-]
ω_{ox}	Oxygen change rate of the oxidized state	[-]
ω_{red}	Oxygen change rate of the reduced state	[-]
ΔT_{heat}	Exothermal heat release	[°C]
$\Delta T_{max,M}$	Highest temperature difference	[°C]
μ	Dynamic viscosity	[kg/ms]

References

1. Manabe, S., *Role of greenhouse gas in climate change**. Tellus A: Dynamic Meteorology and Oceanography, 2019. **71**(1): p. 1620078.

2. *Atmospheric Carbon Dioxide*. 2022 [cited 2024 27.09.2024]; Available from: https://www.globalchange.gov/indicators/atmospheric-carbon-dioxide#:~:text=data%20collection%20began.-,Global%20monthly%20average%20concentrations%20of%20carbon%20dioxide%20have%20risen%20from,Dioxide%22%20is%20an%20adapted%20panel.

3. Abbass, K., et al., *A review of the global climate change impacts, adaptation, and sustainable mitigation measures.* Environmental Science and Pollution Research, 2022. **29**(28): p. 42539-42559.

4. *Technical Summary*, in *Climate Change 2022 – Impacts, Adaptation and Vulnerability: Working Group II Contribution to the Sixth Assessment Report of the Intergovernmental Panel on Climate Change*, C. Intergovernmental Panel on Climate, Editor. 2023, Cambridge University Press: Cambridge. p. 37-118.

5. *Energy consumption worldwide from 2000 to 2022, with a forecast until 2050, by energy source*. 2024 [cited 2024 17.11.2024]; Available from: https://www.statista.com/statistics/222066/projected-global-energy-consumption-by-source/#:~:text=Global%20energy%20consumption%20has%20increased,of%20the%20global%20energy%20consumption.

6. McLaren, D. and N. Markusson, *The co-evolution of technological promises, modelling, policies and climate change targets.* Nature Climate Change, 2020. **10**(5): p. 392-397.

7. *Das Übereinkommen von Paris*. 2024 [cited 2024 27.09.2024]; Available from: https://www.oesterreich.gv.at/themen/umwelt_und_klima/klima_und_umweltschutz/1/Seite.1000325.html.

8. Figueroa, J.D., et al., *Advances in CO2 capture technology—The U.S. Department of Energy's Carbon Sequestration Program.* International Journal of Greenhouse Gas Control, 2008. **2**(1): p. 9-20.

9. Fleiß, B., *Untersuchung zur Übertragbarkeit von Versuchsergebnissen zwischen Versuchsanlagen verschiedener Größe*. 2019.

10. Alalwan, H.A. and A.H. Alminshid, *CO2 capturing methods: Chemical looping combustion (CLC) as a promising technique.* Science of The Total Environment, 2021. **788**: p. 147850.

11. Chao, C., et al., *Post-combustion carbon capture.* Renewable and Sustainable Energy Reviews, 2021. **138**: p. 110490.

12. Theo, W.L., et al., *Review of pre-combustion capture and ionic liquid in carbon capture and storage.* Applied Energy, 2016. **183**: p. 1633-1663.

13. Scholes, C.A., et al., *CO2 capture from pre-combustion processes—Strategies for membrane gas separation.* International Journal of Greenhouse Gas Control, 2010. **4**(5): p. 739-755.

14. Metz, B., O. Davidson, H. C. de Coninck, M. Loos, and L. A. Meyer, *IPCC Special Report on Carbon Dioxide Capture and Storage*. 2005, Cambridge: Cambridge University Press.

15. Merkel, T.C., et al., *Power plant post-combustion carbon dioxide capture: An opportunity for membranes.* Journal of Membrane Science, 2010. **359**(1): p. 126-139.

16. Lee, A., et al., *Chapter 1 - Policies and Incentives Developments in CO2 Capture and Storage Technology: A Focused Survey by the CO2 Capture Project*, in *Carbon Dioxide Capture for Storage in Deep Geologic Formations*, D.C. Thomas, Editor. 2005, Elsevier Science:

Amsterdam. p. 17-35.

17. Kerr, H.R., *Chapter 38 - Capture and Separation Technology Gaps and Priority Research Needs*, in *Carbon Dioxide Capture for Storage in Deep Geologic Formations*, D.C. Thomas, Editor. 2005, Elsevier Science: Amsterdam. p. 655-660.

18. Lewis, W., E. Gilliland, and G. McBride, *Gasification of carbon by carbon dioxide in fluidized powder bed.* Industrial & Engineering Chemistry, 1949. **41**(6): p. 1213-1226.

19. Lewis, W.K. and E.R. Gilliland, *Production of pure carbon dioxide*. 1954, Google Patents.

20. Ishida, M. and H. Jin, *A new advanced power-generation system using chemical-looping combustion.* Energy, 1994. **19**(4): p. 415-422.

21. Liu, G. and G. Lisak, *Cu-based oxygen carriers for chemical looping processes: Opportunities and challenges.* Fuel, 2023. **342**.

22. Brachi, P., et al., *Assessing the feasibility of an integrated CLC-methanation system using solar dried and torrefied biomasses as a feedstock.* Fuel, 2023. **331**.

23. Haugen, N.E.L., et al., *Building the world's largest Chemical Looping Combustion (CLC) unit*, in *6th International Conference on Chemical Looping*. 2022: Zaragoza, Spain.

24. Lyngfelt, A., B. Leckner, and T. Mattisson, *A fluidized-bed combustion process with inherent CO2 separation; application of chemical-looping combustion.* Chemical Engineering Science, 2001. **56**(10): p. 3101-3113.

25. Leion, H., T. Mattisson, and A. Lyngfelt, *Solid fuels in chemical-looping combustion.* International Journal of Greenhouse Gas Control, 2008. **2**(2): p. 180-193.

26. Leion, H., T. Mattisson, and A. Lyngfelt, *The use of petroleum coke as fuel in chemical-looping combustion.* Fuel, 2007. **86**(12): p. 1947-1958.

27. Adánez, J., et al., *Chemical looping combustion of solid fuels.* Progress in Energy and Combustion Science, 2018. **65**: p. 6-66.

28. Pröll, T. and H. Hofbauer, *A dual fluidized bed system for chemical looping combustion of solid fuels.* Proceedings of the AIChE Annual Meeting 2010 Salt Lake City, USA, 2010.

29. Pröll, T., et al., *A novel dual circulating fluidized bed system for chemical looping processes.* AIChE Journal, 2009. **55**(12): p. 3255-3266.

30. Fleiß, B., et al., *Holistic assessment of oxygen carriers for chemical looping combustion based on laboratory experiments and validation in 80 kW pilot plant.* Fuel Processing Technology, 2022. **231**.

31. Lyngfelt, A., *Oxygen Carriers for Chemical Looping Combustion - 4 000 h of Operational Experience.* Oil & Gas Science and Technology – Revue d'IFP Energies nouvelles, 2011. **66**(2): p. 161-172.

32. De Vos, Y., et al., *Development of Stable Oxygen Carrier Materials for Chemical Looping Processes—A Review.* Catalysts, 2020. **10**(8): p. 926.

33. Adanez, J., et al., *Progress in Chemical-Looping Combustion and Reforming technologies.* Progress in Energy and Combustion Science, 2012. **38**(2): p. 215-282.

34. Voon, C.H., et al., *3 - Synthesis and preparation of metal oxide powders*, in *Metal Oxide Powder Technologies*, Y. Al-Douri, Editor. 2020, Elsevier. p. 31-65.

35. Lyngfelt, A., et al., *11,000 h of chemical-looping combustion operation—Where are we and where do we want to go?* International Journal of Greenhouse Gas Control, 2019. **88**: p. 38-56.

36. Mattisson, T., A. Lyngfelt, and H. Leion, *Chemical-looping with oxygen uncoupling for*

combustion of solid fuels. International Journal of Greenhouse Gas Control, 2009. **3**(1): p. 11-19.

37. Fleiß, B., et al., *CO2 capture costs of chemical looping combustion of biomass: A comparison of natural and synthetic oxygen carrier.* Journal of Energy Chemistry, 2024. **92**: p. 296-310.

38. Abdulally, I., et al., *Alstom's chemical looping technology, program update*, in *11th Annual Conference on Carbon Capture Utilization & Sequestration*. 2014: Edinburgh, Scotland.

39. Ströhle, J., M. Orth, and B. Epple, *Design and operation of a 1 MWth chemical looping plant.* Applied Energy, 2014. **113**: p. 1490-1495.

40. Haugen, N.E.L., et al., *Building the world's largest Chemical Looping Combustion (CLC) unit.* International Journal of Greenhouse Gas Control, 2023. **129**: p. 103975.

41. Mayer, K., et al., *The different demands of oxygen carriers on the reactor system of a CLC plant – Results of oxygen carrier testing in a 120kWth pilot plant.* Applied Energy, 2015. **157**: p. 323-329.

42. Fleiß, B., et al., *Synthetic oxygen carrier C28 compared to natural ores for chemical looping combustion with solid fuels in 80 kWth pilot plant experiments.* Fuel, 2023. **334**.

43. Heinrich, S., *Neue Entwicklungen in der Partikel- und Wirbelschichttechnik.* Chemie Ingenieur Technik, 2013. **85**(3): p. 215-215.

44. Grace, J.R., *Introduction, History, and Applications*, in *Essentials of Fluidization Technology*. 2020. p. 1-9.

45. Grace, J.A., A.; Knowlton, T., *Circulatin Fluidized Beds*. 1 ed. Balckie Academic and Professional, ed. 1. 1997: Springer Netherlands.

46. Hofbauer, H., *Vorlesung Wirbelschichttechnik, Kapitel 1-3*. 2018.

47. M., B., *Mechanische Verfahrenstechnik*. 1. 2004: Weinheim : Wiley-VCH.

48. Geldart, D., *Types of gas fluidization.* Powder Technology, 1973. **7**(5): p. 285-292.

49. Schmid, J., et al., *Cold Flow Model Investigation on a Modified Riser with Enhanced Gas-Solid Contact: Locating the Regions of Operation in a Fluidization Regime Map*, in *21st International Conference on Fluidized Bed Combustion (FBC)*. 2012: Naples, Italy.

50. Kalman, H., *Role of Reynolds and Archimedes numbers in particle-fluid flows.* Reviews in Chemical Engineering, 2022. **38**(2): p. 149-165.

51. Song, C., *Global challenges and strategies for control, conversion and utilization of CO2 for sustainable development involving energy, catalysis, adsorption and chemical processing.* Catalysis Today, 2006. **115**(1): p. 2-32.

52. Ekemezie, I.O. and W.N. Digitemie, *Carbon Capture and Utilization (CCU): A review of emerging applications and challenges.* Engineering Science & Technology Journal, 2024. **5**(3): p. 949-961.

53. Kontou, V., et al., *Transforming CO2 into Synthetic Fuels: Modeling, Simulation, and Optimization Analysis of Methanol Production from Industrial Wastes.* Eng, 2024. **5**(3): p. 1337-1359.

54. Abanades, J.C., et al., *On the climate change mitigation potential of CO2 conversion to fuels.* Energy & Environmental Science, 2017. **10**(12): p. 2491-2499.

55. Muggeridge, A., *The Geotechnical Challenges Associated with CCS.*

56. *Where is CO2 Stored and How Do We Know it Works?* [cited 2024 13.09.2024]; Available from: https://www.globalccsinstitute.com/ccs-101-storage/.

57. *Understanding carbon capture and storage*. [cited 2025 02.02.2025]; Available from: https://www.bgs.ac.uk/discovering-geology/climate-change/carbon-capture-and-storage/.

58. Scott, V., et al., *Last chance for carbon capture and storage.* Nature Climate Change, 2013. **3**(2): p. 105-111.

59. *Carbon capture and storage – what you need to know*. [cited 2024 12.09.2024]; Available from: https://www.greenpeace.org.uk/challenges/fossil-fuels/carbon-capture-and-storage/.

60. Duncan, I.J. and H. Wang, *Estimating the likelihood of pipeline failure in CO2 transmission pipelines: New insights on risks of carbon capture and storage.* International Journal of Greenhouse Gas Control, 2014. **21**: p. 49-60.

61. Duncan, I. and H. Wang, *Evaluating the likelihood of pipeline failures for future offshore CO2 sequestration projects.* International Journal of Greenhouse Gas Control, 2014. **24**: p. 124-138.

62. Fleiß, B., et al., *Innovative laboratory unit for pre-testing of oxygen carriers for chemical-looping combustion.* Biomass Conversion and Biorefinery, 2021.

63. Parzer, S., *Design, Errichtung und Inbetriebnahme einer Versuchsanlage für innovative Wirbelschichtprozesse*, in *Institut für Verfahrenstechnik, Umwelttechnik und Technische Biowissenschaften*. 2018, TU Wien: Wien.

64. Mayer, K., et al., *Chemical Looping Combustion Using Two Different Perovskite Based Oxygen Carriers: A Pilot Study.* Energy Technology, 2018.

65. Jerndal, E., et al., *NiO particles with Ca and Mg based additives produced by spray- drying as oxygen carriers for chemical-looping combustion.* Energy Procedia, 2009. **1**(1): p. 479-486.

66. Linderholm, C., T. Mattisson, and A. Lyngfelt, *Long-term integrity testing of spray-dried particles in a 10-kW chemical-looping combustor using natural gas as fuel.* Fuel, 2009. **88**(11): p. 2083-2096.

67. Cabello, A., et al., *Evaluation of a highly reactive and sulfur resistant synthetic Fe-based oxygen carrier for CLC using gaseous fuels.* Energy Procedia, 2013. **37**: p. 580-587.

68. Piesenberger, S., *Evaluierung von Mn-basierten Sauerstoffträgern für Chemical Looping Combustion*, in *Technische Universität Wien | Fakultät für Technische Chemie | Institut für Verfahrenstechnik, Umwelttechnik und technische Biowissenschaften*. 2018: Technische Universität Wien. p. 85.

69. Cabello, A., et al., *Qualification of operating conditions to extend oxygen carrier utilization in the scaling up of chemical looping processes.* Chemical Engineering Journal, 2022. **430**.

70. Cho, P., T. Mattisson, and A. Lyngfelt, *Comparison of iron-, nickel-, copper- and manganese-based oxygen carriers for chemical-looping combustion.* Fuel, 2004. **83**(9): p. 1215-1225.

71. Gayán, P., et al., *Effect of Support on the Behavior of Cu-Based Oxygen Carriers during Long-Term CLC Operation at Temperatures above 1073 K.* Energy & Fuels, 2011. **25**(3): p. 1316-1326.

72. Cabello, A., et al., *On the attrition evaluation of oxygen carriers in Chemical Looping Combustion.* Fuel Processing Technology, 2016. **148**: p. 188-197.

73. *Curie point of iron* [cited 2024 17.03.2024].